MICROCOPY RESOLUTION TEST CHART

②

CHARGE ACCUMULATION AND ARC DISCHARGES ON SPACECRAFT
MATERIALS AND COMPONENTS

November 1985

DTIC
SELECTED
APR 01
D

K.G. Balmain
Department of Electrical Engineering
University of Toronto
Toronto, Canada M5S 1A4

86 4 1 049

REPORT DOCUMENTATION PAGE *AD-A 166 216*

1a. REPORT SECURITY CLASSIFICATION		1b. RESTRICTIVE MARKINGS			
UNCLASSIFIED					
2a. SECURITY CLASSIFICATION AUTHORITY		3. DISTRIBUTION/AVAILABILITY OF REPORT			
		Approved for public release; distribution unlimited.			
2b. DECLASSIFICATION/DOWNGRADING SCHEDULE					
4. PERFORMING ORGANIZATION REPORT NUMBER(S)		5. MONITORING ORGANIZATION REPORT NUMBER(S)			
		AFOSR-TR. 86-0057 ~~AFOSR-84-0042~~			
6a. NAME OF PERFORMING ORGANIZATION	6b. OFFICE SYMBOL *(If applicable)*	7a. NAME OF MONITORING ORGANIZATION			
University of Toronto		AFOSR/NE			
6c. ADDRESS *(City, State and ZIP Code)*		7b. ADDRESS *(City, State and ZIP Code)*			
Toronto, Canada M5S 1A4		Building 410 Bolling AFB, DC 20332-6448			
8a. NAME OF FUNDING/SPONSORING ORGANIZATION	8b. OFFICE SYMBOL *(If applicable)*	9. PROCUREMENT INSTRUMENT IDENTIFICATION NUMBER			
AFOSR	NE	*AFOSR-84-0342*			
8c. ADDRESS *(City, State and ZIP Code)*		10. SOURCE OF FUNDING NOS.			
Building 410 Bolling AFB Washington, DC 20332-6448		PROGRAM ELEMENT NO.	PROJECT NO.	TASK NO.	WORK UNIT NO.
		61102F	2306	B1	
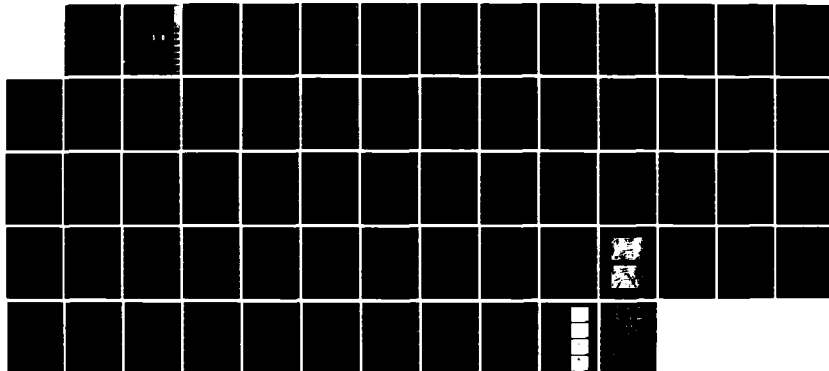
11. TITLE *(Include Security Classification)*
Charge Accumulation and Arc Discharges on Spacecraft Materials and Components

12. PERSONAL AUTHOR(S)
K. G. Balmain

13a. TYPE OF REPORT	13b. TIME COVERED	14. DATE OF REPORT *(Yr., Mo., Day)*	15. PAGE COUNT
Final	FROM 1 SEP 84 TO 31 AUG85	11 Nov 85	60

16. SUPPLEMENTARY NOTATION

17.	COSATI CODES		18. SUBJECT TERMS *(Continue on reverse if necessary and identify by block number)*
FIELD	GROUP	SUB. GR.	
			"ion spot phenomenon" 20 keV, luminescence.

19. ABSTRACT *(Continue on reverse if necessary and identify by block number)*

A study of arc discharge strength was carried out, emphasising its variation with the thickness of the dielectric-sheet specimens which had been exposed to an incident 20 keV electron beam at a current density of a thickness at which the peak current and the energy released into a load resistor are maximized. The addition of a low-energy ion beam was found to reduce discharge strength without significantly altering thickness-scaling. Also, experimental evidence was presented for a new effect called the "ion spot phenomenon" in which the incident ions are focussed into a central spot which then glows due to electron-impact luminescence. The first stage in the analysis of the ion spot phenomenon has been carried out and is described in this report. A two-dimensional analysis reveals complex ion trajectories which produce not only a strip (equivelent to a spot) of ion deposition, but are also such as to produce a spot with very sharply defined edges, just as observed experimentally. As for the spacecraft-charging experimental facility, a chamber capable of holding specimens up to 30 cm diameter has been completed. Arc discharges of 700 A peak have been recorded for the largest specimens

20. DISTRIBUTION/AVAILABILITY OF ABSTRACT	21. ABSTRACT SECURITY CLASSIFICATION	
UNCLASSIFIED/UNLIMITED ☑ SAME AS RPT. ☑ DTIC USERS ☐	UNCLASSIFIED	
22a. NAME OF RESPONSIBLE INDIVIDUAL	22b. TELEPHONE NUMBER *(Include Area Code)*	22c. OFFICE SYMBOL
Capt Kevin Malloy	202-767-4931	NE

DD FORM 1473, 83 APR   EDITION OF 1 JAN 73 IS OBSOLETE.

and a system for making surface potential measurements has been tested.

CHARGE ACCUMULATION AND ARC DISCHARGES ON SPACECRAFT
MATERIALS AND COMPONENTS

November 1985

K.G. Balmain
Department of Electrical Engineering
University of Toronto
Toronto, Canada M5S 1A4

TABLE OF CONTENTS

Accesion For

NTIS CRA&I		☒
DTIC TAB		☐
U.announced		☐
Justification		

By ....

Dist.ibution /

Availability Codes

Dist	Avail and / or Special
A-1	

1. SUMMARY

Objectives: Arc discharges on exposed spacecraft dielectric materials can occur as a result of charge accumulation from the energetic electrons and ions which are always present in synchronous orbit and which represent an increased danger to spacecraft systems under "magnetic storm" conditions. The main objective of this research is to use laboratory measurements and theoretical computations to evaluate the variation in arc discharge strength as a function of dielectric material thickness, under exposure to mono-energetic electron beams and low-energy ions.

Results: A study of arc discharge strength was carried out, emphasizing its variation with the thickness of the dielectric-sheet specimens which had been exposed to an incident 20 keV electron beam at a current density of 25 nA/cm^2. It was found that there exists a "worst" thickness around 50 μm, a thickness at which the peak current and the energy released into a load resistor are maximized. The addition of a low-energy ion beam was found to reduce discharge strength without significantly altering thickness-scaling. Also, experimental evidence was presented for a new effect called the "ion spot phenomenon", in which the incident ions are focussed into a central spot which then glows due to electron-impact luminescence. This work is all described in a paper to be published (by Balmain, Battagin and Dubois), which is attached to this report as the Appendix.

The first stage in the analysis of the ion spot phenomenon has been carried out and is described in this report. A two-dimensional analysis reveals complex ion trajectories which produce not only a strip (equivalent to a spot) of ion deposition, but also are such as to produce a spot with very sharply defined edges, just as observed experimentally.

As for the spacecraft-charging experimental facility, a chamber capable of holding specimens up to 30 cm diameter has been completed. Arc discharges of 700 A peak have been recorded for the largest specimens, and a system for making surface potential measurements has been tested.

Interactions: The Principal Investigator, K.G. Balmain, attended the IEEE Nuclear and Space Radiation Effects Conference, held in Monterey, California, July 22-24, 1985. He presented the paper "Thickness Scaling for Arc Discharges on Electron-Beam-Charged Dielectrics", by K.G. Balmain, A. Battagin, and G.R. Dubois, the final publication version of which is in the Appendix.

2. PERSONNEL

K.G. Balmain,	Principal Investigator
G.R. Dubois,	Professional Engineering Officer 2
T. Nozaki,	Engineering Technologist 3
G. McKeil,	Graduate Student (Ph.D. candidate)
A. Battagin,	Graduate Student (M.A.Sc. candidate)

3. ANALYSIS OF THE ION SPOT PHENOMENON
G. McKeil

3.1 Introduction

Theoretical investigations have been undertaken into the effect of the inclusion of positive ions with the incident electron beam during dielectric charging. Earlier [1] and concurrent [2] work here has shown that the introduction of ions at relative current densities comparable to those existing in the magnetosphere (about 10% of the electron current density) results in a reduction in strength or elimination of electrical discharges. Further, evidence was seen [2] to indicate that strong focussing of the incident ions was occurring. The ions appeared not to be deposited over the entire dielectric surface but to be concentrated on a small central "spot". This "ion spot" was stable in location and general features, and had a very definite and sharp boundary. A more gradual and continuous transition between regions of high and low ion concentration might have been expected, if spot formation had been predicted.

As a first step in theoretical investigations, the ion trajectories and resultant ion beam focussing are studied numerically for low energy ions in the field of a simplified charge distribution representative of those thought to exist on exposed dielectrics. A 2-dimensional geometry with constant surface charge density is used. To simulate the laboratory work, low energy lithium ions are used. Subsequently, protons are substituted. It is shown, however, that the trajectories, and hence the focussing, of ions with equal initial energy are independent of the ion mass. Further, the paths are shown to be independent of ionic charge and average dielectric charge density, provided the initial energy of the ions is scaled in a prescribed manner.

The simple model used results in a profile of the ion density incident at the dielectric surface which displays the essential features of the laboratory observations. The ion spot with sharp edges is reproduced. The profile pattern is also found to be stable over a wide range of simulation parameters. The mechanism by which smoothly varying ion trajectories produce the discontinuously sharp ion spot is found and discussed. A model is proposed to describe the effect of the inclusion of ions on the external electric field. In this model, the main result is the production of a region where the negative charge due to the electrons is substantially or, for a large class of situations, exactly neutralized. The remaining dielectric surface is affected to a much lesser degree.

3.2 Results and Analysis

The charge distribution used to represent the surface charge on exposed dielectrics is a constant-width, infinitely long ribbon of surface charge of uniform density held in free space over a grounded plane. This is intended to model the charge distribution which exists on a long strip of dielectric lying on a grounded metal substrate after exposure to an electron beam. The steps used to arrive at this model are illustrated in Figure 1. Effects due to the finite length of the dielectric strip and extent of the metal substrate are ignored. The ground plane is replaced by the image charges, and

the charge on the dielectric is replaced by the equivalent free space distribution. The side edge faces of the dielectric would be in the shadow of the beam and the fields there would be predominantly perpendicular to the grounded plane. Therefore the free and bound charge on these side faces would be relatively small and is neglected. The resultant ribbon of surface charge in free space is taken as a first approximation to be of uniform density. The image force of the ion in the ground plane is also included. This force, however, can be shown to be insignificant. This model and some of the computer code used are extensions and modifications of work by R.D. Reeves [3]. The electric potential at the dielectric surface is the physical quantity monitored to establish the appropriate range of charge densities to be used.

A common dielectric sheet thickness of 50 μm is used. A low value of 10 eV was chosen for the initial ion beam energy. Scaling analysis, however, is used to show that results for energies ranging from .7 to 700 eV may be inferred. Free space charge densities ranging from -1 to 1000 nC/cm² are used resulting in surface potentials from -.06 to -56 kV respectively.

Results are presented mainly in two forms, the ion trajectories and the resultant focussing profile. The orientations of the y and z coordinate axes used are shown in Figure 1. Also included with the trajectory plots is a rough plot of the potential across the strip at its surface level. Figure 2 shows a wide view for a typical trajectory plot. For clarity of display only half of the trajectories, those originating to the left of centre, are shown. The remainder can be inferred by symmetry. The potential at surface level is shown by the lightly dotted line, with the scale to the right. The position of the dielectric strip is indicated on the horizontal base axis by two small dotted arrows.

The details of focussing are better seen with a narrower, judiciously chosen, scale, but the wide view of Figure 2 shows the outer trajectories. Notable is the region where the ions completely rebound. The dipole-like fields and the low ion energies produce this effect. The image forces of the ion in the ground plane are included but are insignificant and cannot overcome the repulsion.

The effect of varying the dielectric strip width is shown in Figures 3 to 12. Here the trajectories and the ion focussing at the dielectric surface are displayed for various strip widths. These plots are the results for lithium ions with an initial energy of 10 eV over 50 μm thick samples charged to the free space equivalent of -70 nC/cm² producing a surface potential of -4 kV. Five strip widths are included; 5, 15, 25, 50 and 100 millimeters. The ion spot becomes more sharply defined as the width increases. The central region of high ion focussing surrounded by lower ion density constitutes the ion spot. The spot boundary is seen to be very sharp.

Figure 13 shows, for a typical case, the relationship between the initial ion position in the direction parallel to the dielectric surface ("INITIAL Z") and the final position when the ion strikes the dielectric ("FINAL Z"). The figure also illustrates how this position curve compares with the location of the ion spot. The position curve is produced by cubic-spline interpolation of the values obtained from the individual trajectories. The plot of the ion

positions is continuous, as would be expected, and has no sudden jumps. However, due to the reversal points, as indicated on the figure, this smooth curve produces the concentrated ion spot with its discontinuously sharp edges. The local ion density at the surface of the dielectric is proportional to the absolute value of the slope of the position curve as drawn. For areas between the reversal points, ions are incident from three separate initial regions and the sum must be taken. In addition, the reversals necessitate steep slopes and hence high ion densities in the ion spot region. The slopes at the reversal points themselves are infinite! These factors result in the ion spot receiving a total ion density much greater than the surrounding dielectric. Furthermore, the reversal points provide the mechanism for absolutely sharp spot boundaries. Any "monotonic" position curve would result in gradual transitions, as in the 5 and 15 cm strip width cases of Figures 3 to 6. It can be said that, once the reversal is established, the smoother, more gradual the position curve, the sharper and the more intense the ion spot.

The ion spot formation is found to be stable over a wide range of surface charge densities and potentials. Results are presented in Figures 14 to 27 for lithium ions with initial energy of 10 eV over charge distributions of width 50 mm placed 50 μm above the ground plane. Free space charge densities of -1, -5, -10, -70, -200, -400, -1000 nC/cm^2 are used resulting in surface potentials of about -.06, -.3, -.6, -4, -11, -22, and -56 kV. Over this range of three orders of magnitude, only in the case of the least charge density does the ion spot begin to break down.

To simulate conditions encountered by spacecraft in orbit, studies were done with the lithium ions replaced by protons. Results for 10 eV protons over a few charge configurations are presented in Figures 28 to 33 . Comparison of these plots with the plots in Figures 14 to 27 for lithium ions over the same charge configurations shows that the results are identical. This is due to the general fact that the paths of charged particles of like sign in a static electric field are independent of the particle mass. To derive this and other conditions for path degeneracy, consider the equation and initial conditions below.

$$\ddot{\bar{x}}(t) = \bar{F}(\bar{x})$$

(1)

$$\dot{\bar{x}}(0) = \hat{V}_o v_o \quad , \quad \bar{x}(0) = \bar{X}_o$$

where $\dot{\bar{x}} = \dfrac{d}{dt} \bar{x}$ and $\hat{V}_o$ is a unit vector.

If $\bar{X}(t)$ is the solution to equation (1), what is the solution to the related problem below?

$$\ddot{\bar{x}}(t) = \alpha^2 \, \bar{F}(\bar{x})$$

(2)

$$\dot{\bar{x}}(0) = \alpha \hat{V} v_o \quad , \quad \bar{x}(0) = \bar{X}_o$$

The solution to equation (2) is

$$\bar{X}'(t) = \bar{X}(\alpha t) .$$

This can be easily verified by substitution. This result is now applied to ions falling over a charge distribution. Take $\bar{f}(\bar{x})$ to be the electric field due to some static charge distribution, $\rho(\bar{x})$, with unit average charge density. Consider two ions, charges q, q', and masses m, m', travelling over charge distributions $C\rho(\bar{x})$, $C'\rho(\bar{x})$, respectively, where C, C' are the average charge densities. The fields involved are, by super-position, $C\bar{f}(\bar{x})$, and $C'\bar{f}(\bar{x})$. The parameters are restricted so that (Cq) and (C'q') are non-zero and have the same sign. In this analysis, we neglect the ion images in the ground plane. This force for our case of interest is insignificant except when the total surface charge is comparable to the charge of the ion; a ridiculously tiny surface charge. The equations governing the motion are,

$$\ddot{\bar{X}}(t) = \frac{q}{m} C\bar{f}(\bar{X})$$

$$\dot{\bar{X}}(0) = \hat{V}_0 v_0 = \hat{V}_0 \sqrt{\frac{2E_0}{m}}$$

$$\bar{X}(0) = \bar{X}_0$$

and

$$\ddot{\bar{X}}'(t) = \frac{q'}{m'} C'\bar{f}(\bar{X}')$$

$$\dot{\bar{X}}'(0) = \hat{V}_0' v_0' = \hat{V}_0' \sqrt{\frac{2E_0'}{m'}}$$

$$\bar{X}(0) = \bar{X}_0'$$

The resultant paths will therefore be identical provided the initial conditions scale as required; namely,

$$\bar{X}_0' = \bar{X}_0$$

$$\hat{V}_0' v_0' = \hat{V}_0 v_0 \sqrt{\frac{q'C'}{qC} \frac{m}{m'}}$$

or, equivalently

$$\vec{X}' = \vec{X}_o$$

$$\hat{V}_o' = \hat{V}_o$$

$$E_o' = E_o \left(\frac{q'C'}{qC} \right) \tag{3}$$

It can be seen from equation (3) that the paths of ions of equal initial energy and charge will be independent of the ionic mass. In addition, variations in initial energy, ionic charge, and overall charge density (or, equivalently, electric field or potential) magnitude are shown, through equation (3), to be interchangeable, as far as resultant ion trajectories and focussing are concerned. A caution is expressed at this point. The paths taken by ions have been shown to be the same, but the speeds at which these paths are traversed, of course, vary. Furthermore, because the impact energies are different, the secondary emission and sputtering properties will also vary greatly, and the net charge deposition will vary. Nevertheless, the ion spot will cover the same region and retain its sharp edges. More is said about this in the concluding section.

A demonstration of the scaling equivalence of initial ion energy and overall surface charge density is included as Figures 34 and 35. For the -1 nC/cm² case, as in Figures 26 and 27, the initial energy was rescaled to produce the same trajectories as the -70 nC/cm² case, as in Figures 20 and 21. The initial energy was rescaled via equation (3) as below.

$$E_o' = E_o \left(\frac{C'}{C} \right)$$

$$= 10 \text{ eV} \left(\frac{-1 \text{ nC/cm}^2}{-70 \text{ nC/cm}^2} \right)$$

$$= .143 \text{ eV}$$

Comparison of Figures 34 and 35 with Figures 20 and 21 shows that the trajectories and focussing are identical.

Using the scaling law of equation (3), Figures 14 to 27 may be viewed, not as results for surface charge variation, but for variation of initial ion energy. Using the -70 nC/cm² case as standard and scaling the others to it, the results obtained using a 10 eV initial energy with charge densities of -1000, -400, -200, -70, -10, -5, and -1 nC/cm² are equivalent to results for a -70 nC/cm² charge density with initial energies of .7, 3.5, 10, 70, 140, 280, and 700 eV respectively. Thus the ion spot formation is shown to be stable over a wide range of initial ion energies for this charge configuration.

3.3 Conclusions

Using a simplified, two-dimensional model of the surface charge,

positively charged ions incident on an electron-beam-charged dielectric sheet are shown to focus to a central region of high concentration with the remaining dielectric surface receiving a much lower and uniform ion current. The boundaries of this spot of high concentration are extremely sharp. The mechanism for the creation of the ion spot with sharply defined edges is found in the dynamics of the ion trajectories in the electric field above the dielectric surface. This mechanism is sufficiently general that the existence and features of the ion spot are stable over a wide range of incident ion energies and dielectric surface charge densities and strip widths, as is demonstrated. Further, the ion trajectory dynamics are shown to scale with ion mass, leaving the ion spot unaffected. Additional scaling rules are also found.

The effect of the ion spot is to produce a region in which the charge due to the electron beam is substantially neutralized. The high focussing of ions at the ion spot and the additional reduction of negative charge, not considered here, due to impact emission of electrons will effectively eliminate much or all of the charge due to the electron beam. However, no positive charge will build up in the ion spot region due to the abundance of low energy secondary electrons present during dielectric exposure. These secondary electrons will migrate to any positive potential and pin it at a low value. Experimental verification of this prevention by secondary electrons of positive potentials has been reported in the literature [4].

For many situations, the incident ion density and the secondary electron emission rate is greater than the primary electron density. For such cases, exact charge neutralization will occur at the ion spot. That is, the surface potential will be held to nearly exactly zero volts. The exact profile and magnitude of the focussing at the ion spot is therefore of little importance for this class of situations. Further, the importance of the exact ion impact emission, dependent as it is on impact energy, mass, and angle, will be greatly reduced. The position and sharp boundaries of the ion spot define a region of complete neutralization, regardless. This increases the significance of the scaling properties of the ion spot, particularly the pattern independence with the ion mass. Equivalence of ion trajectory solutions is reflected as an equivalence in the neutralization region.

For the purpose of external field modelling, the ion effect on the net surface charge distribution on dielectrics exposed to an electron beam is thus expected to have two general features. Primarily, a region with sharply defined boundaries is produced where in the electron charge is substantially reduced or, for a class of situations, exactly neutralized. Secondly, a low, even density of ions is deposited over the remainder of the dielectric surface. A more complete model, including particularly the effect of the ion neutralization on the trajectories of subsequently incident ions, will certainly show variation in the exact ion spot size and shape. However, the spot pattern has been shown to be robust, surviving wide variation of the simulation parameters. Scaling laws exist to confirm this stable behaviour. The mechanism responsible for the sharp edges is simple and basic. Further, as discussed in this section, for many cases the results are independent of the exact ion density and secondary emission parameters. For these reasons, the general features of the ion spot are expected to be present in more complicated charging situations.

3.5 <u>References</u>

[1] M. Gossland, K.G. Balmain, "Incident ion effects on polymer surface discharges," IEEE Trans. Nucl. Sci., Vol. NS-30, no.6, pp. 4302-4306, Dec., 1983.

[2] K.G. Balmain, A. Battagin, G.R. Dubois, "Thickness scaling for arc discharges on electron-beam-charged dielectrics," (attached).

[3] R.D. Reeves, Two-dimensional electron beam charging model for polymer films, M.A.Sc. Thesis, Department of Electrical Engineering, University of Toronto, 1981.

[4] M.S. Leung, M.B. Tueling, E.R. Schnauss, "Effects of Secondary Emission on Charging," NASA Conf. Proc. 2182, Spacecraft Charging Technology, 1980.

4. EXPERIMENTAL EVALUATION OF THE ELECTROSTATIC PROBE
G.R. Dubois

The electrostatic probe (Trek Model 340 HV) has been modified to mount inside the chamber as shown in Figures 36 and 37. The probe itself has been placed inside a grounded aluminum case to protect it from the e-beam. The cable leading to the probe connects to an electrical feedthrough and runs inside a grounded aluminum tube to the probe head. The probe head is mounted on an arm which is connected through a transmission assembly and rotational feedthrough and allows the probe to be swung across the sample surface in an arc by manually adjusting the rotational feedthrough from outside the chamber.

In experiments to evaluate the probe performance, the probe height was adjusted to produce a gap of 6-8 mm from the sample surface. A circular sample defined by a 100 mm diameter aluminum aperture was used as a test specimen. A 75 µm thick piece of Mylar was used as the first test specimen. The accelerating voltage was set at 20 kV and the filament current at approximately 2.2 A. The actual e-beam current density at the sample was not measured for these tests but previous results indicated that for this filament current the current density would be about 15-30 nA/cm^2.

The probe head was moved out of the way of the e-beam and the sample was irradiated for approximately 15 seconds. The accelerating voltage was then shut off and the probe was swung across the sample and voltage readings were taken every one-eighth turn of the rotational feedthrough. This corresponds to a movement of approximately 2.3 mm on the sample surface. Figure 38 shows the voltage profile obtained after the 15 second exposure to the 20 kilovolt e-beam.

The sample was then exposed to the same beam until a discharge occurred. The discharge under visual observation appeared to cover approximately one-third of the area of the sample and the arc direction was normal to the direction of the path of probe head. The voltage profile obtained is shown in Figure 39. It can be seen that the area which discharged corresponds to the visual observation and has a considerably lower charge. The area of lower voltage covers about one-half of the sample which is larger than the discharge area observed, also, the area of the sample which had a higher accumulation of charge in Fig.38, was the area that discharged.

The sample was again exposed to the same e-beam in an attempt to determine a maximum or near-maximum voltage accumulation. The luminescence of the sample was observed and when it dimmed to a point where a discharge was anticipated the beam was shut off. One discharge which visually appeared to cover the complete sample area occurred, after which the sample was continually exposed while observing the luminescence. When the beam was shut down the sample was scanned by the probe and the resulting voltages were plotted in Figure 40. The maximum voltages obtained were over -13 kilovolts but the half of the sample which had previously discharged remained approximately 20 % lower.

The same experiment was completed on a 50 µm thick sample of FEP Teflon. In Figure 41 which is the voltage profile measured after 45 seconds of beam exposure, the maximum voltage obtained is over -13.5 kilovolts and is

relatively uniform (within 10%) across the sample surface.

Figure 42 shows the voltage profile of the FEP Teflon sample immediately after a discharge which, under visual observation, appeared to cover the complete sample area. The voltage profile shows that almost all of the voltage build-up shown in Figure 41, has been eliminated after the discharge.

Figure 43 shows the profile obtained after the complete discharge and an additional 1 minute of exposure to the e-beam. The voltage build-up does not reach the same level as before the discharge and is not as uniform.

The electrostatic probe with some minor modifications should be a useful tool in measuring the voltage profiles of a sample exposed to an electron beam. The sample mounting mechanism is built to rotate the sample so the voltage at any point on the surface of the sample can be measured.
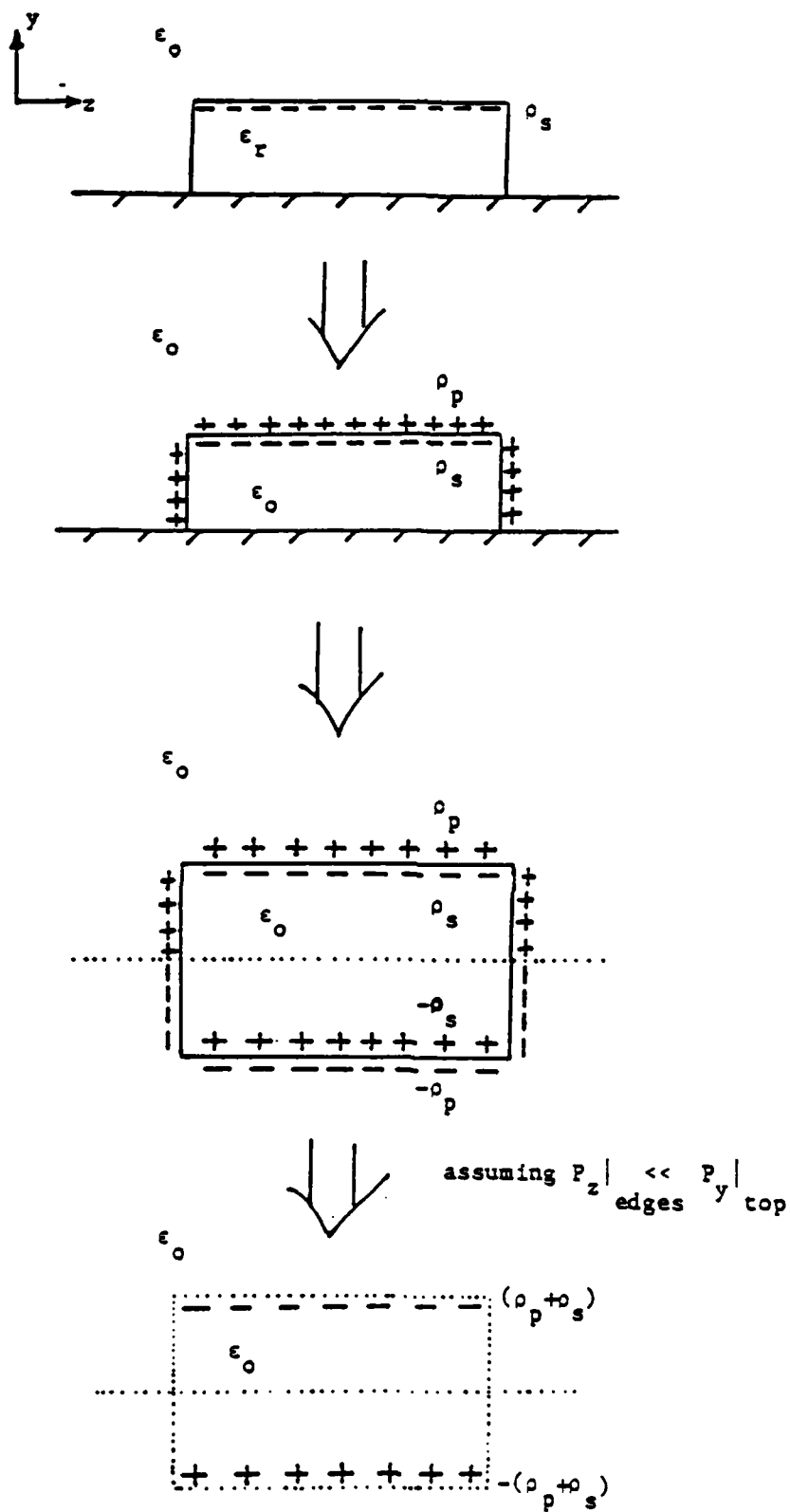
Fig.1 Development of Surface Charge Model

FREE SPACE CHG CONF USED:

-70.00 NC/CM**2

25.00 MM

50.00 MICRONS
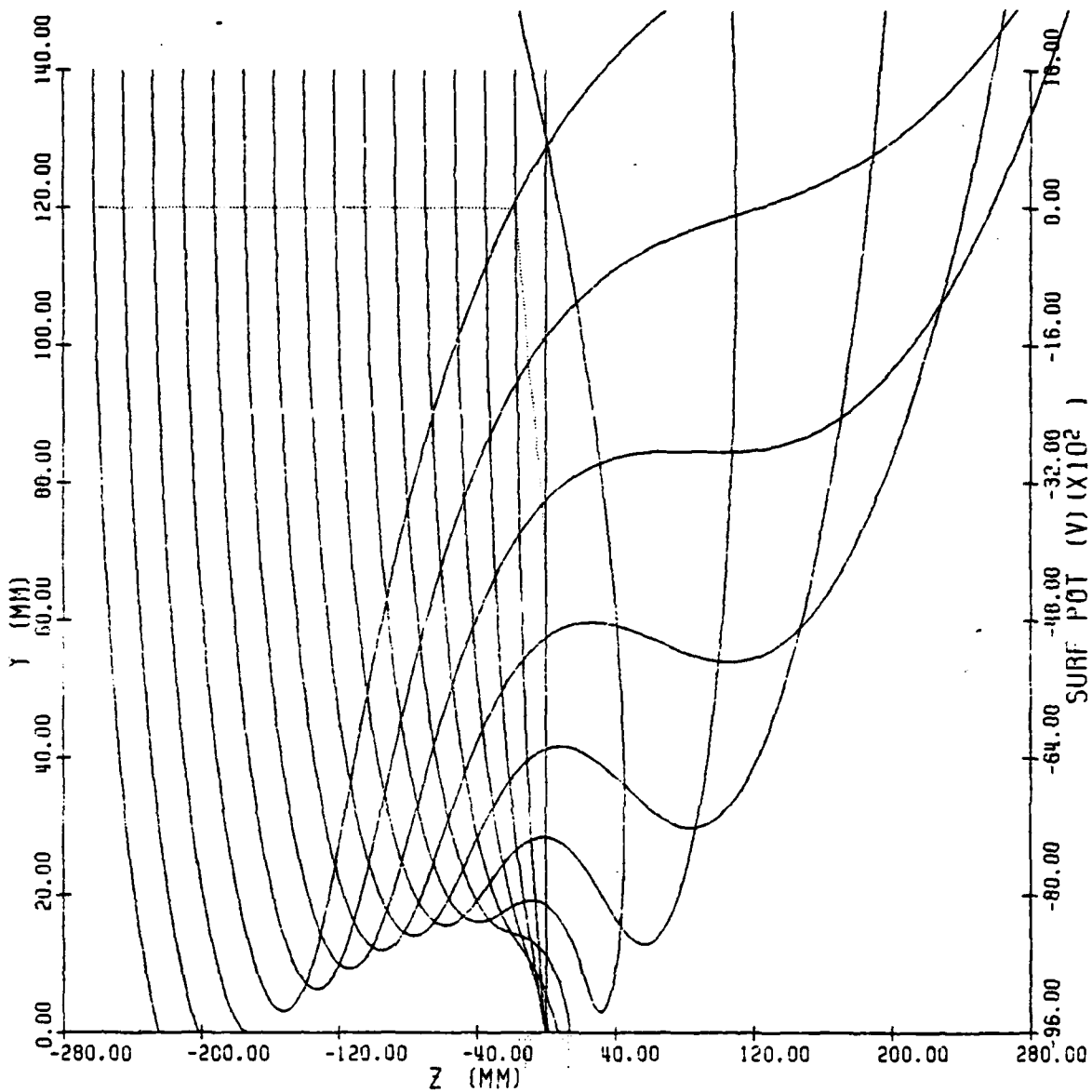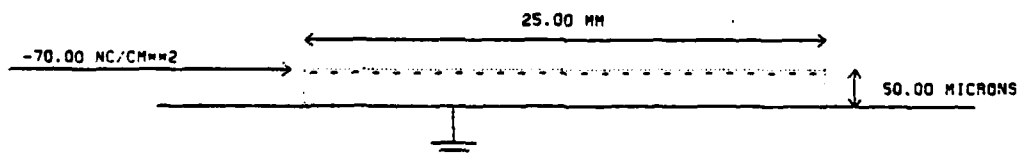
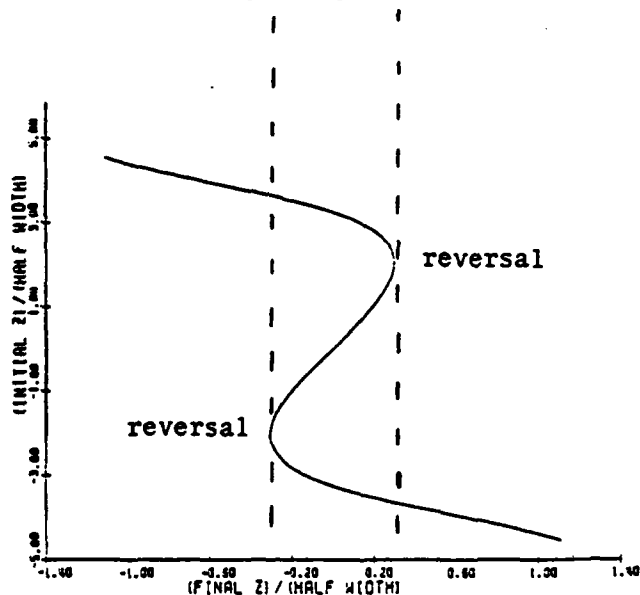IØN TRACKS: M=6.9 AMU, Q=1 E, E0=10.0 EV

Fig.2
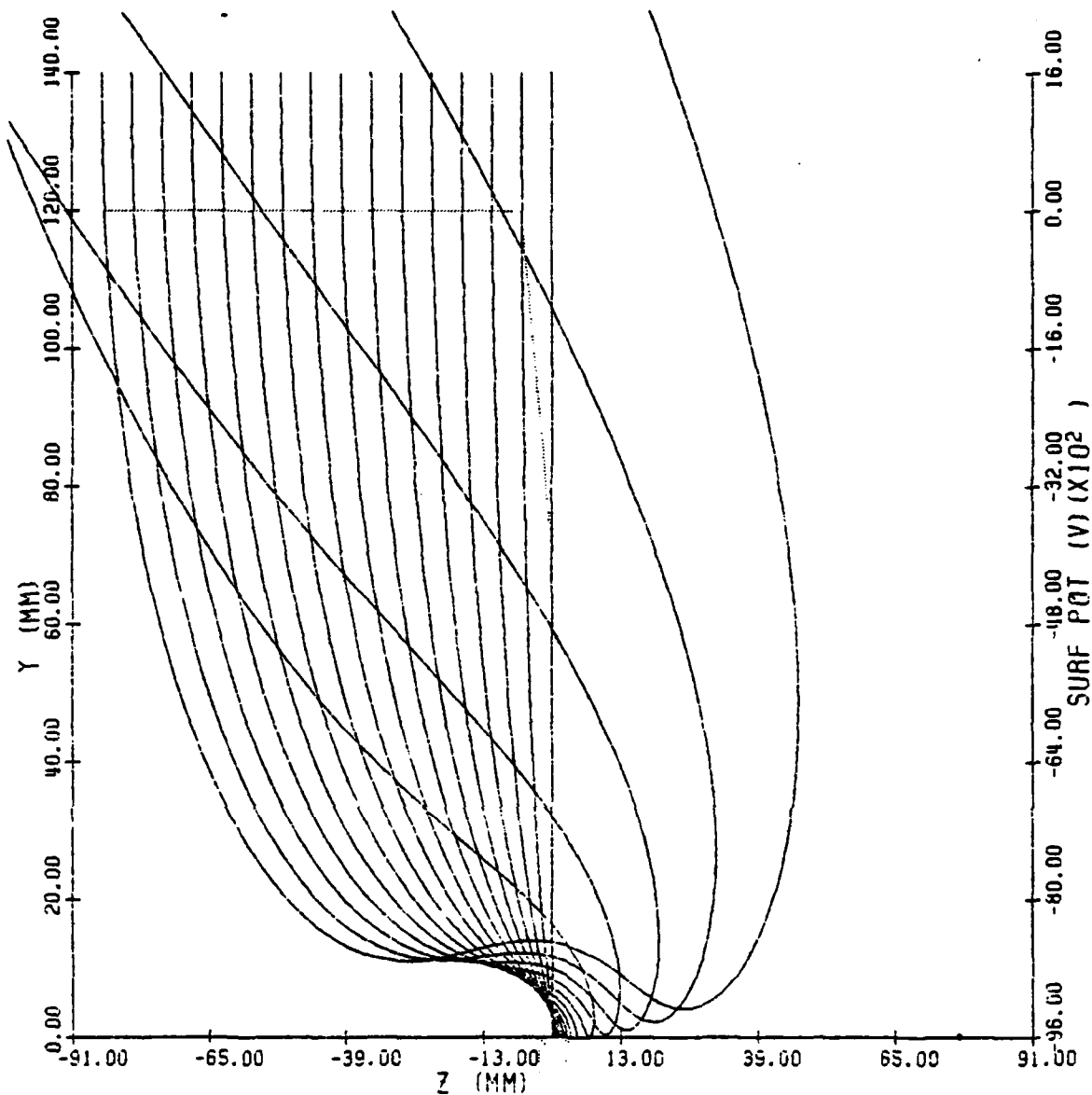
FREE SPACE CHG CONF USED:
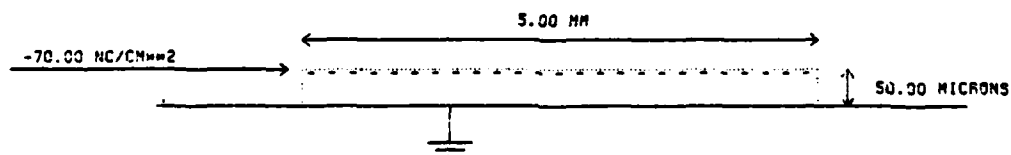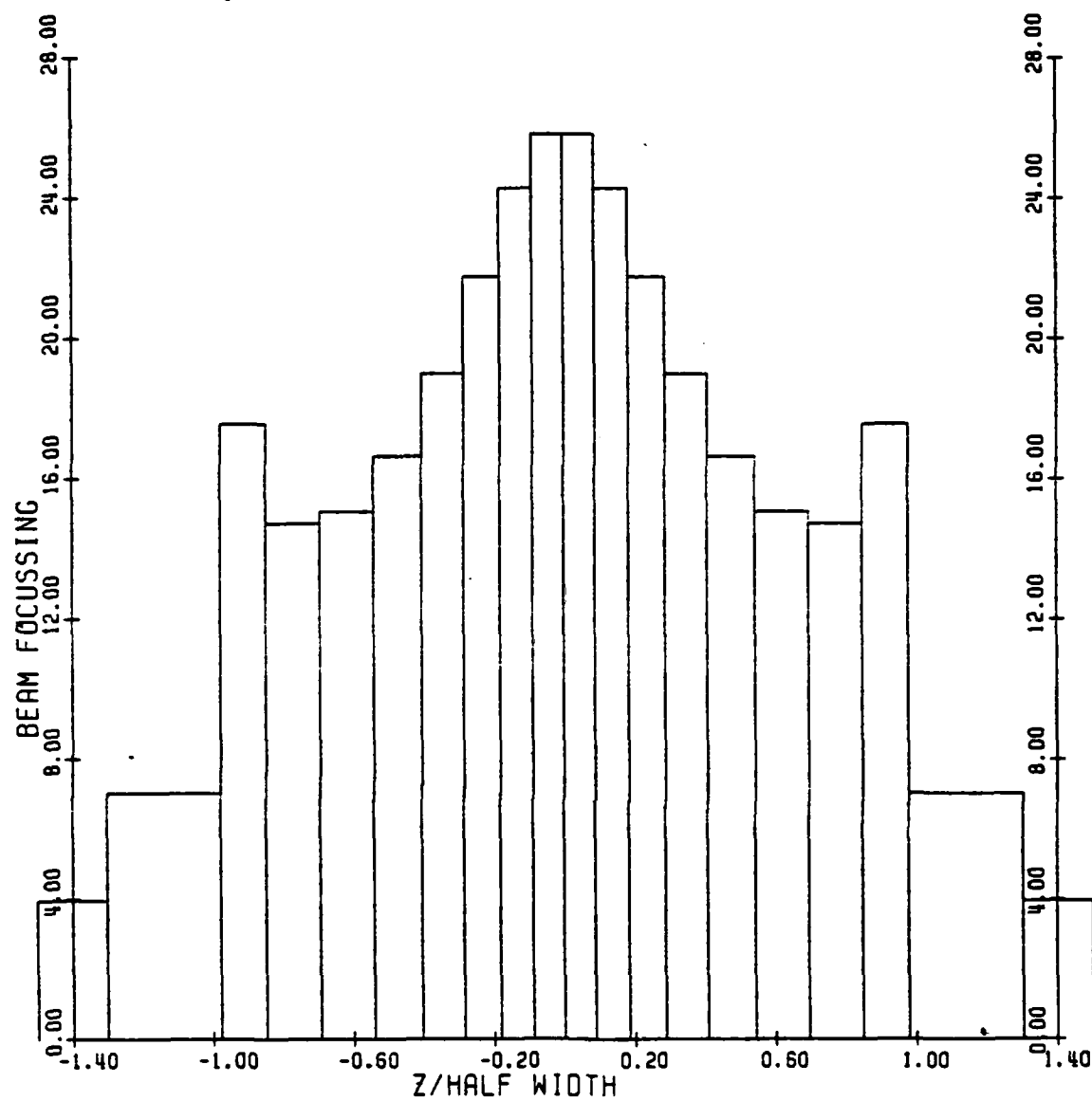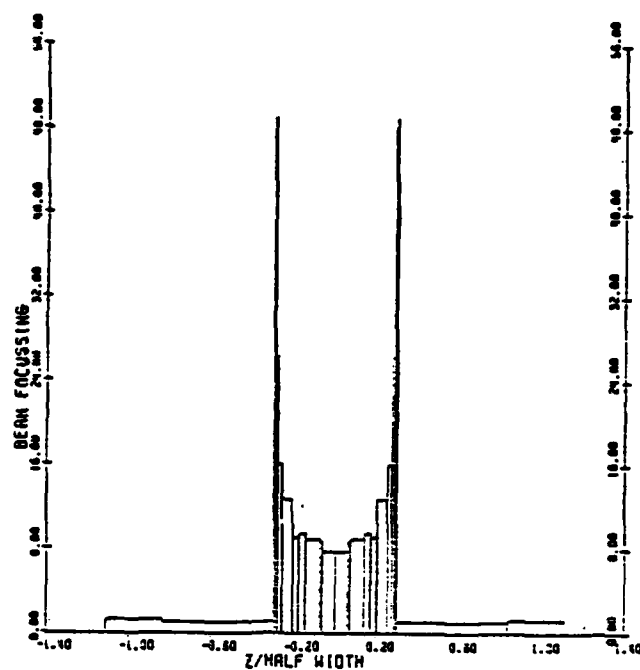
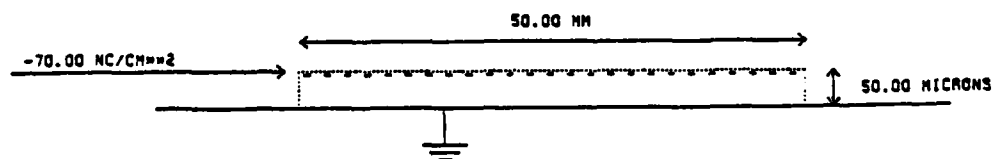IØN TRACKS: M=6.9 AMU,   Q=1 E,   E0=10.0 EV

Fig.3

FREE SPACE CHG CONF USED:
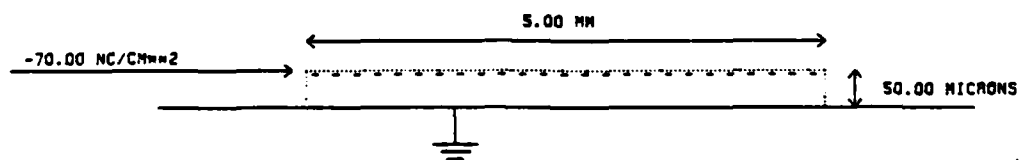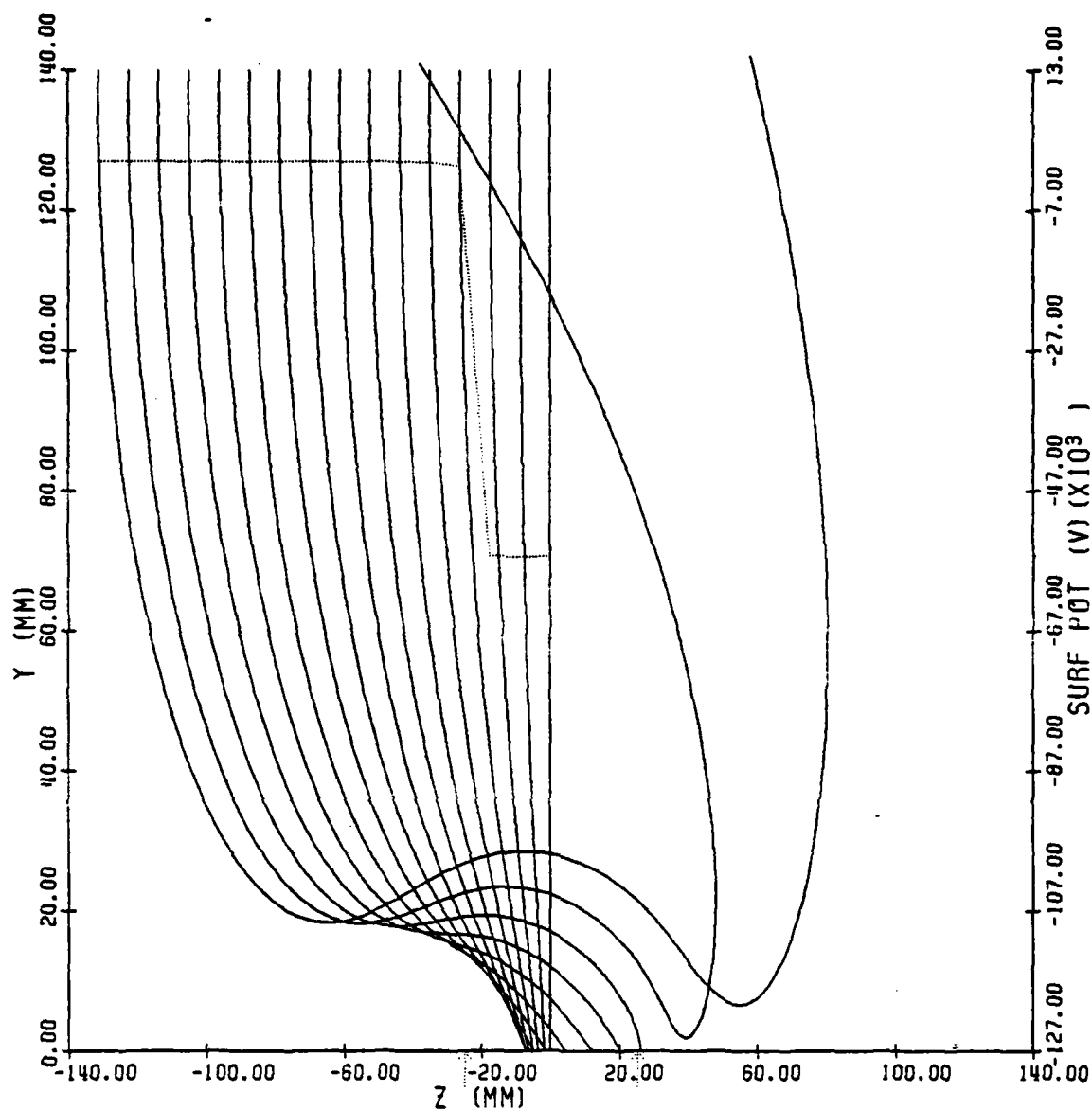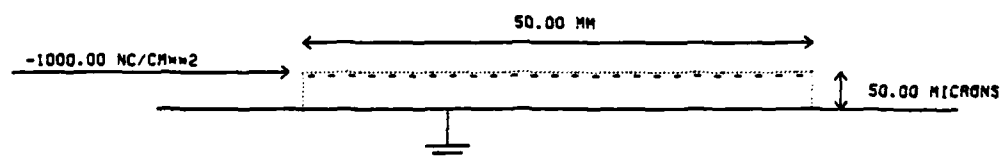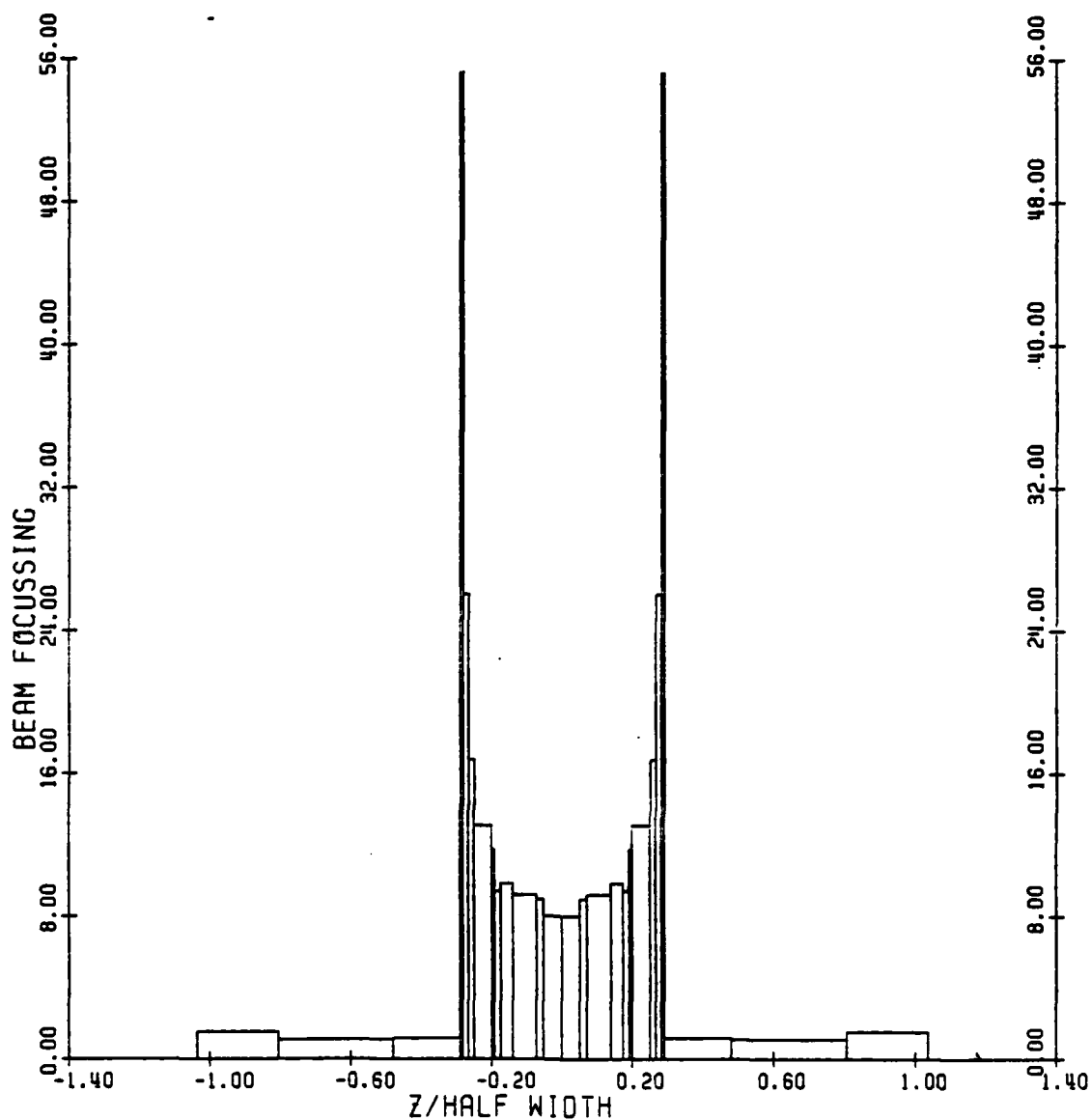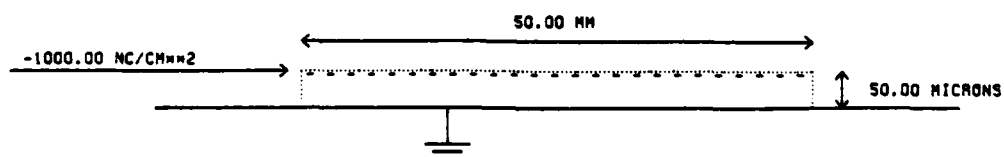
ION SPOT: M=6.9 AMU, Q=1 E, EO=10.0 EV

Fig.4

Y (MM)

140.00

120.00

100.00

80.00

60.00

40.00

20.00

0.00

-91.00   -65.00   -39.00   -13.00   13.00   39.00   65.00   91.00

Z (MM)

SURF POT (V) (X10²)

16.00
0.00
-16.00
-32.00
-48.00
-64.00
-80.00
-96.00

FREE SPACE CHG CONF USED:

15.00 MM

-70.00 NC/CM**2

50.00 MICRONS
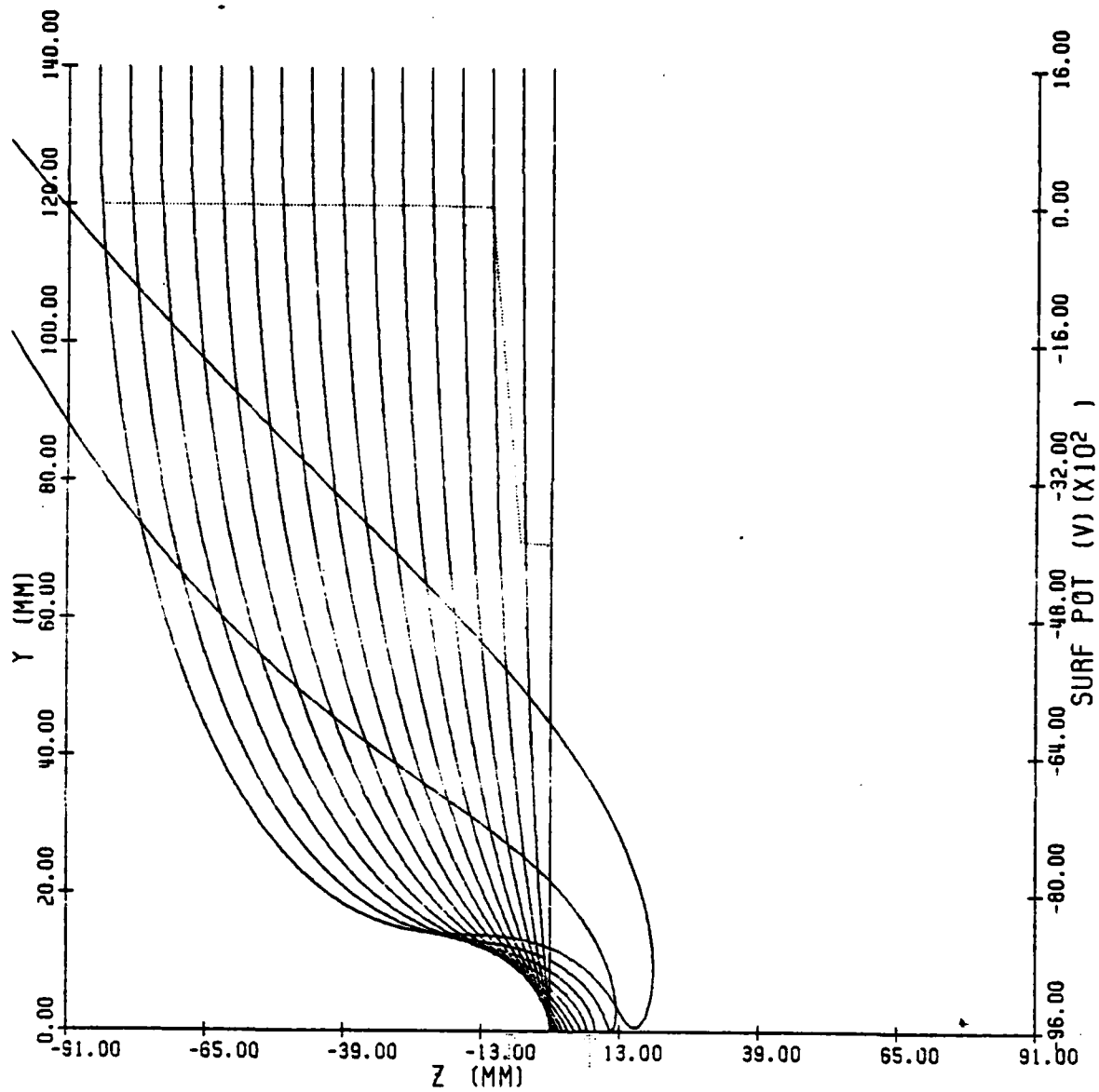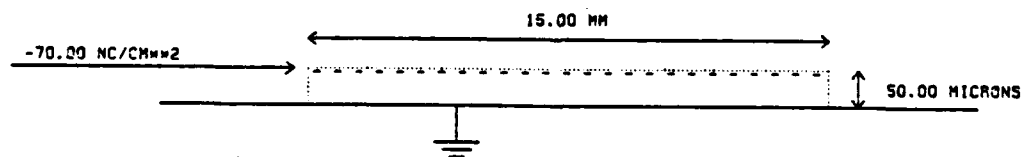
IØN TRACKS: M=6.9 AMU,   Q=1 E,   EO=10.0 EV

Fig.5
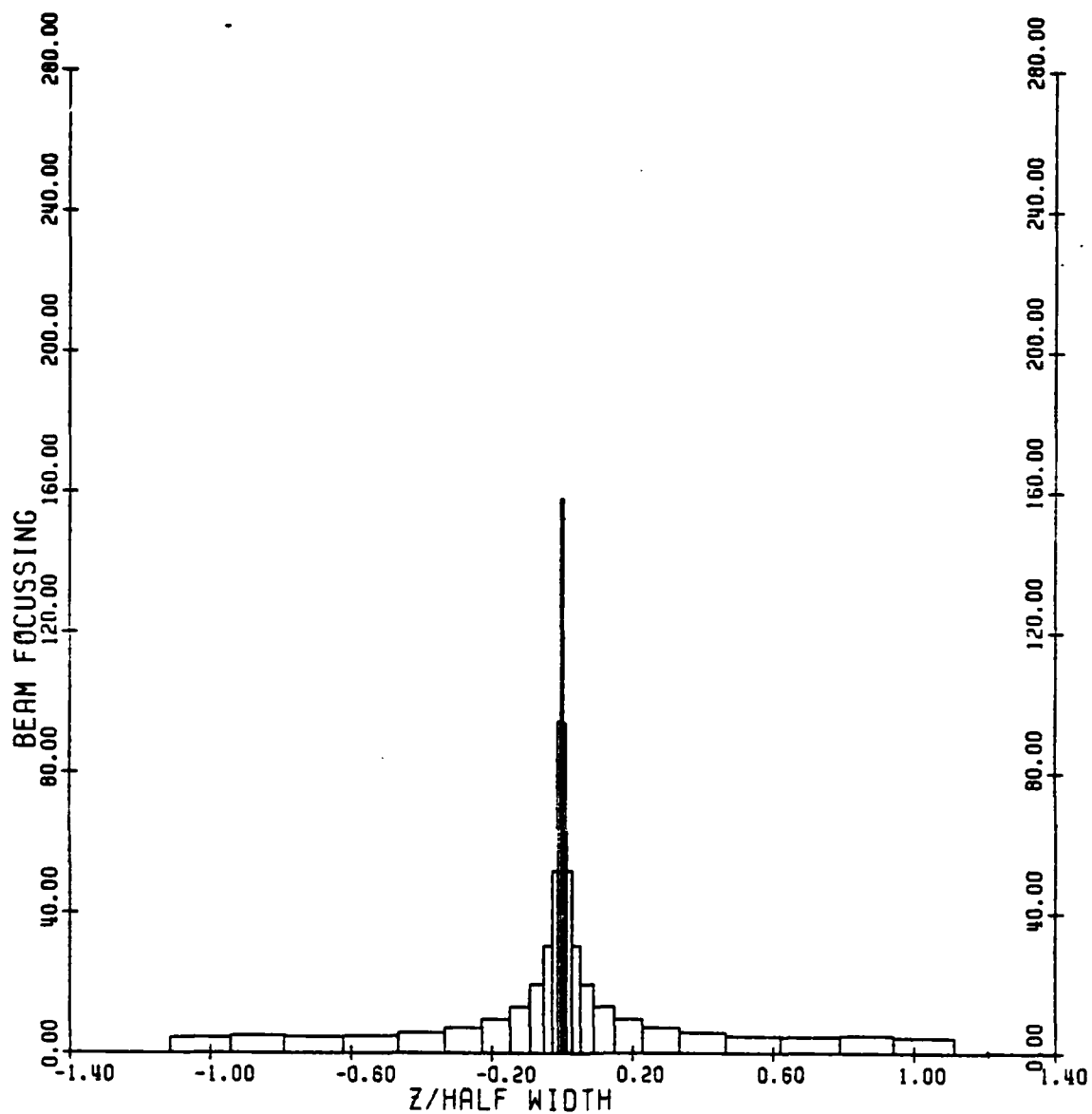
FREE SPACE CHG CONF USED:
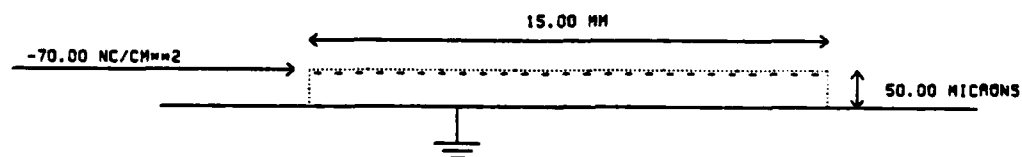
ION SPOT: M=6.9 AMU, Q=1 E. EO=10.0 EV

Fig.6
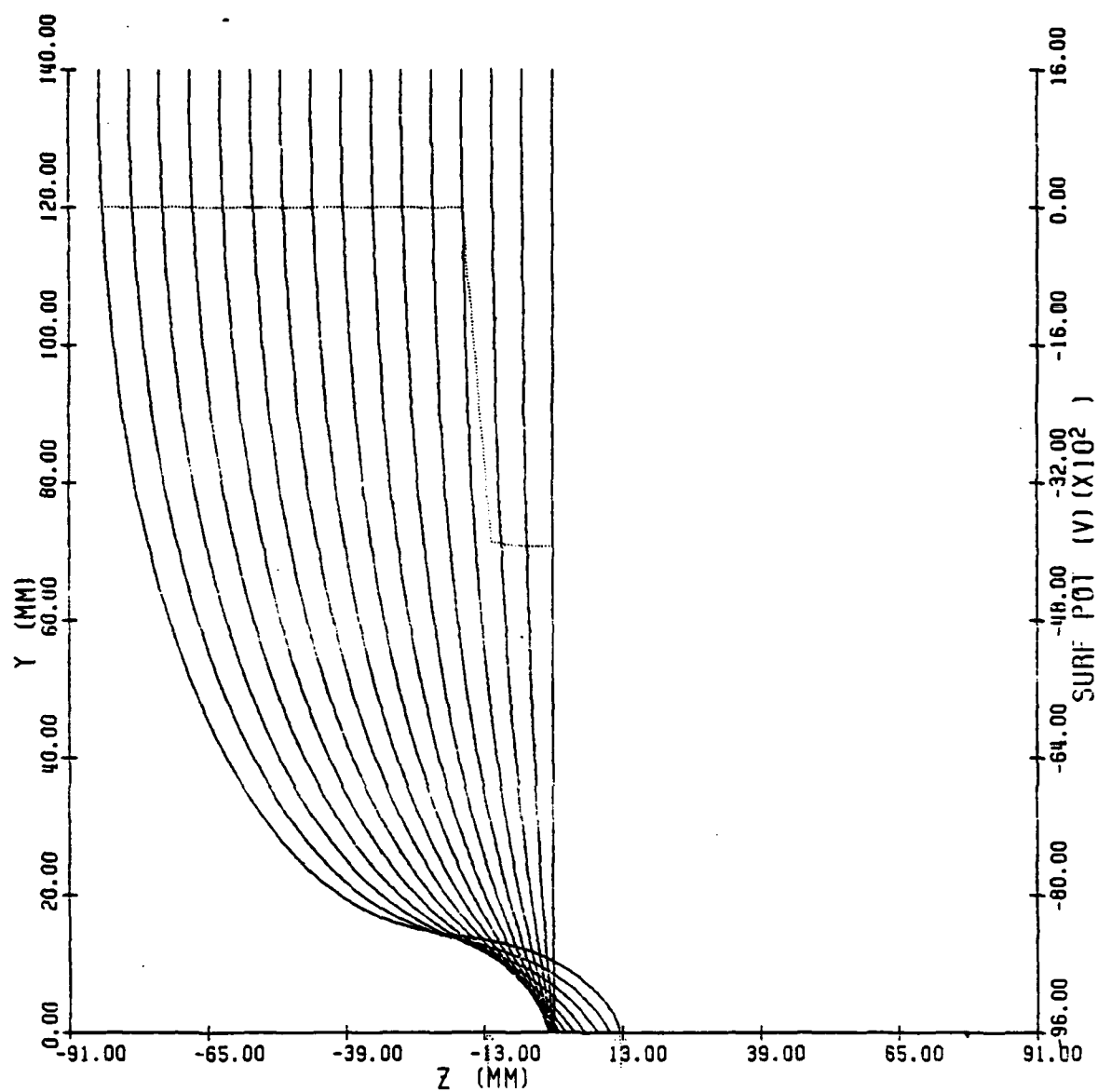
FREE SPACE CHG CONF USED:
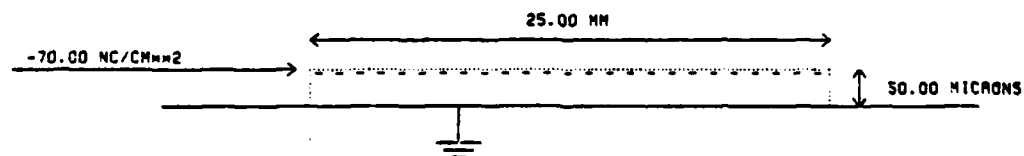
ION TRACKS: M=6.9 AMU,   Q=1 E,   EO=10.0 EV

Fig.7
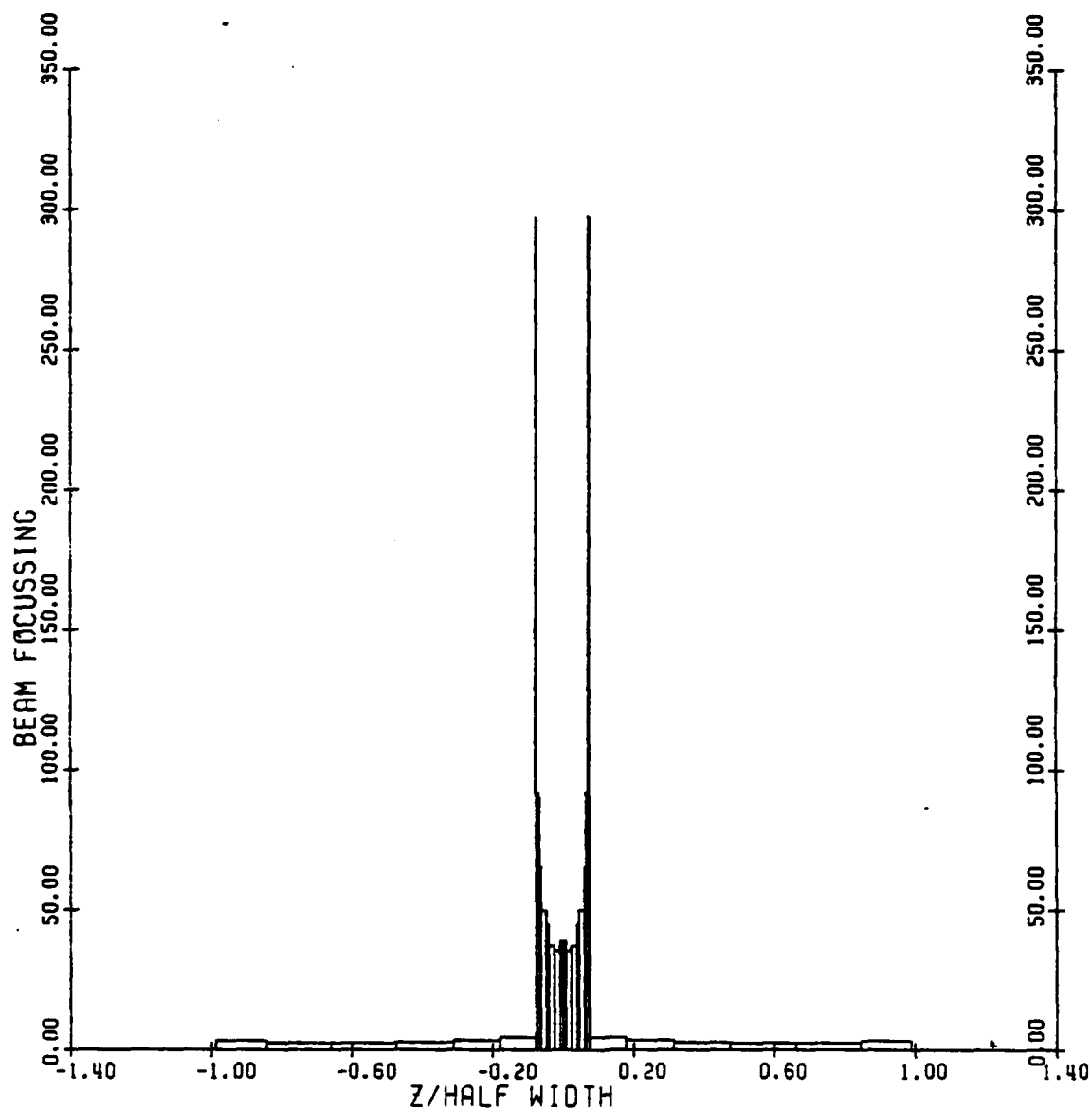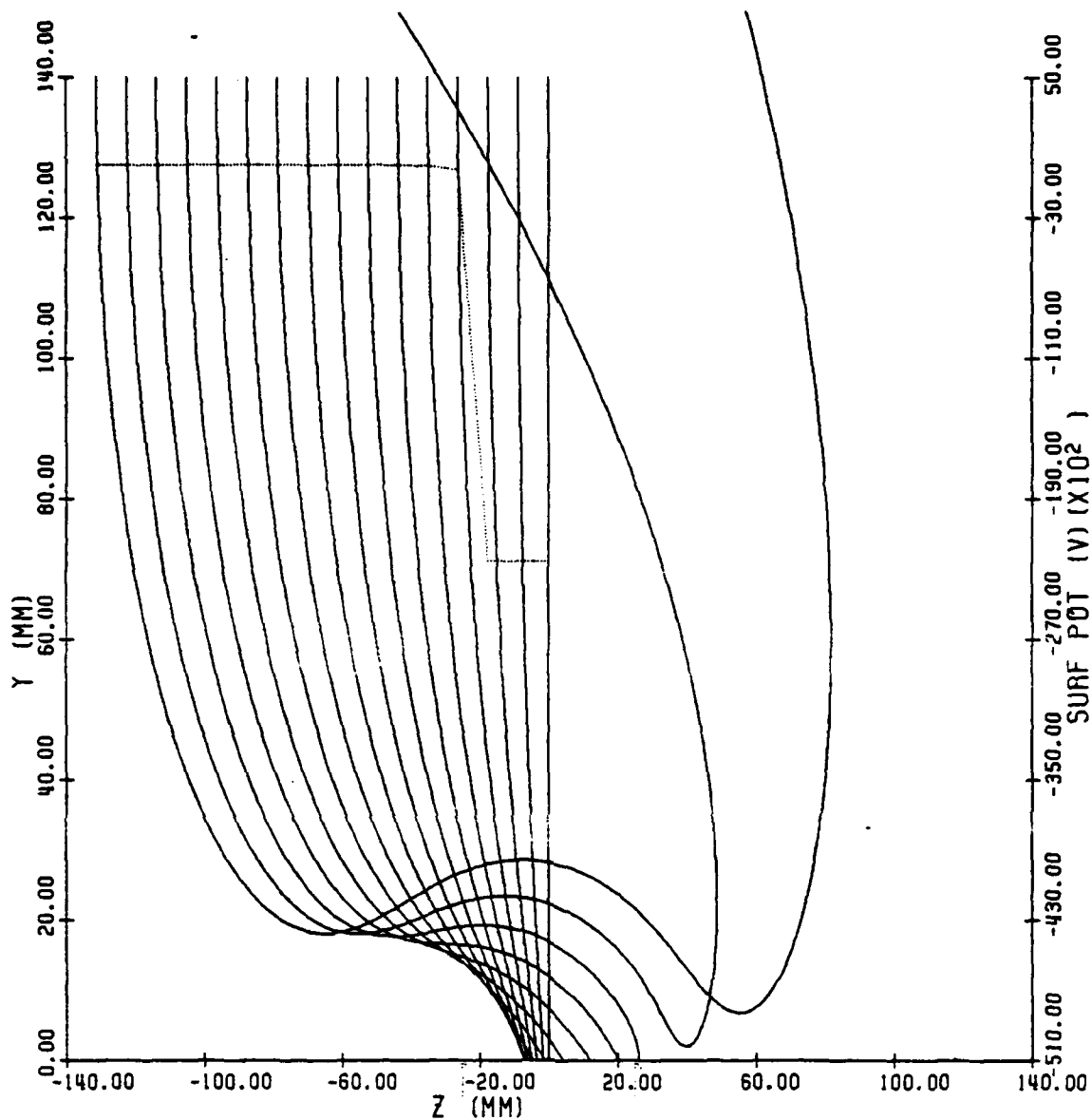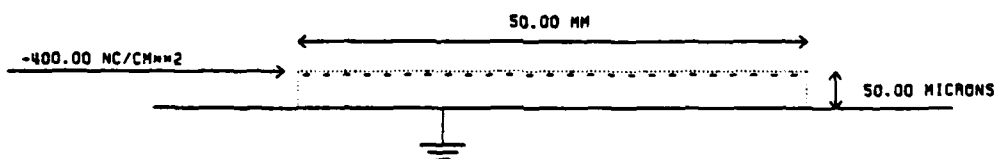
FREE SPACE CHG CONF USED:
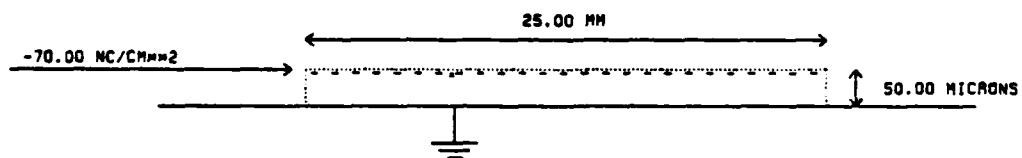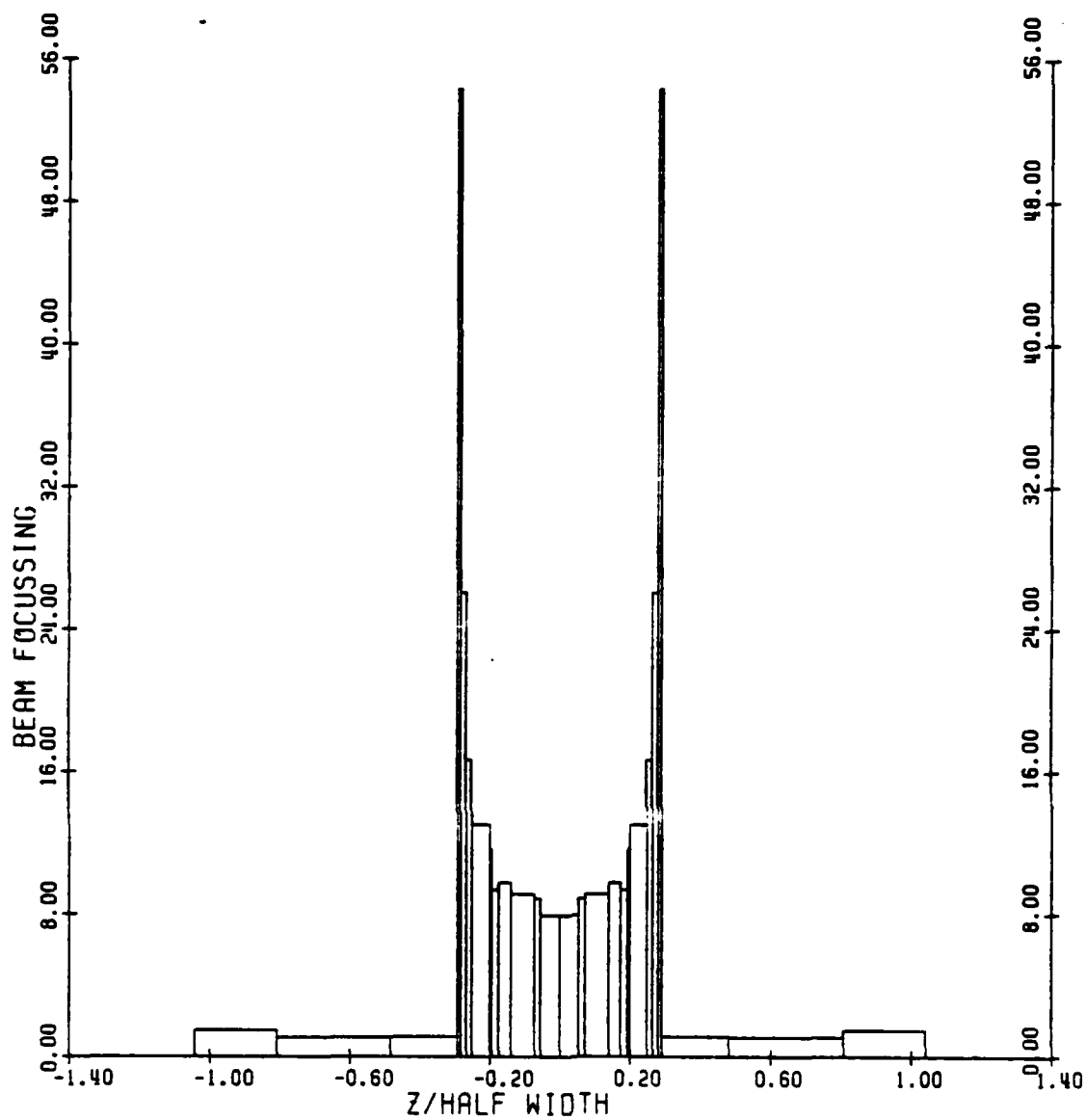
ION SPOT: M=6.9 AMU, Q=1 E, EO=10.0 EV

Fig.8
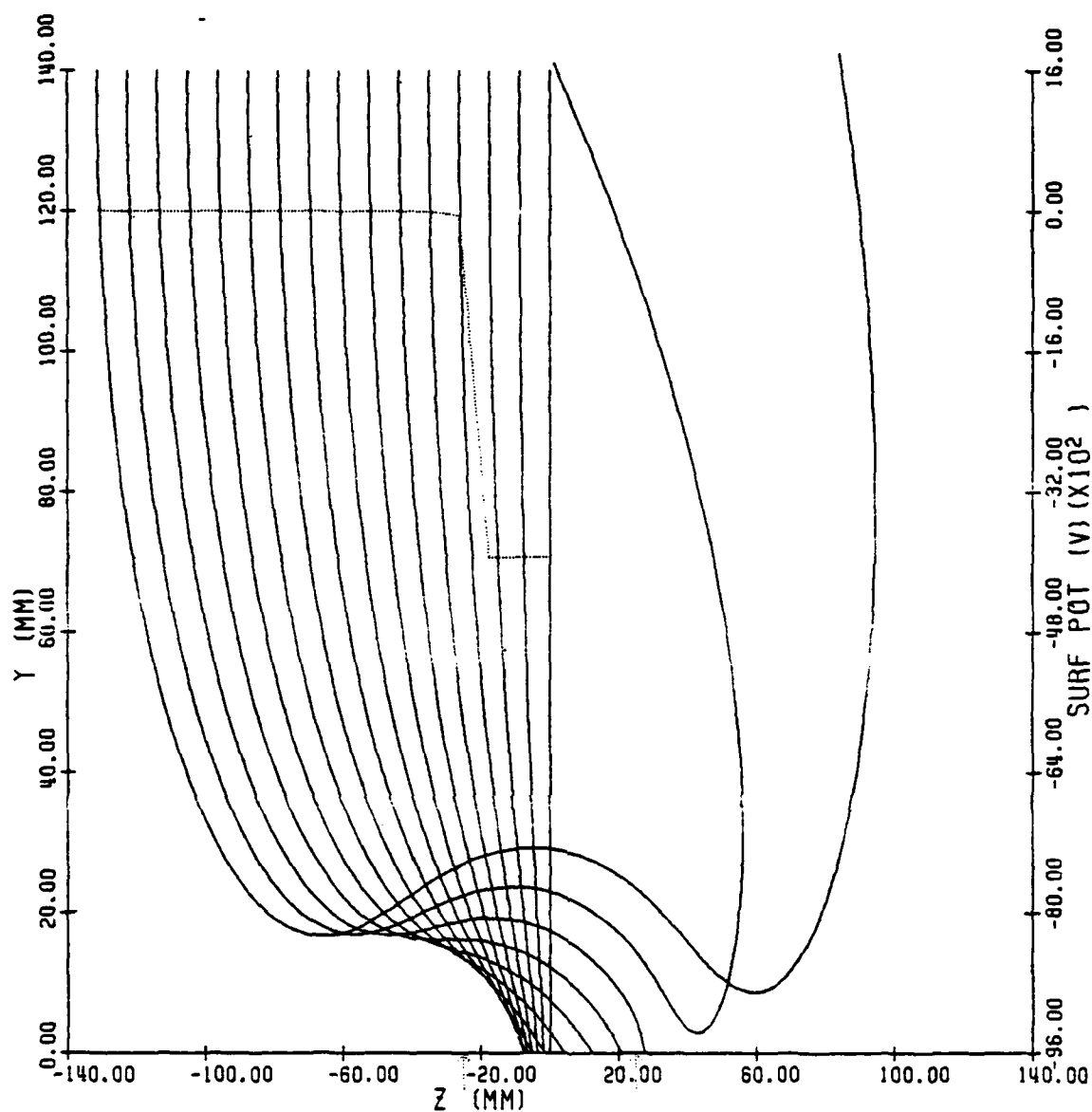
FREE SPACE CHG CONF USED:
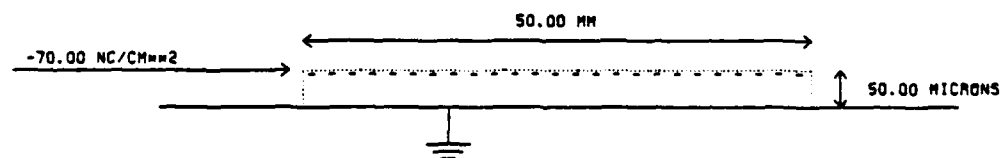
ION TRACKS: M=6.9 AMU,   Q=1 E,   EO=10.0 EV

Fig.9
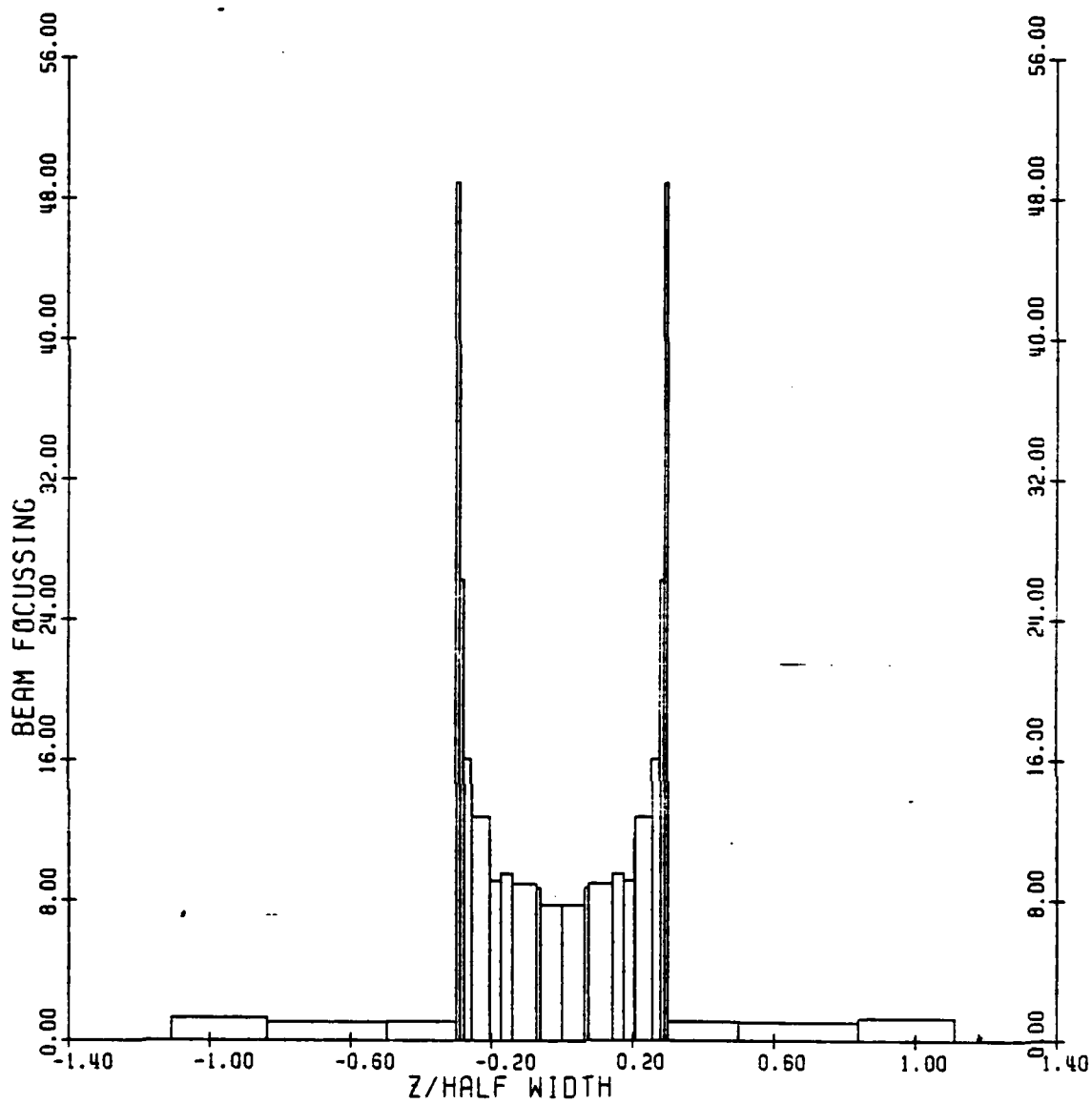
FREE SPACE CHG CONF USED:
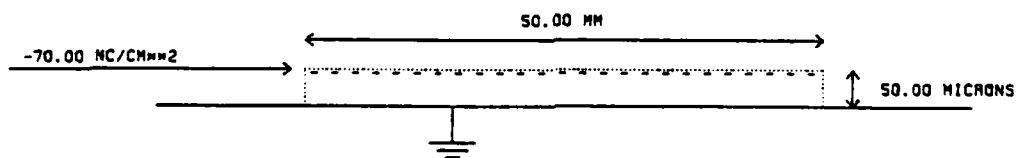
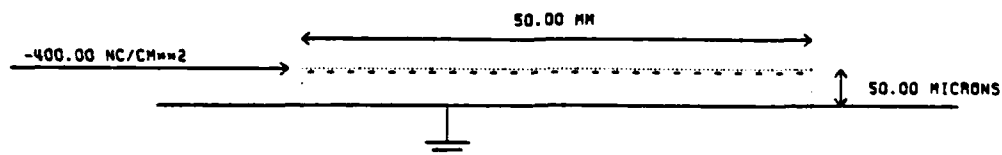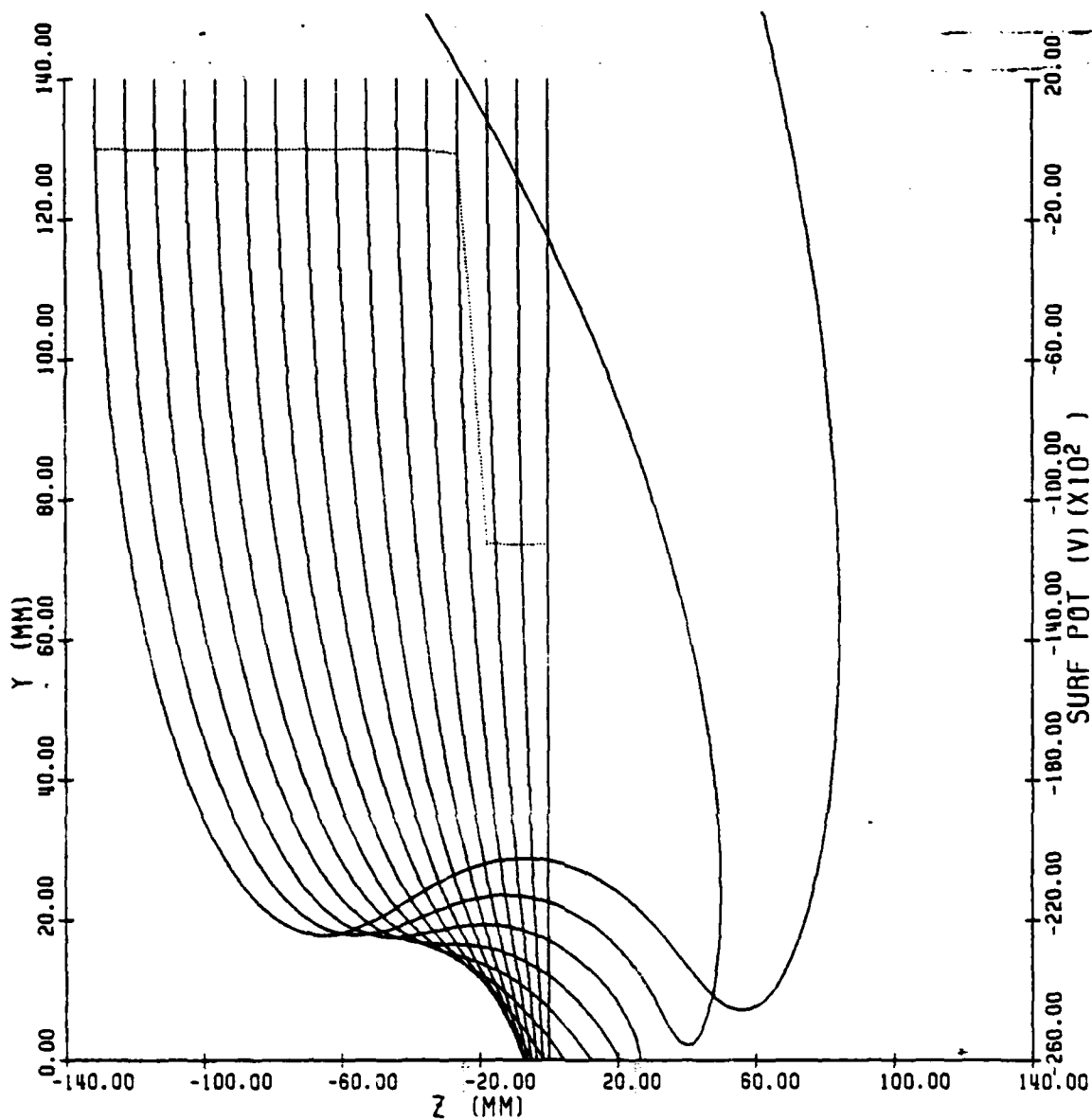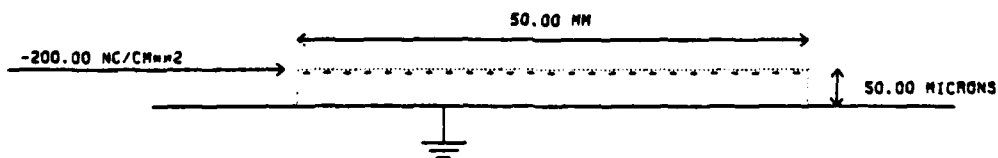ION SPOT: M=6.9 AMU, Q=1 E, EO=10.0 EV

Fig.10
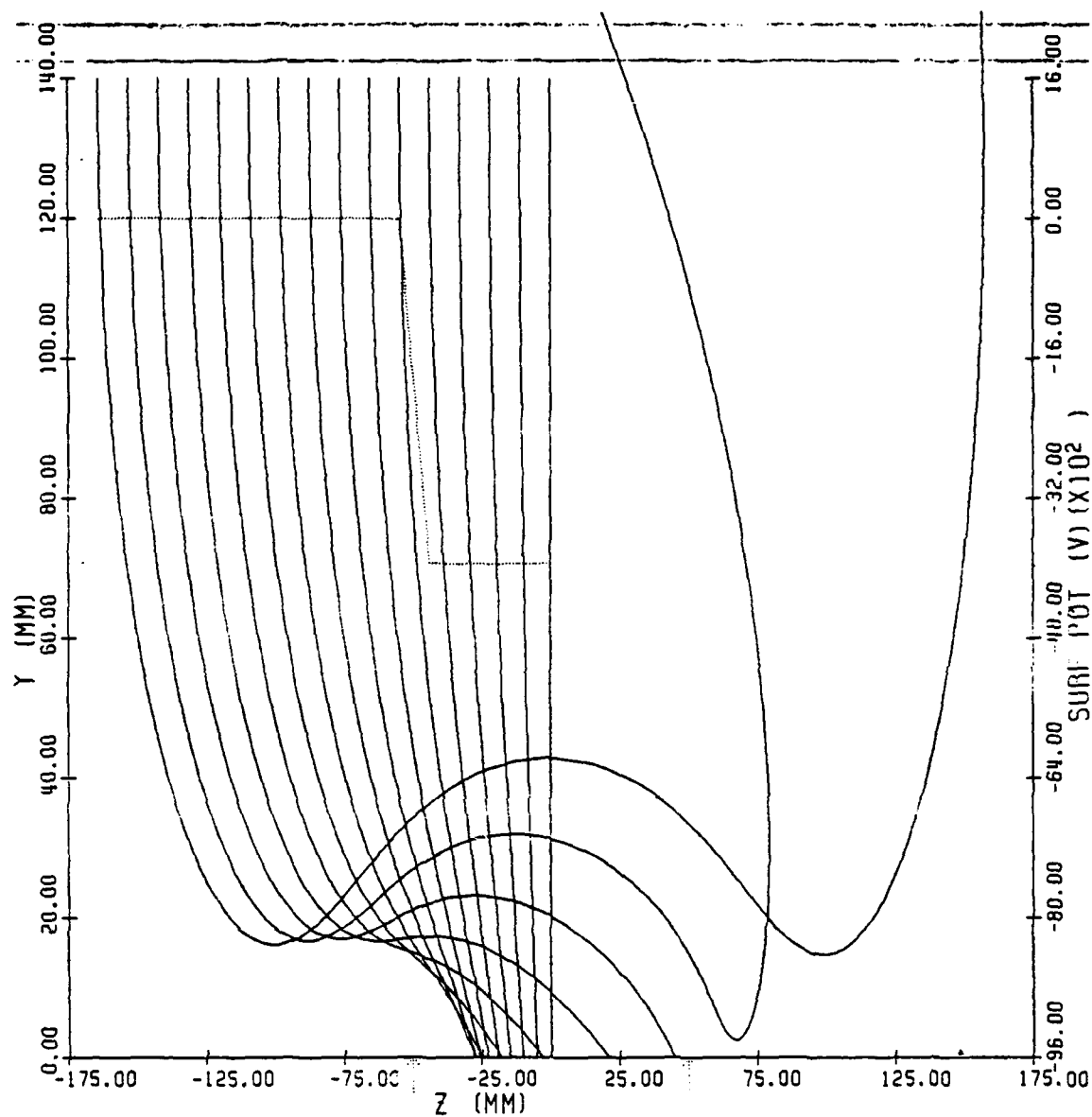
FREE SPACE CHG CONF USED:
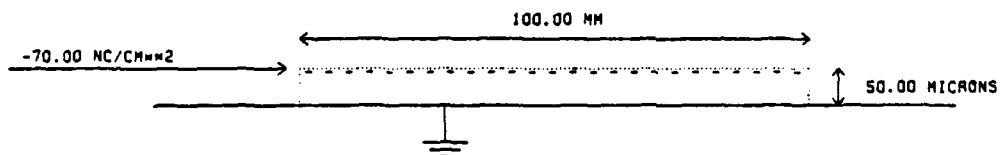
ION TRACKS: M=6.9 AMU, Q=1 E, E0=10.0 EV

Fig.11
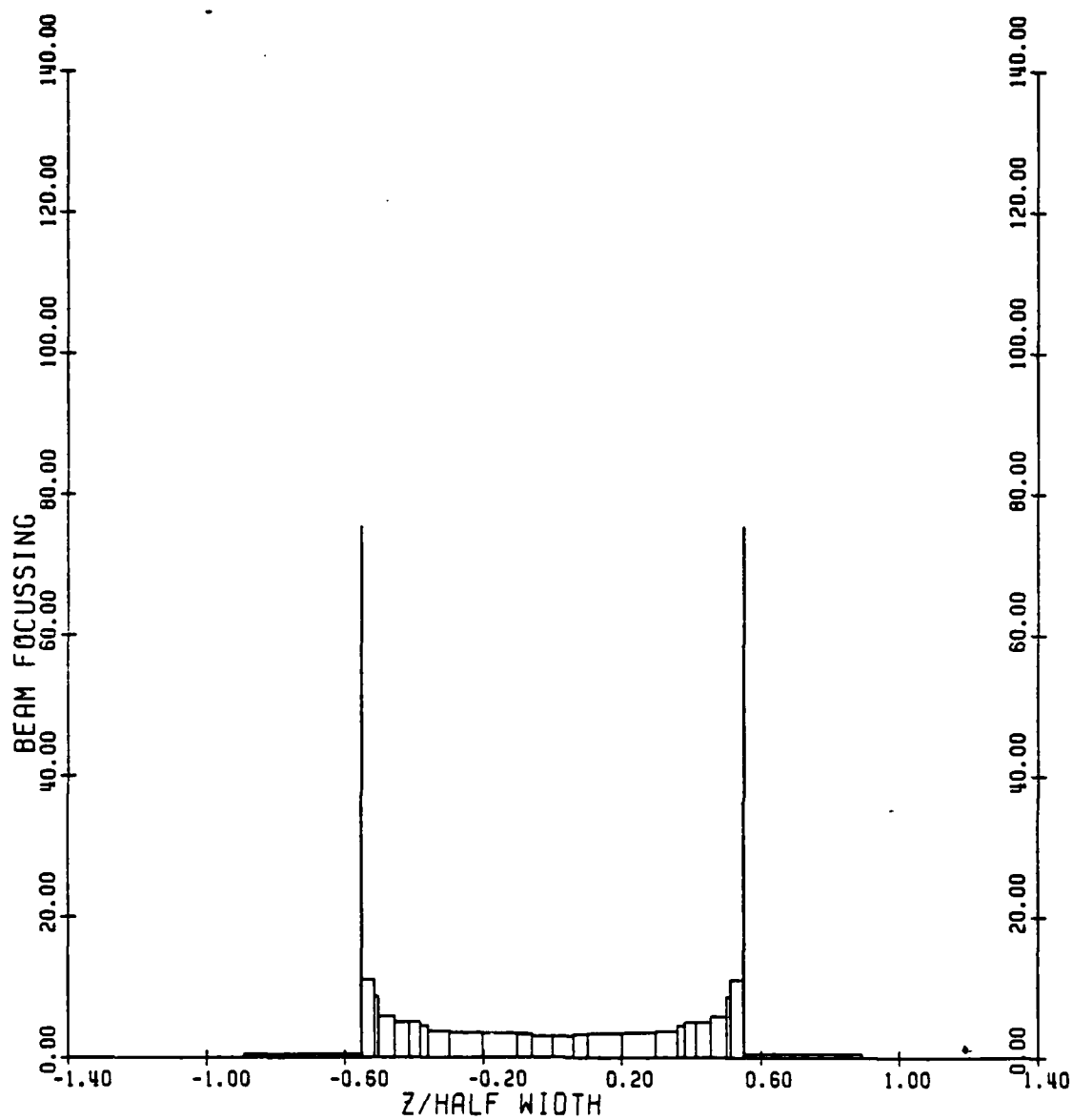
FREE SPACE CHG CONF USED:
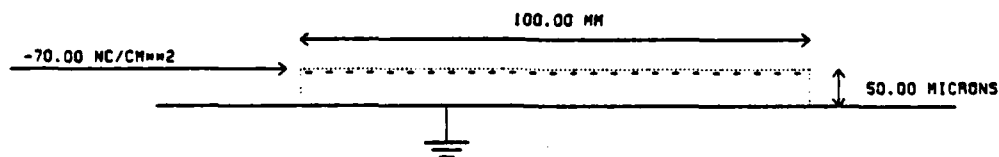
ION SPOT: M=6.9 AMU,   Q=1 E,   E0=10.0 EV

Fig.12

FREE SPACE CHG CONF USED:

ION SPOT: M=6.9 AMU, Q=1 E, E0=10.0 EV

Fig.13 Comparison of initial v.s. final ion
        position curve with resulting ion
        focussing pattern

FREE SPACE CHG CONF USED:

ION TRACKS: M=6.9 AMU, Q=1 E, EO=10.0 EV

Fig.14

FREE SPACE CHG CONF USED:

ION SPOT: M=6.9 AMU,   Q=1 E,   EO=10.0 EV

Fig.15

FREE SPACE CHG CONF USED:

ION TRACKS: M=6.9 AMU, Q=1 E, EO=10.0 EV

Fig.16

FREE SPACE CHG CONF USED:
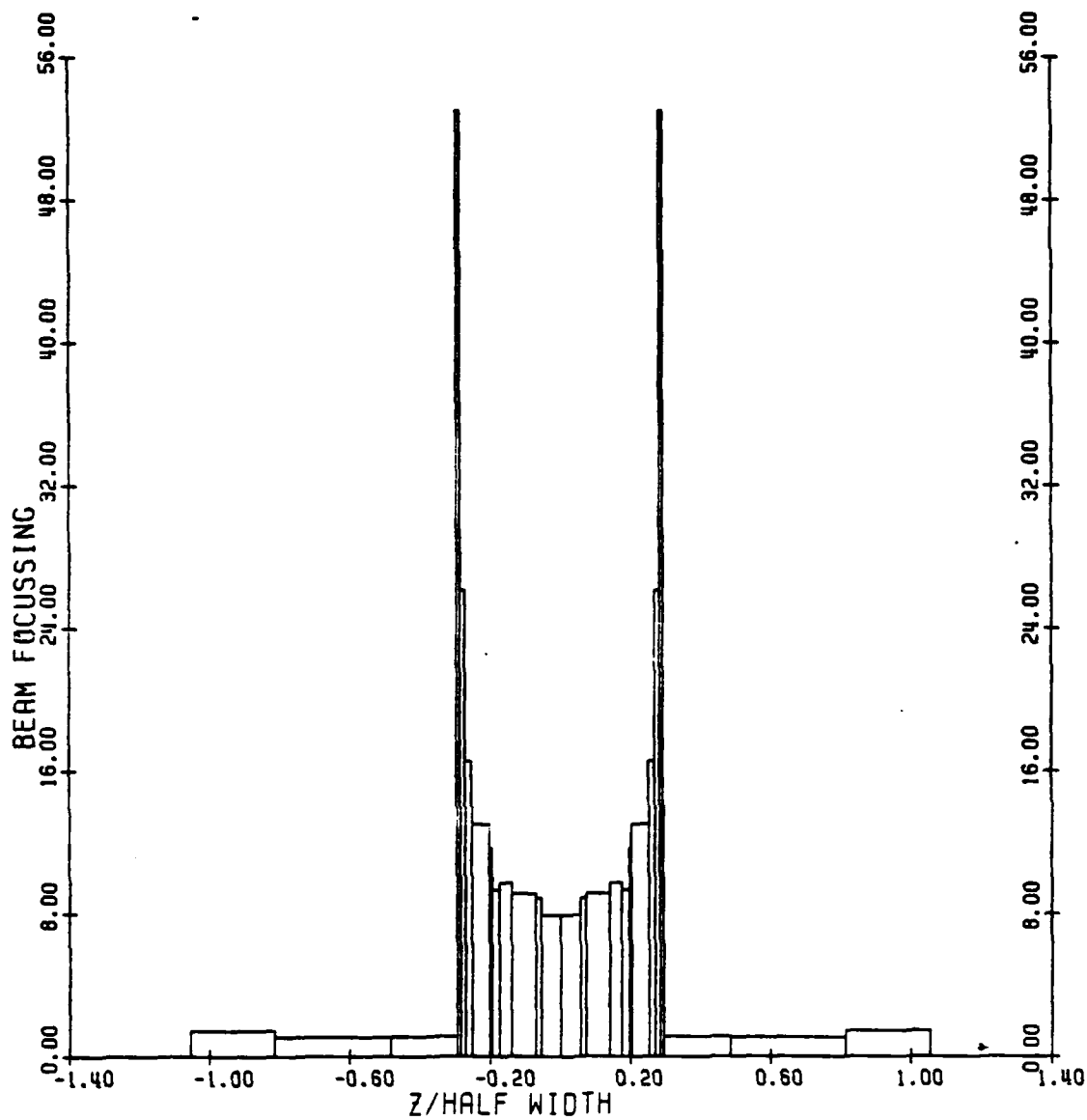
ION SPOT: M=6.9 AMU, Q=1 E, E0=10.0 EV

Fig.17

FREE SPACE CHG CONF USED:

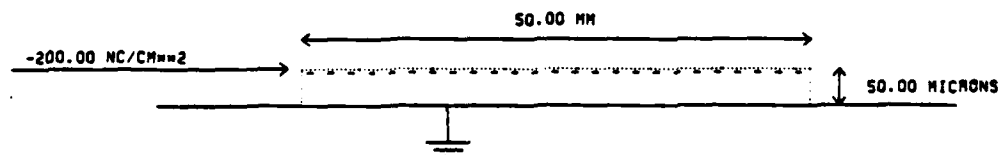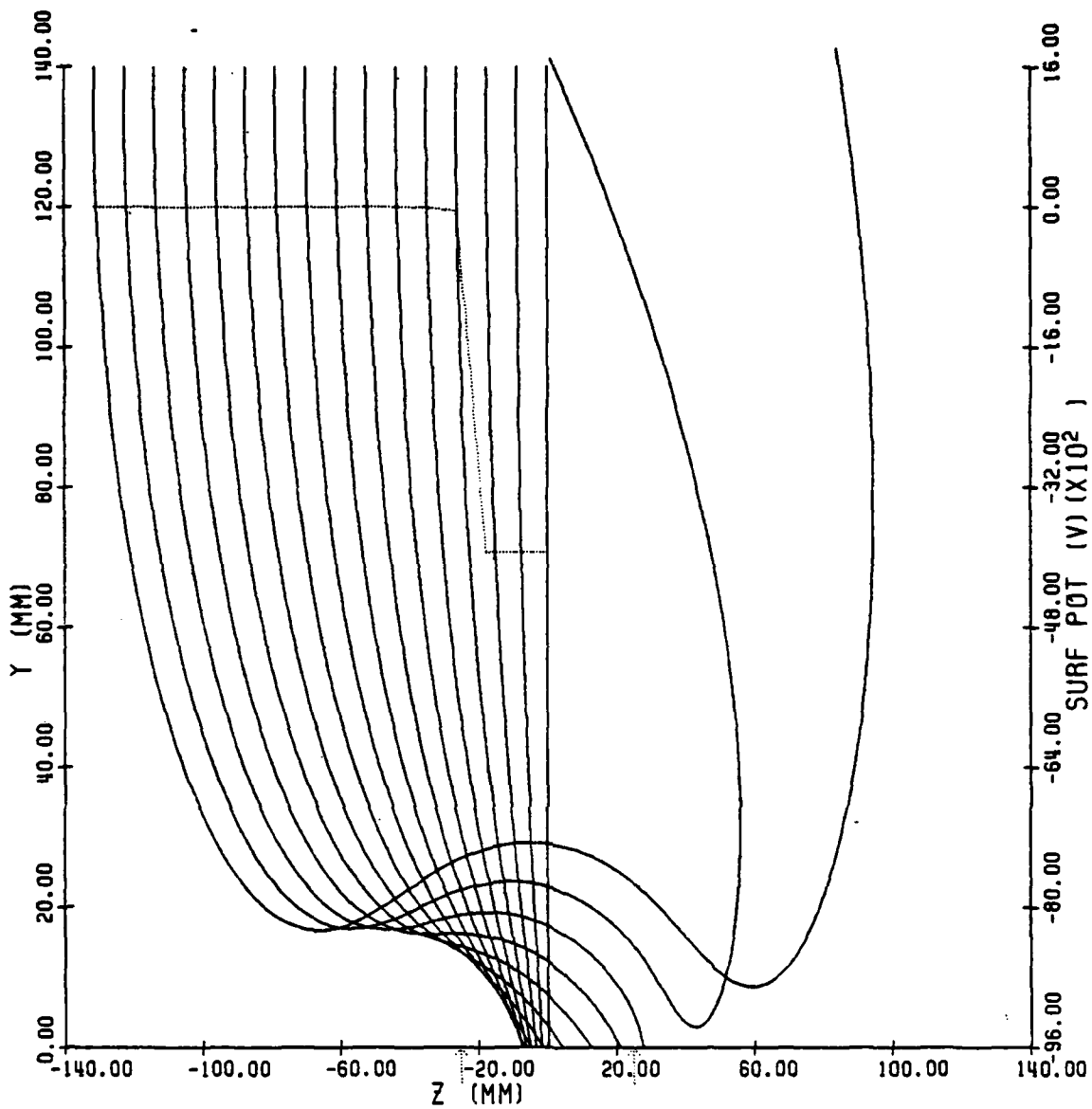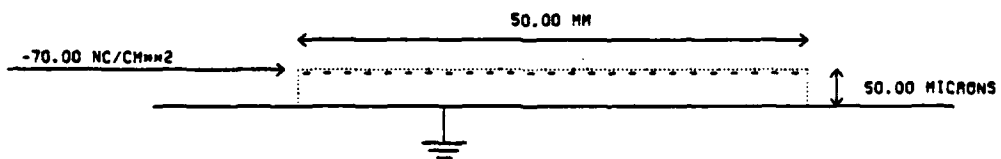ION TRACKS: M=6.9 AMU, Q=1 E, E0=10.0 EV

Fig.18

FREE SPACE CHG CONF USED:

ION SPOT: M=6.9 AMU, Q=1 E, EO=10.0 EV

Fig.19

FREE SPACE CHG CONF USED:

-70.00 NC/CM**2

50.00 MM

50.00 MICRONS

ION TRACKS: M=6.9 AMU, Q=1 E, E0=10.0 EV

Fig.20

FREE SPACE CHG CONF USED:

-70.00 NC/CM==2

50.00 MM

50.00 MICRONS
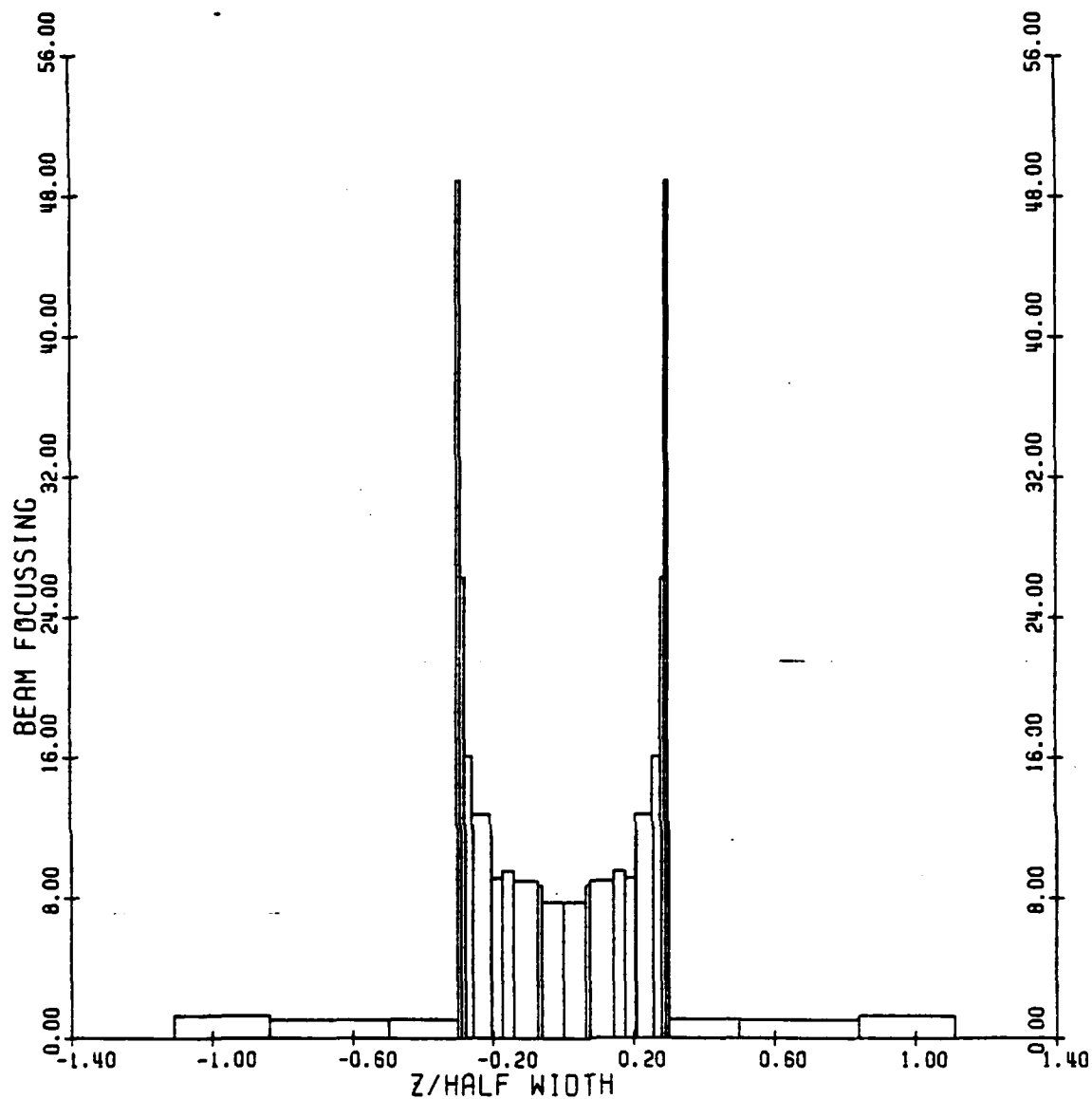
ION SPOT: M=6.9 AMU,   Q=1 E,   E0=10.0 EV

Fig.21

FREE SPACE CHG CONF USED:

ION TRACKS: M=6.9 AMU,   Q=1 E,   E0=10.0 EV

Fig.22

FREE SPACE CHG CONF USED:

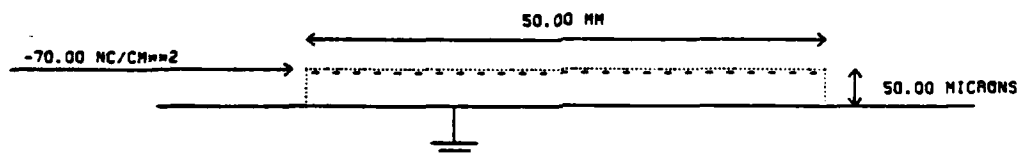ION SPOT: M=6.9 AMU, Q=1 E, EO=10.0 EV

Fig.23

FREE SPACE CHG CONF USED:

ION TRACKS: M=6.9 AMU,   Q=1 E,   E0=10.0 EV

Fig.24

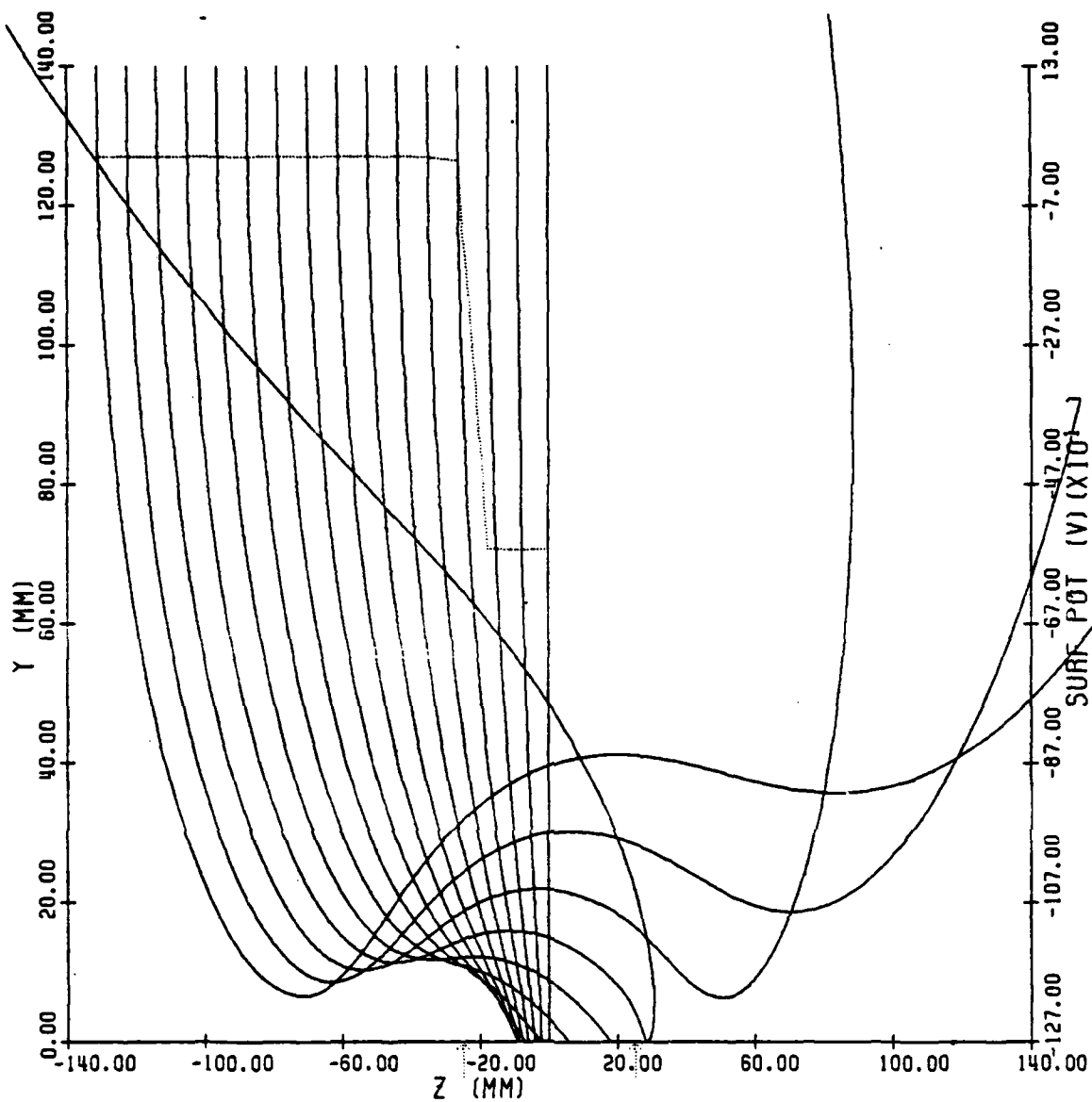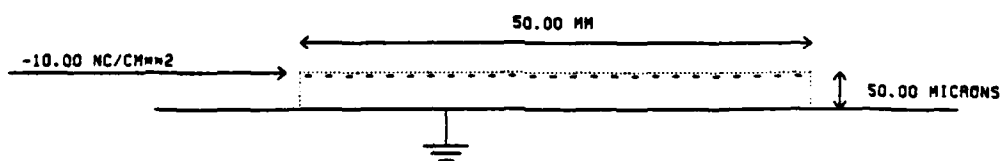FREE SPACE CHG CONF USED:

ION SPOT: M=6.9 AMU, Q=1 E, E0=10.0 EV

Fig.25
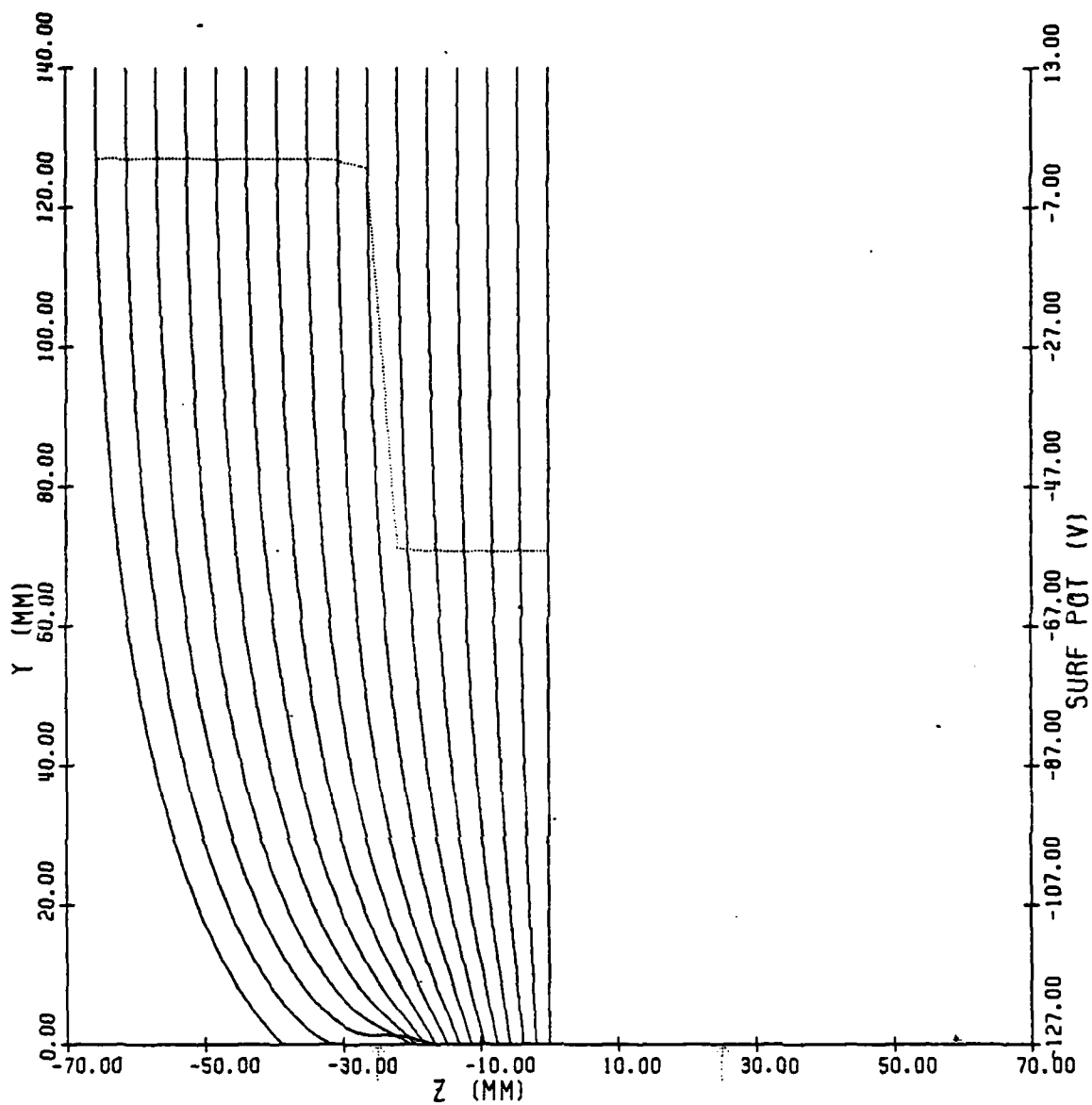
FREE SPACE CHG CONF USED:
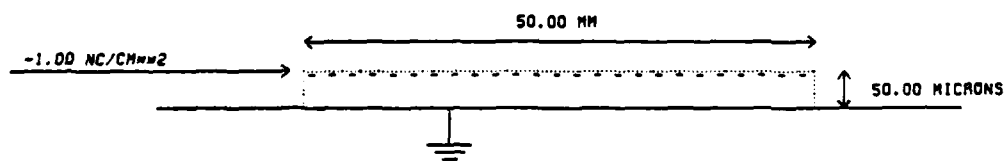
ION TRACKS: M=6.9 AMU, Q=1 E, EO=10.0 EV

Fig.26
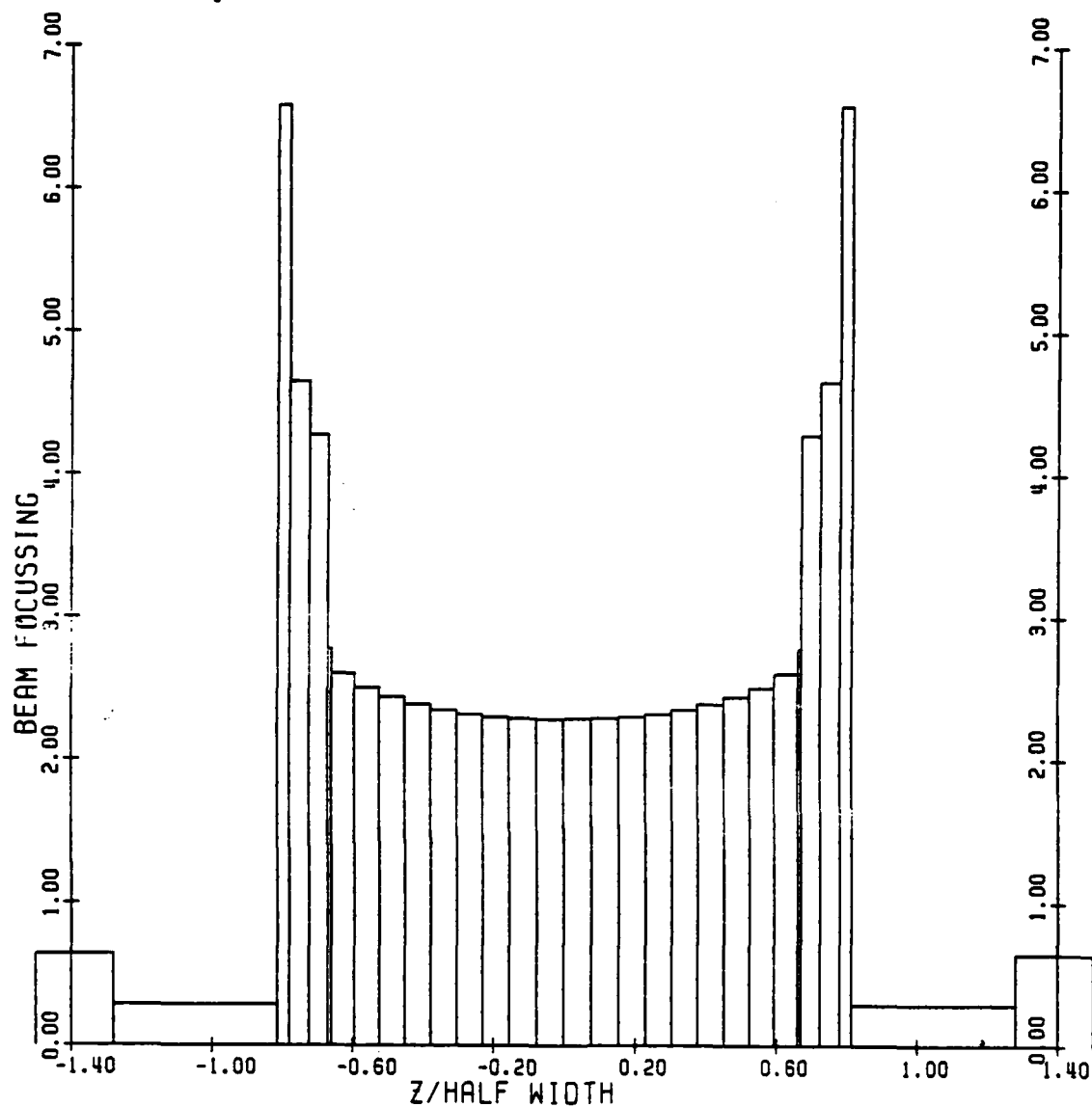
FREE SPACE CHG CONF USED:
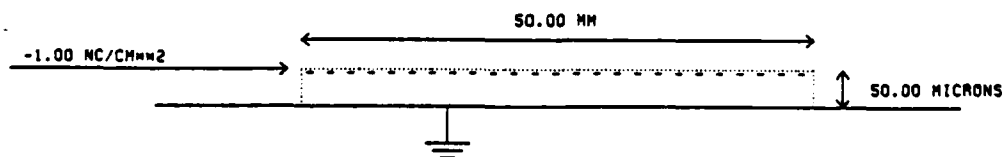
ION SPOT: M=6.9 AMU, Q=1 E, E0=10.0 EV

Fig.27
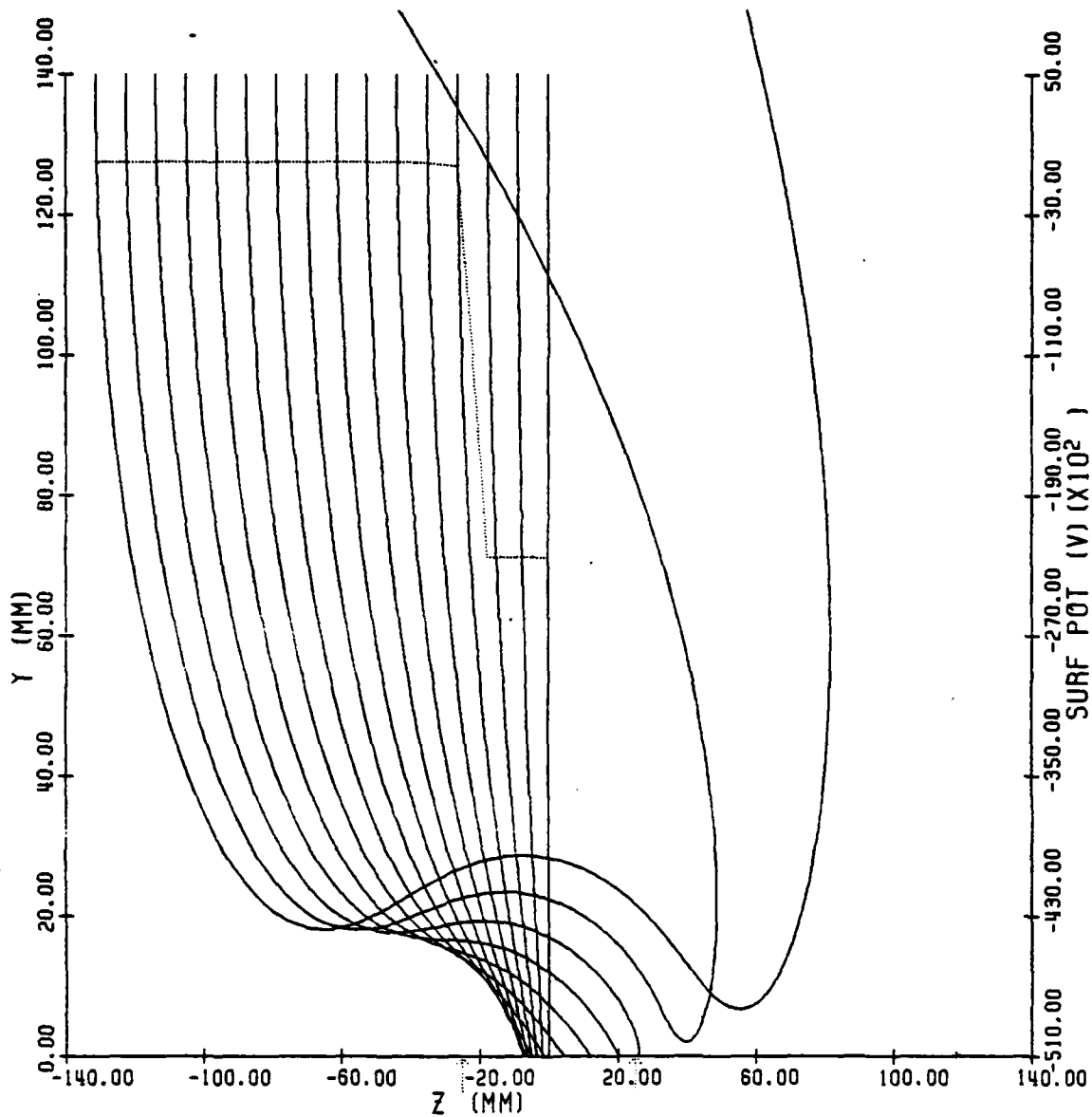
FREE SPACE CHG CONF USED:
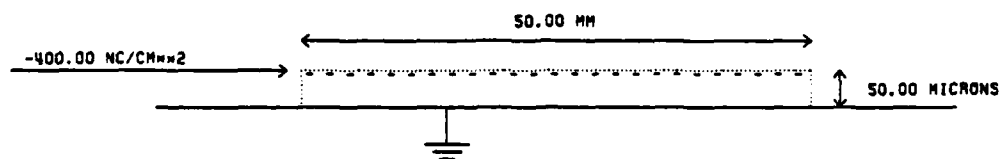
ION TRACKS: M=1.0 AMU,   Q=1 E,   E0=10.0 EV

Fig.28
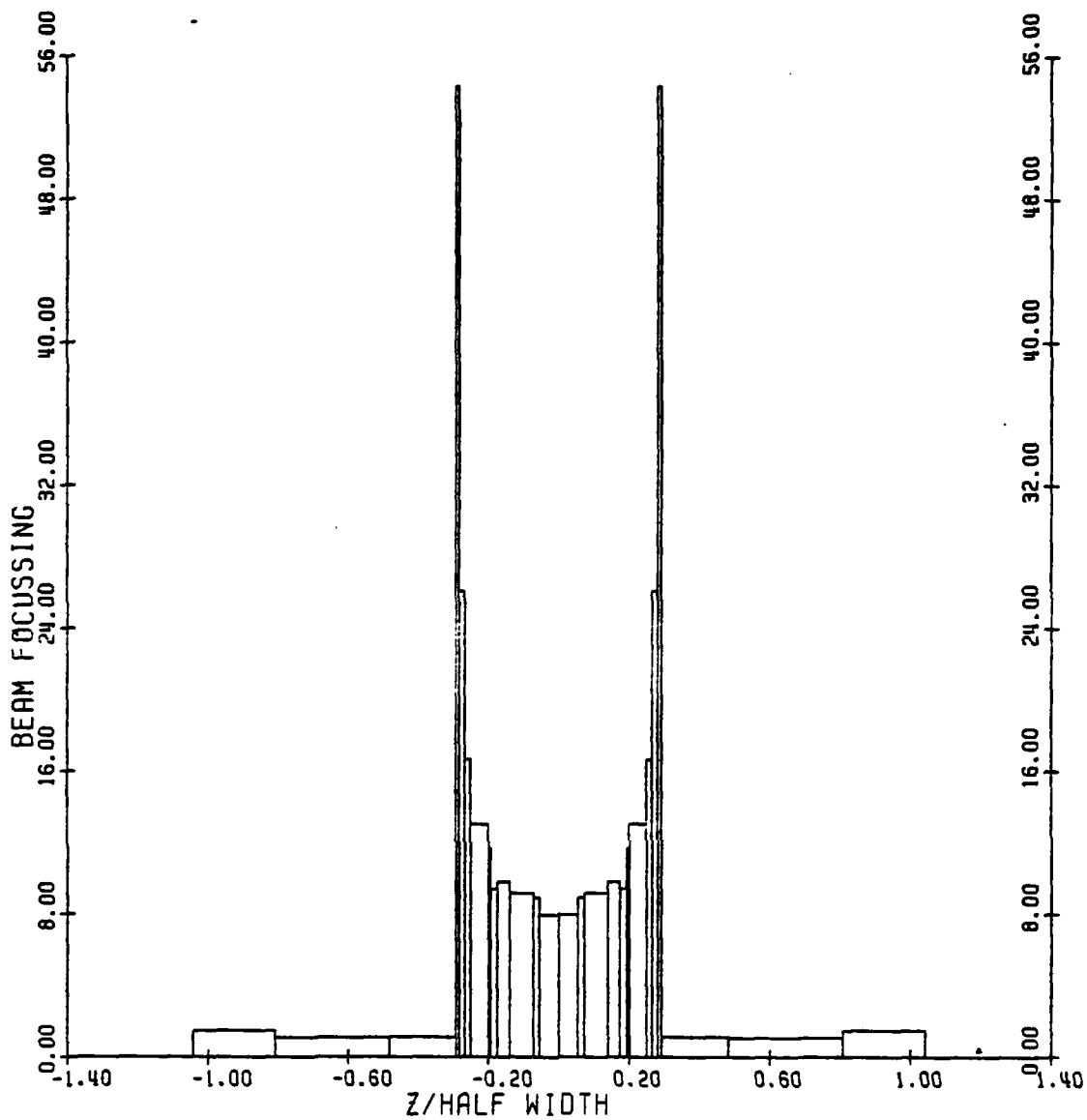
FREE SPACE CHG CONF USED:
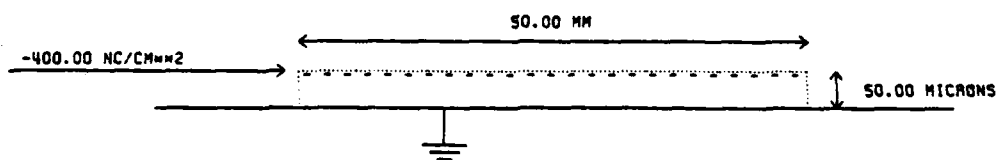
ION SPOT: M=1.0 AMU,   Q=1 E,   EO=10.0 EV

Fig.29
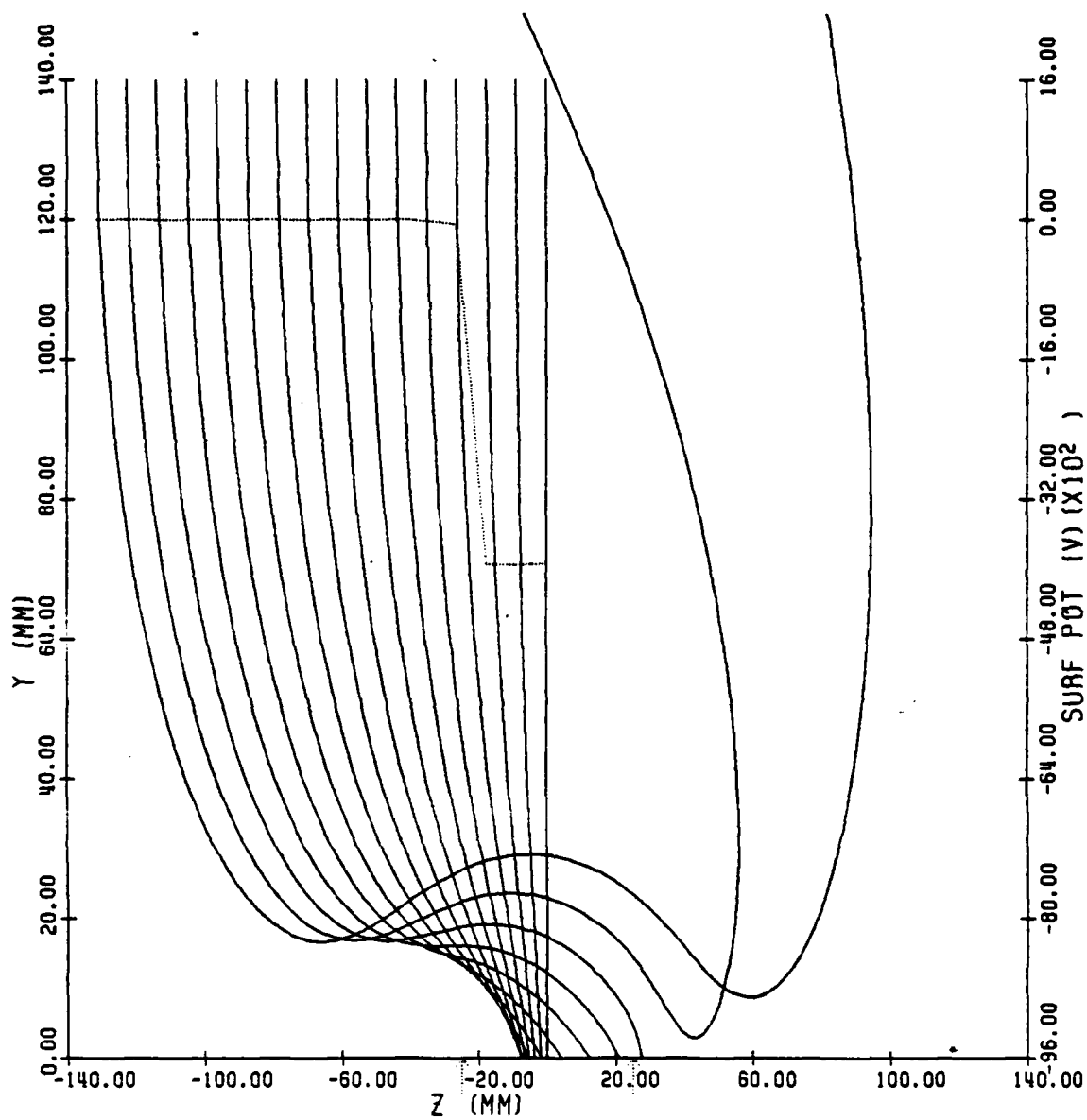
FREE SPACE CHG CONF USED:
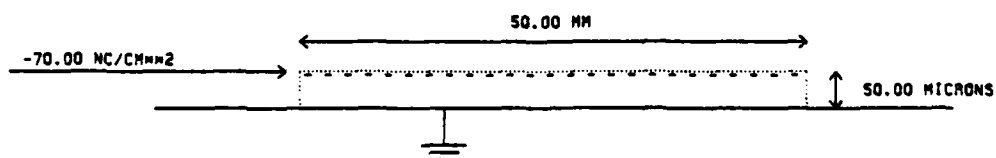
ION TRACKS: M=1.0 AMU, Q=1 E, E0=10.0 EV

Fig.30

FREE SPACE CHG CONF USED:

-70.00 NC/CM==2

50.00 MM

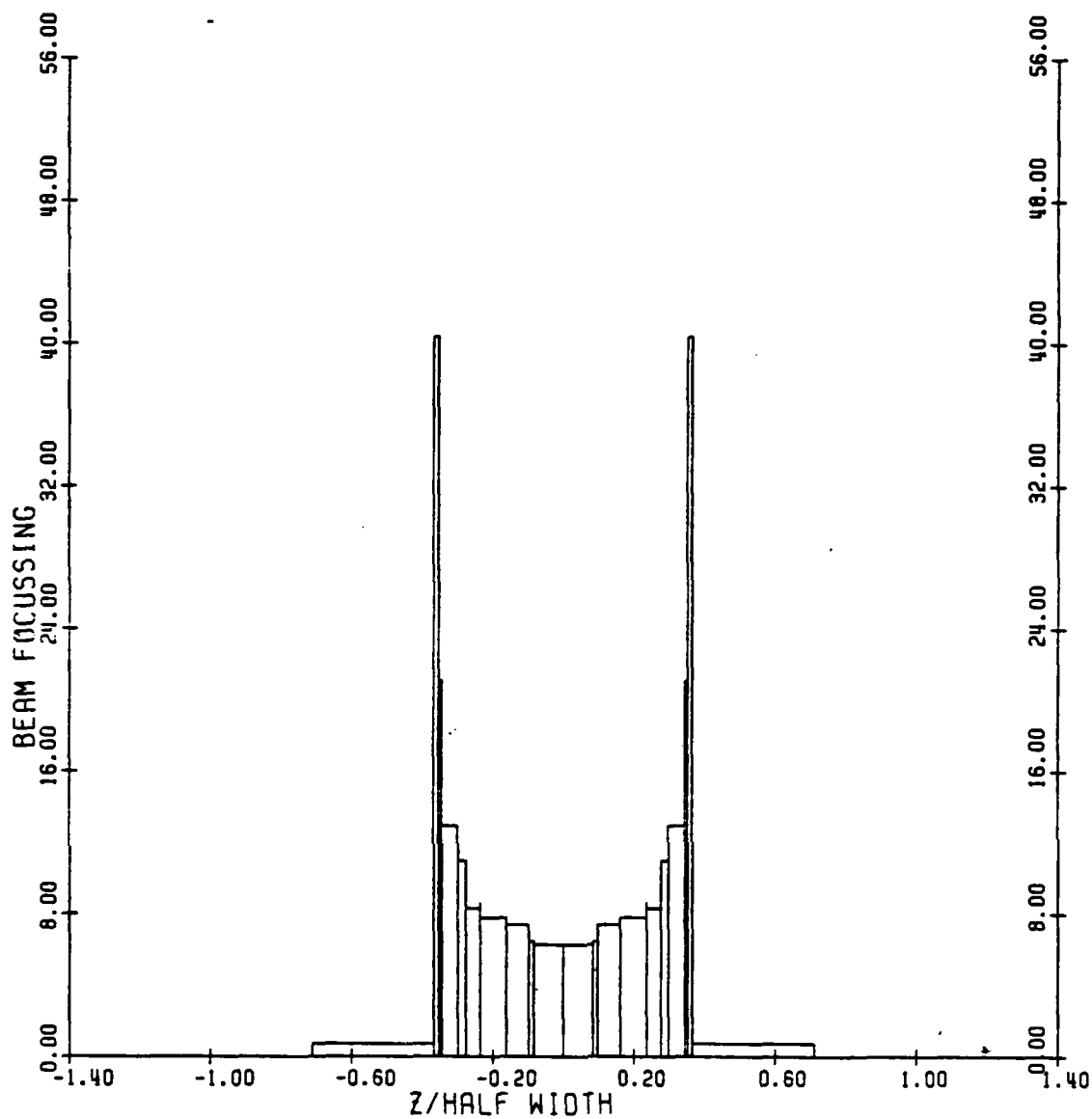50.00 MICRONS
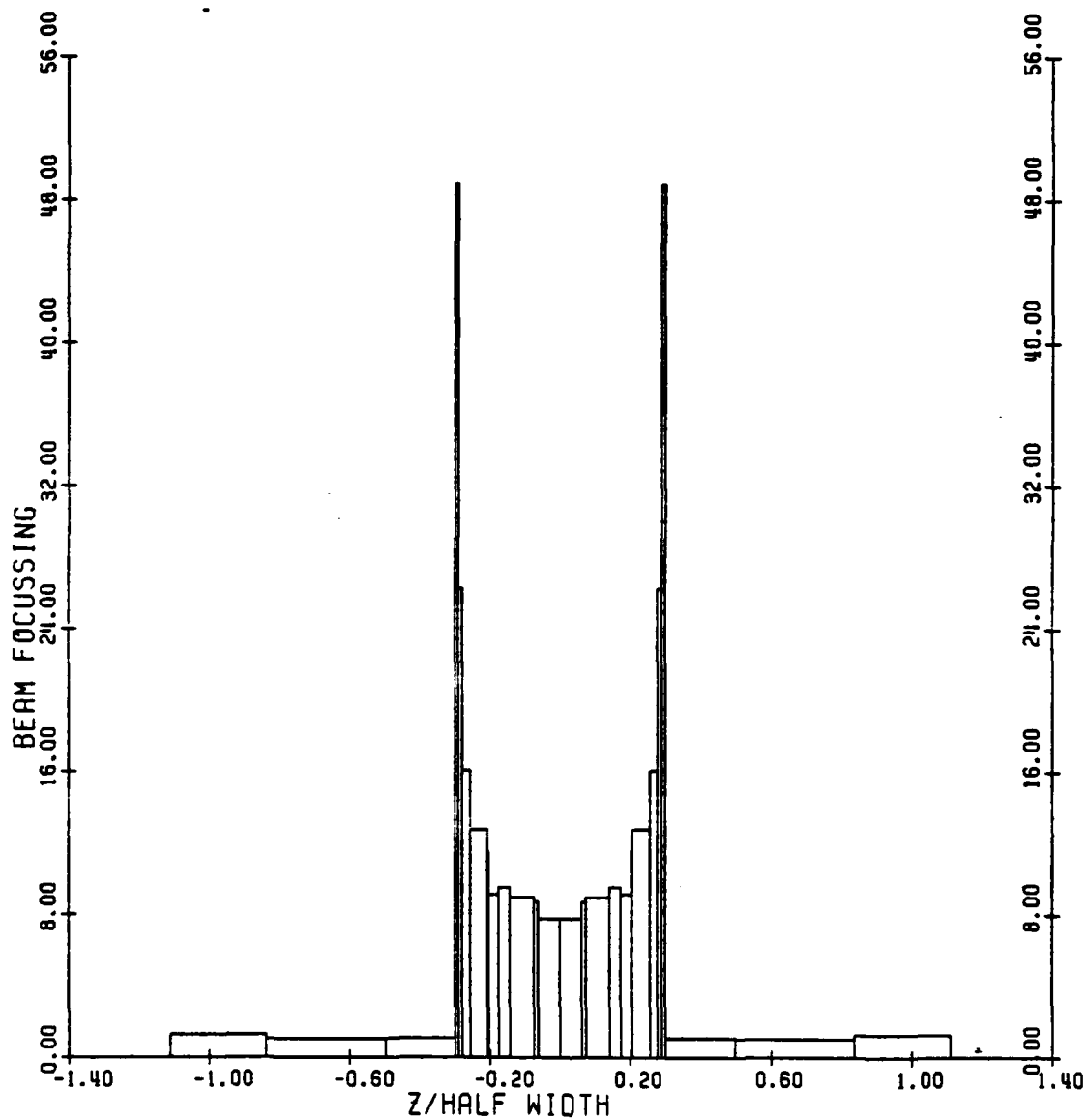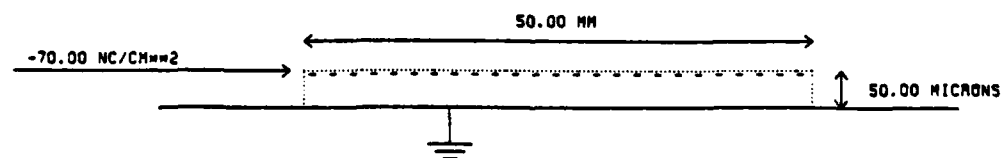
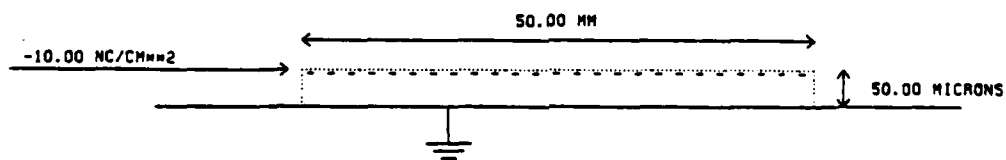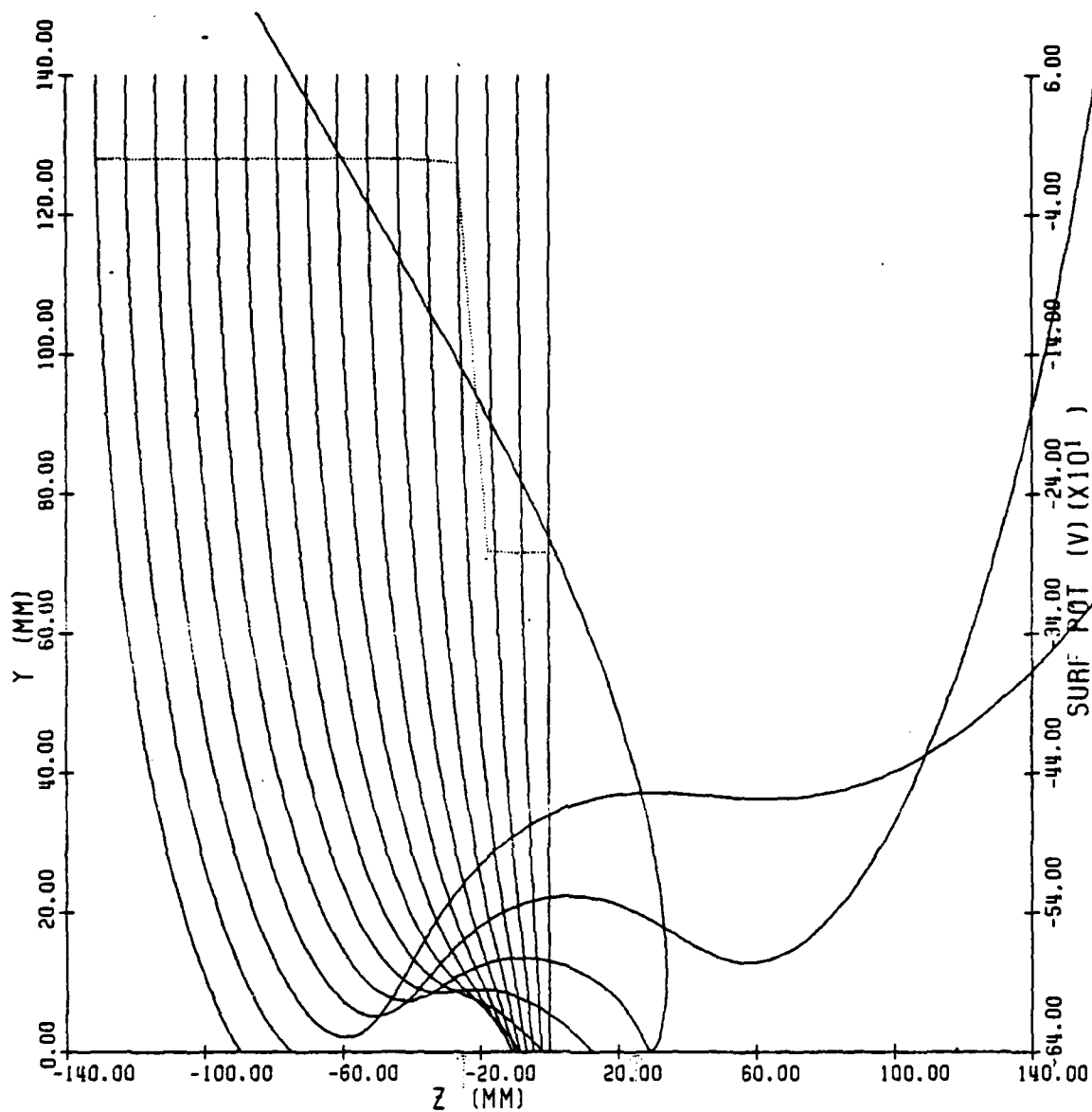ION SPOT: M=1.0 AMU, Q=1 E, EO=10.0 EV

Fig.31
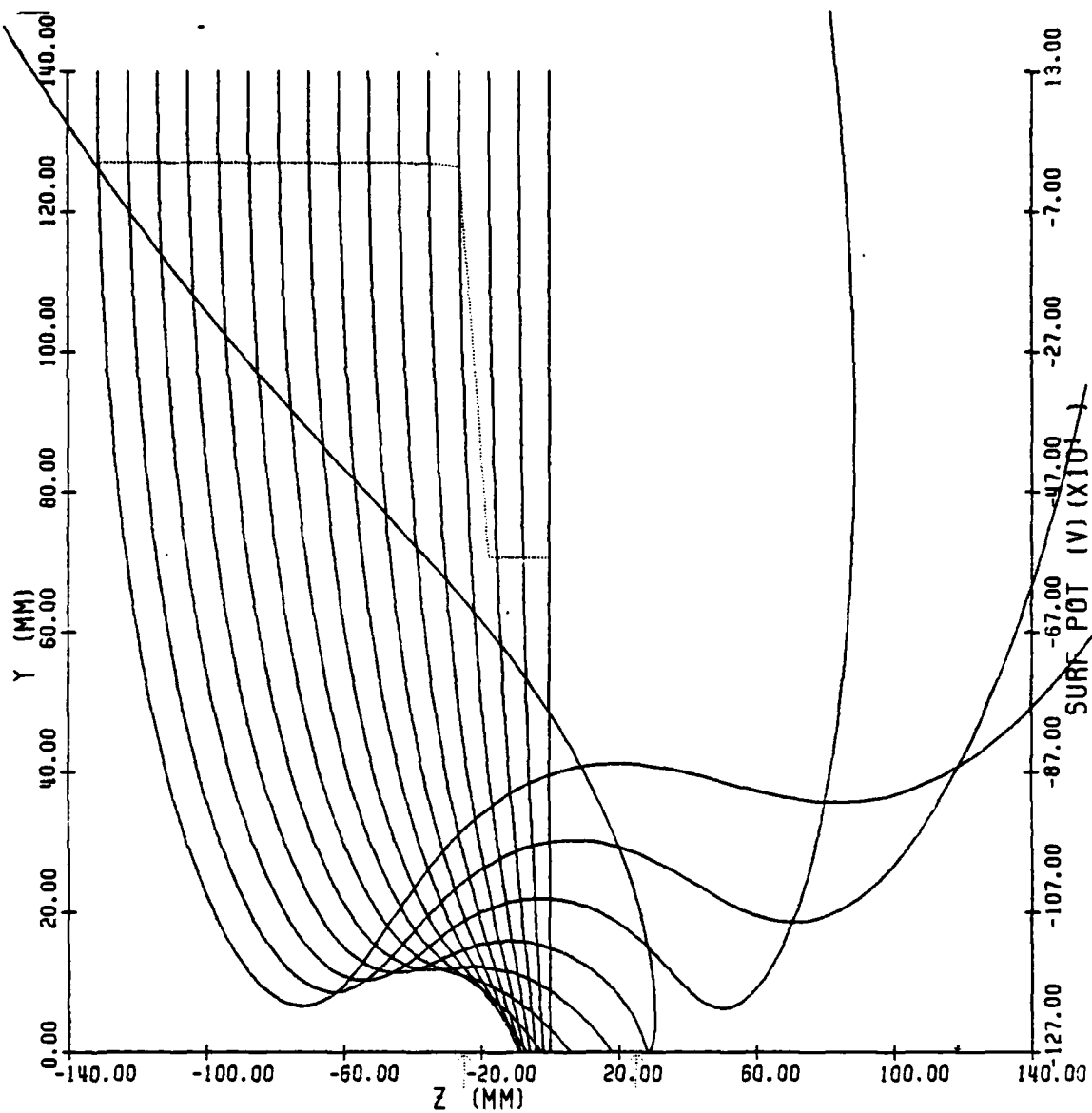
FREE SPACE CHG CONF USED:
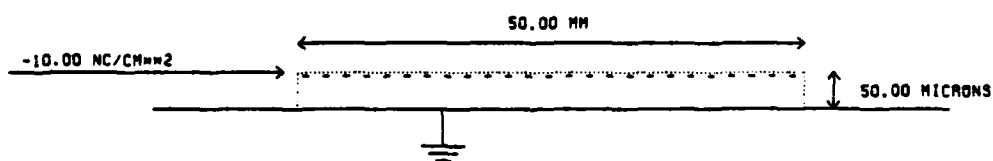
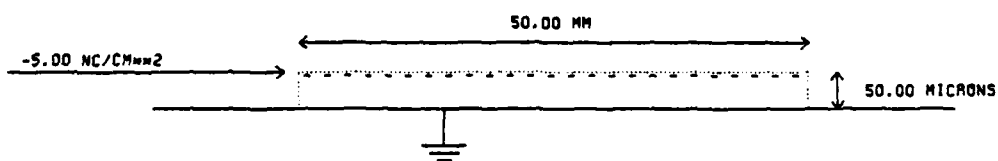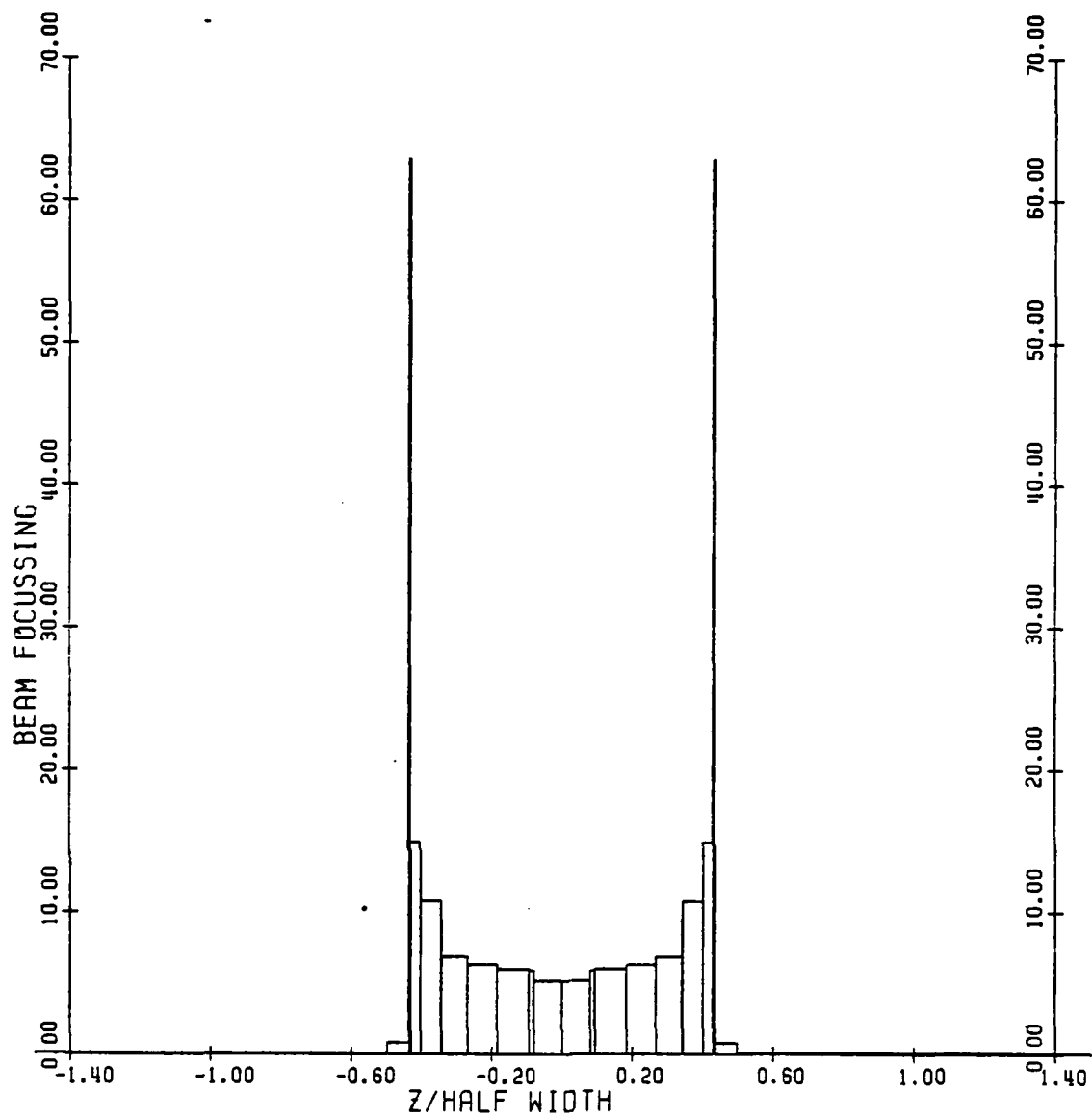ION TRACKS: M=1.0 AMU, Q=1 E, E0=10.0 EV

Fig.32
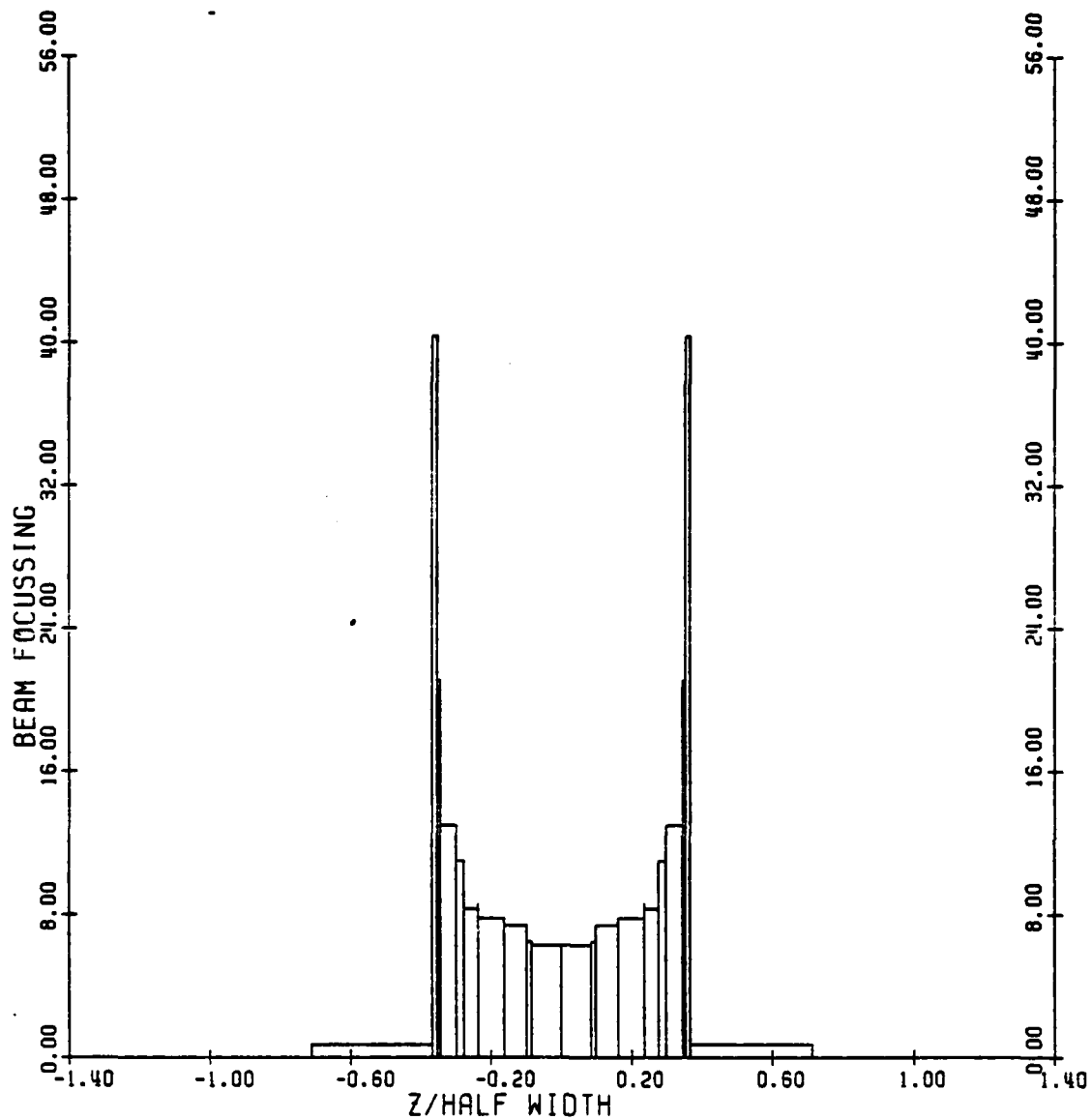
FREE SPACE CHG CONF USED:

ION SPOT: M=1.0 AMU,   Q=1 E,   EO=10.0 EV

Fig.33

Y (MM)

Z (MM)

SURF POT (V)

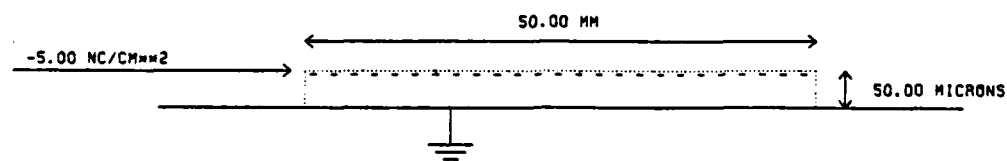FREE SPACE CHG CONF USED:

50.00 MM

-1.00 NC/CM**2

50.00 MICRONS
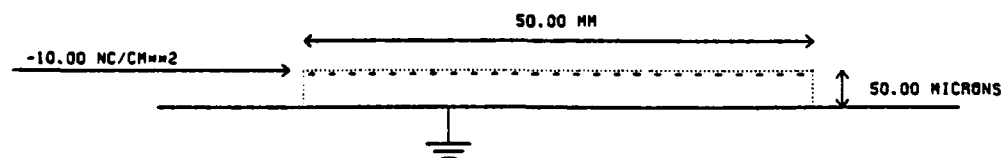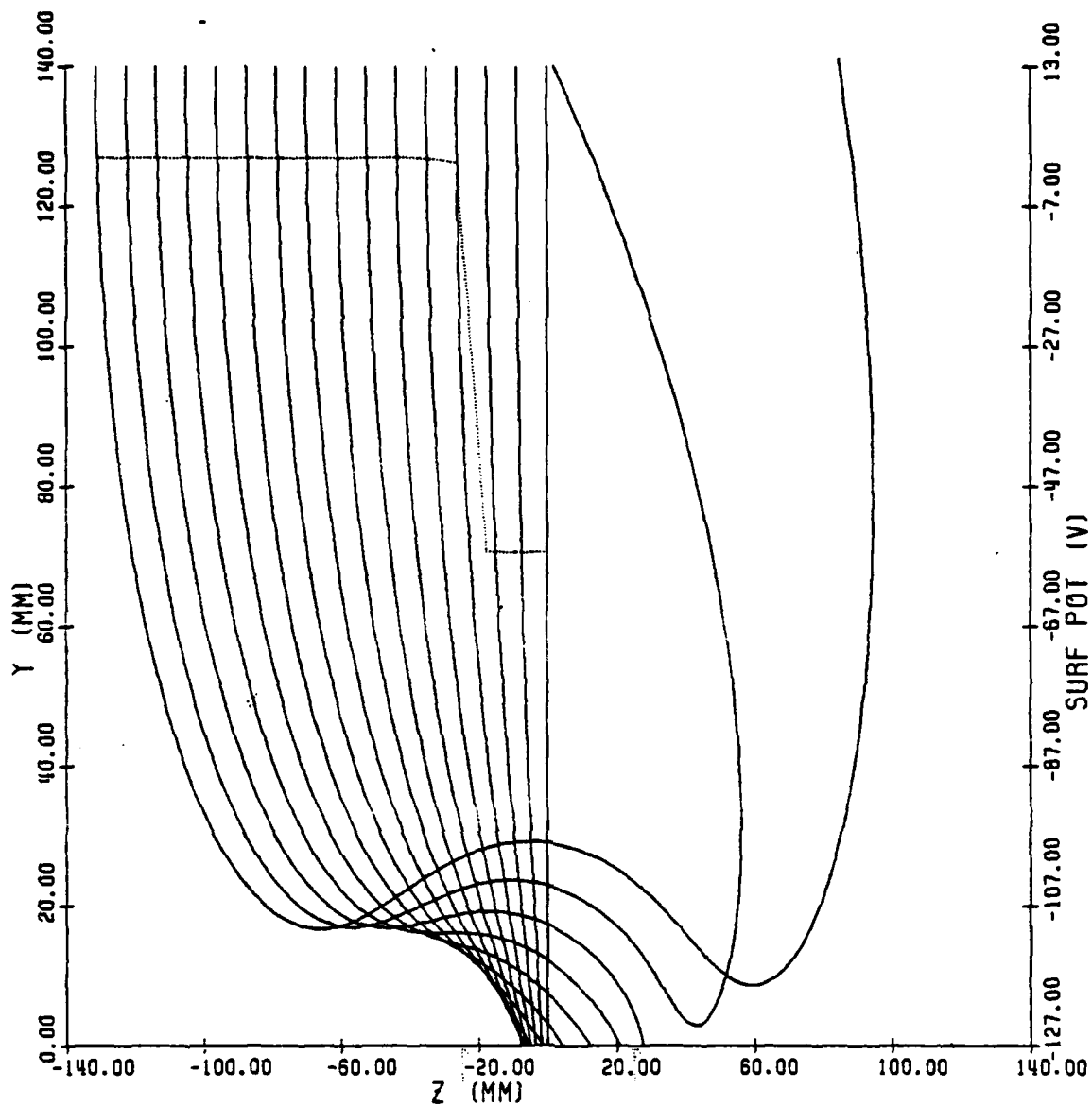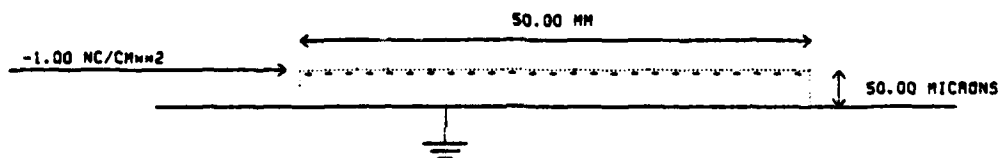
ION TRACKS: M≈6.9 AMU, Q=1 E, E0=0.143 EV

Fig.34
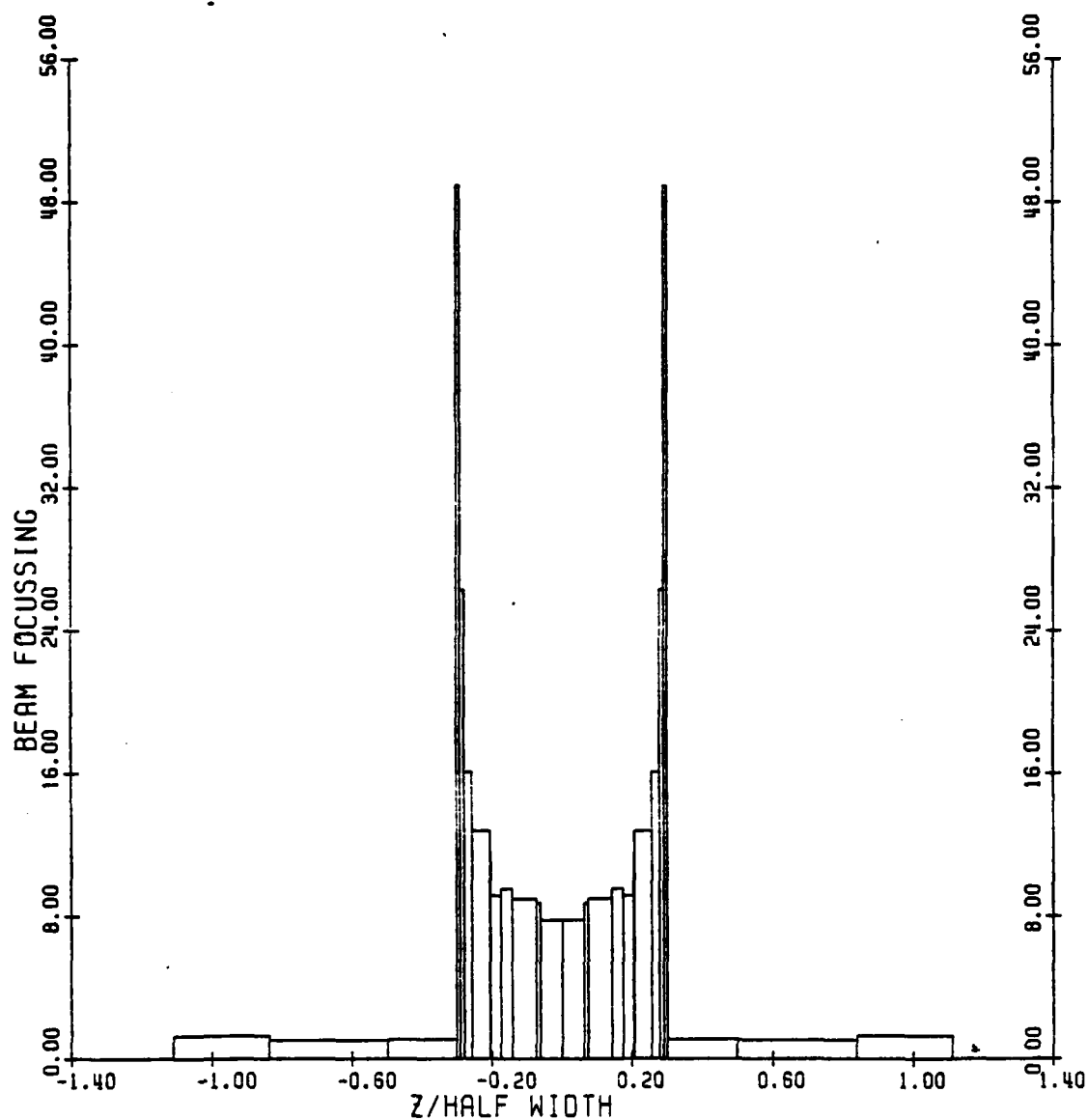
FREE SPACE CHG CONF USED:
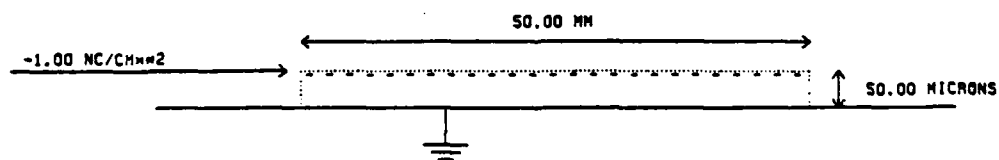
ION SPOT: M=6.9 AMU,   Q=1 E,   EO=0.143 EV

Fig.35
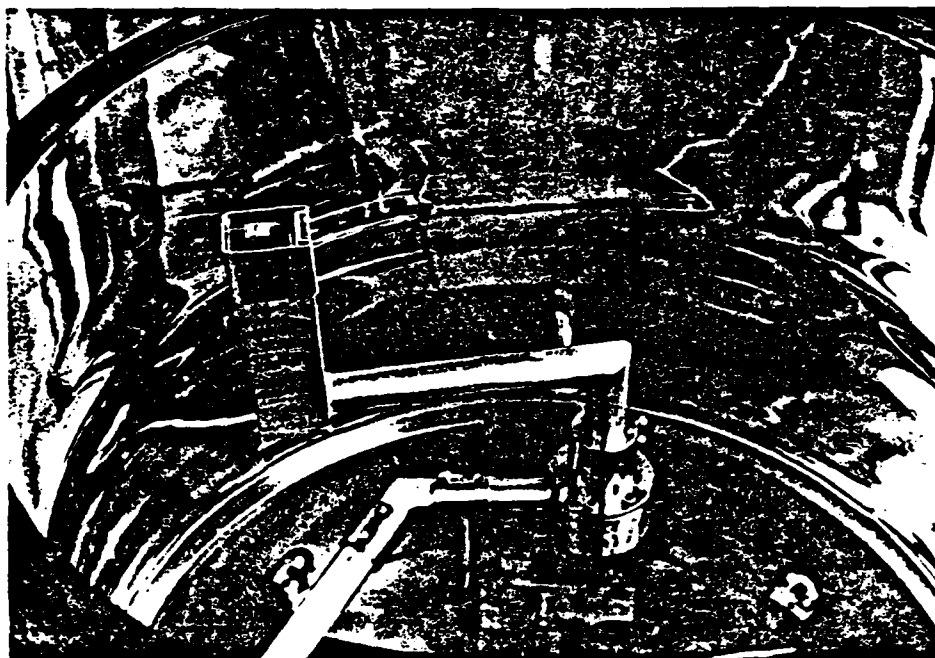
Fig.36 Electrostatic Probe Head Mounted Inside Chamber
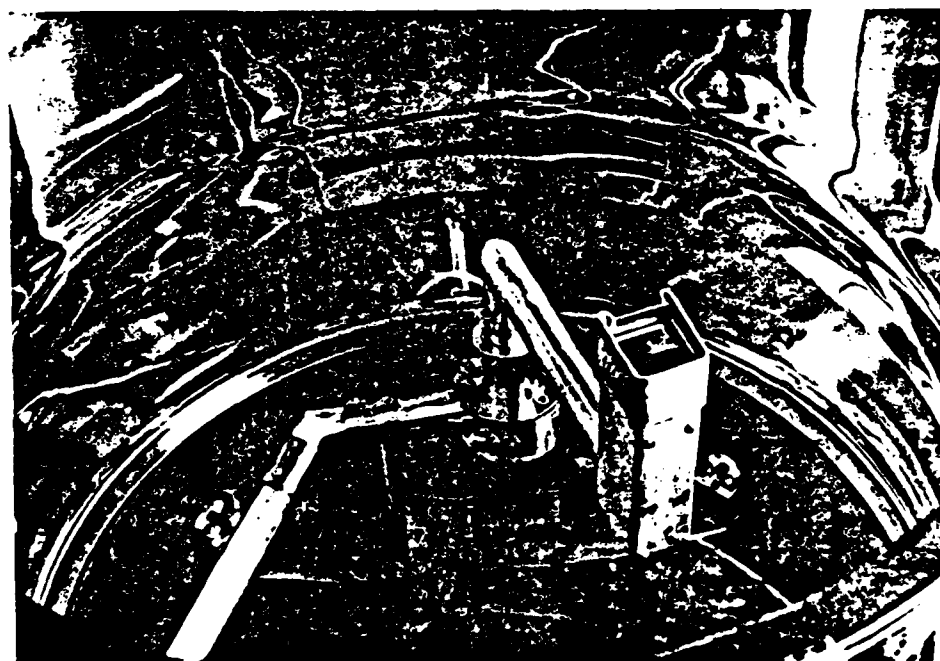
Fig.37 Probe Head Rotated Approx. 90° from Fig.36

VOLTAGE PROFILE ON A MYLAR SAMPLE

100mm dia. exposed to a 20kv e–beam

Sample exposed to e–beam
for approx. 15 sec.
No discharges occurred.

Sweep (millimeters)

Voltage (kilovolts)
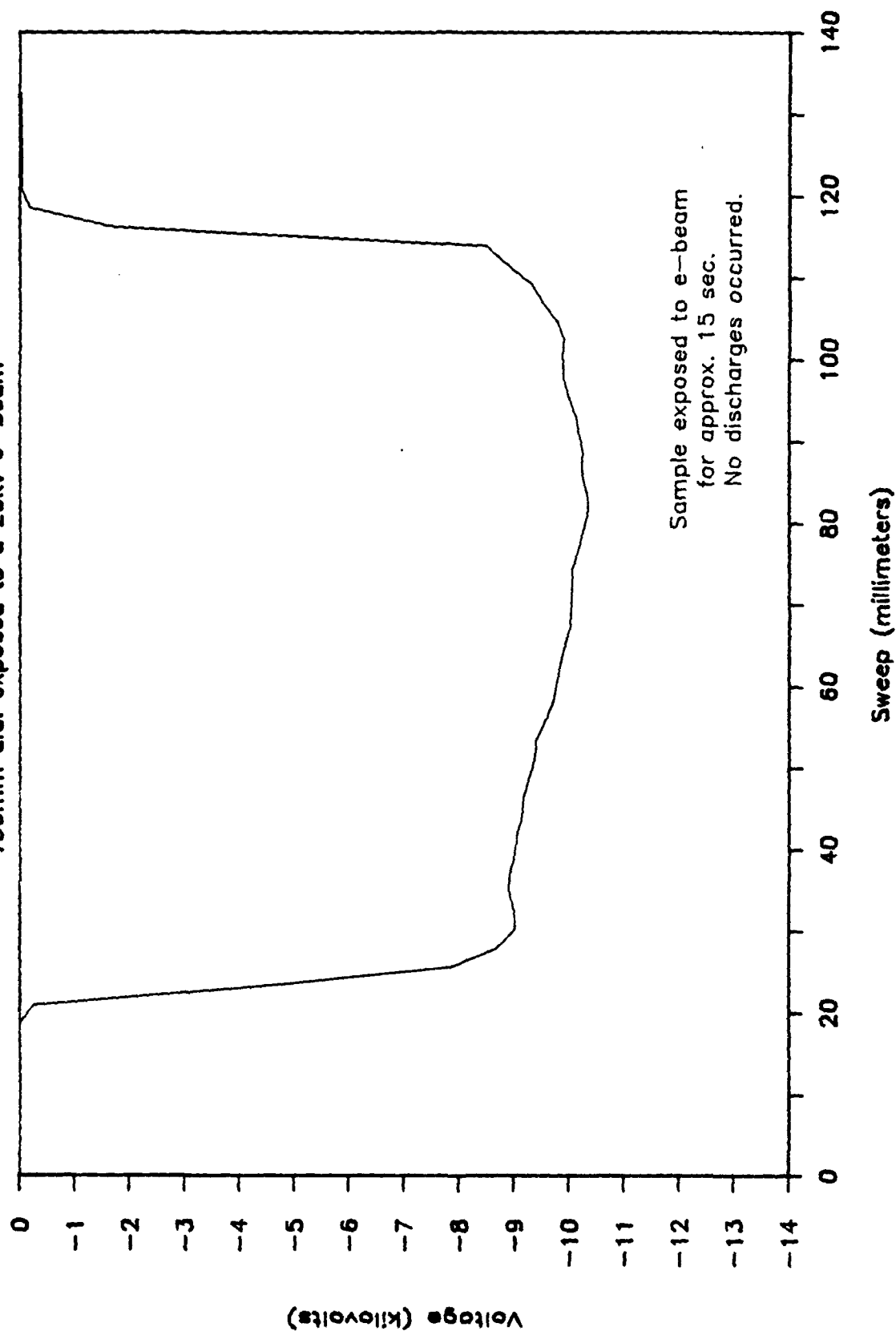
Figure 38

VOLTAGE PROFILE ON A MYLAR SAMPLE

100mm dia. exposed to a 20kv e-beam

Sample exposed until a
discharge occurred. Discharge
covered 1/2 sample area

Sweep (millimeters)

Voltage (kilovolts)
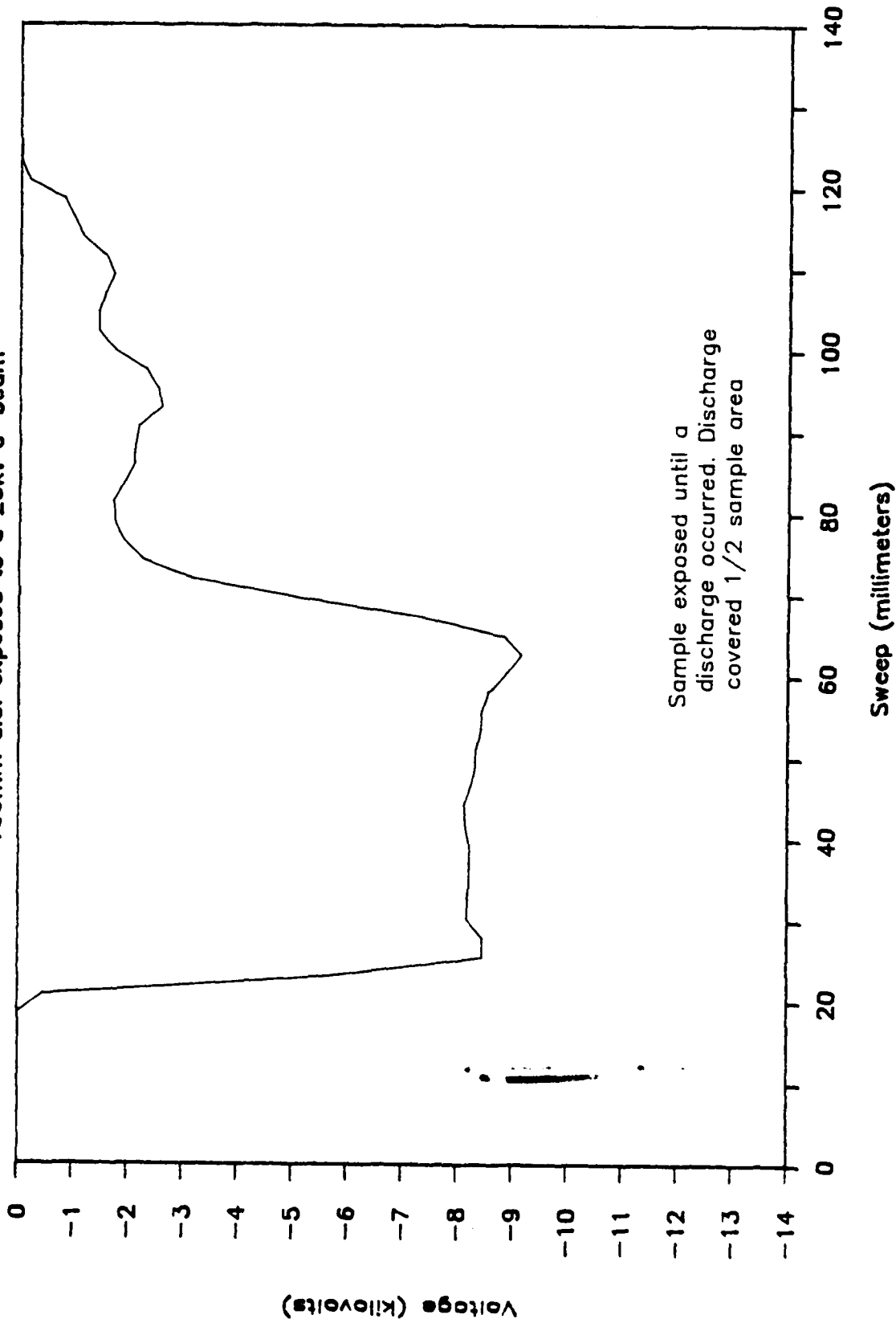
Figure 39

VOLTAGE PROFILE ON A MYLAR SAMPLE

100mm dia. exposed to a 20kv e-beam

Max. voltage obtained.
Sample irradiated after
initial discharge covered
1/2 sample area.

Sweep (millimeters)

Voltage (kilovolts)
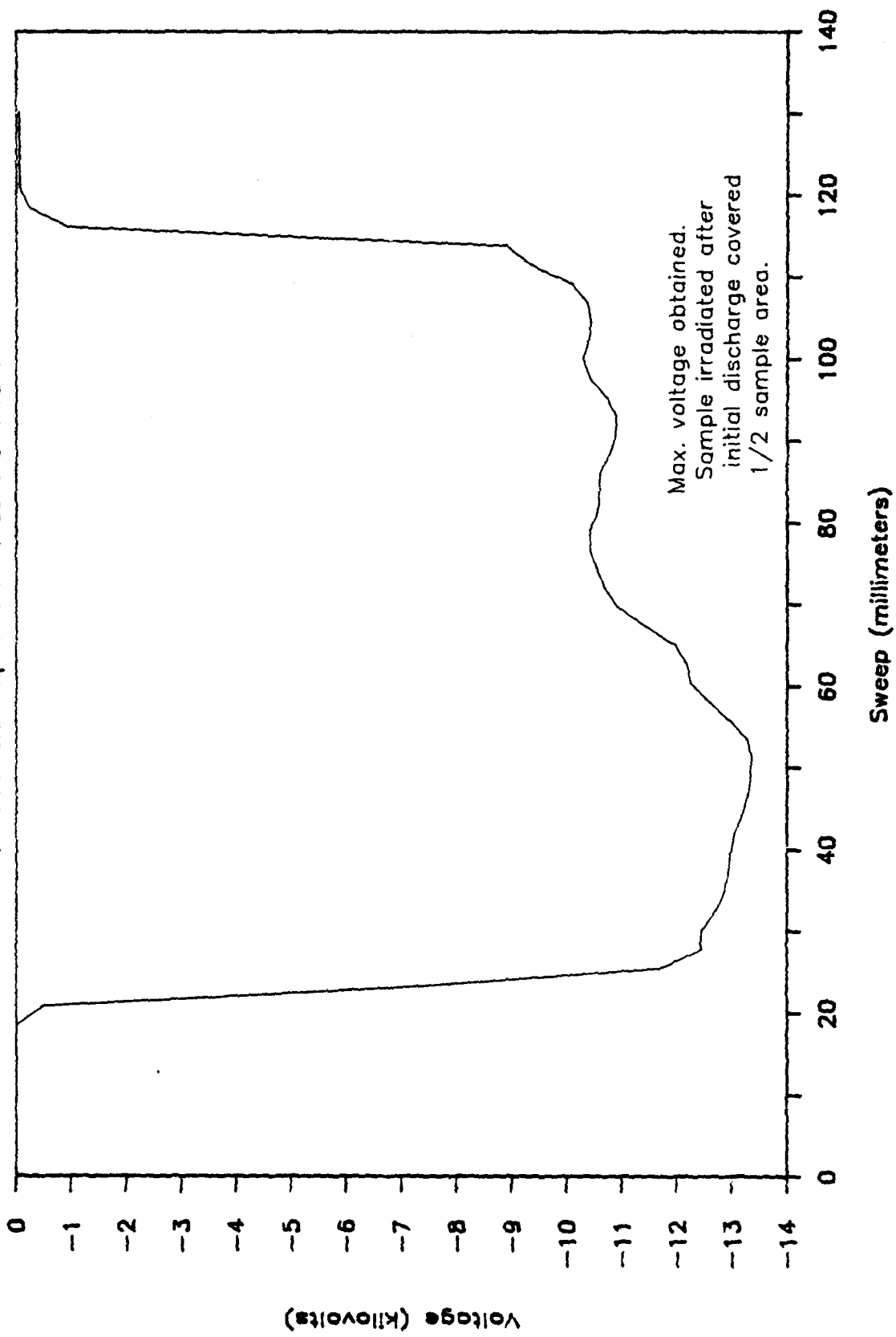
Figure 40

VOLTAGE PROFILE ON A TEFLON SAMPLE

100mm dia. exposed to a 20kv e-beam

After 45 sec.no
previous discharges.

Sweep (millimeters)

Voltage (kilovolts)
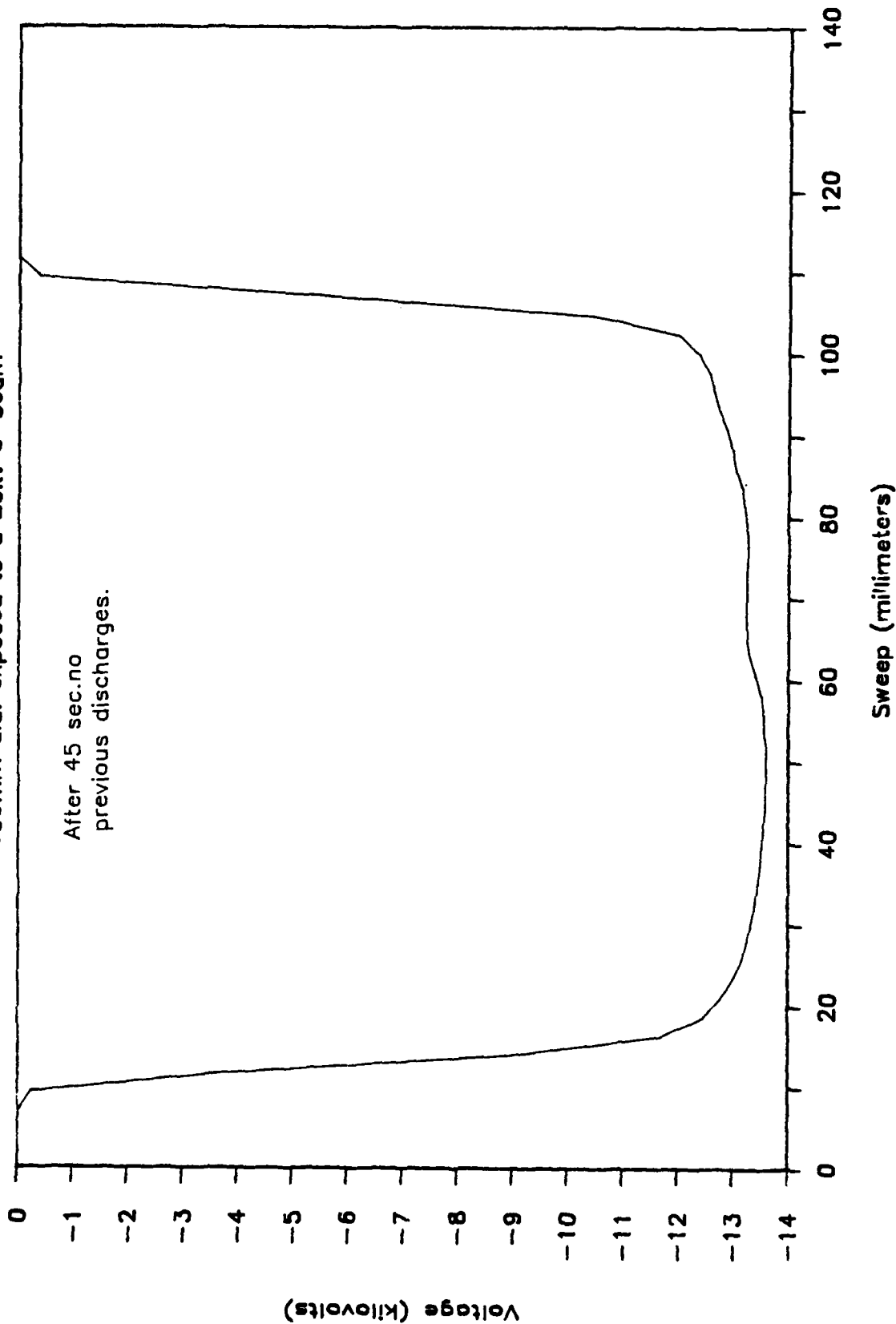
Figure 41

VOLTAGE PROFILE ON A TEFLON SAMPLE

100mm dia. exposed to a 20kv e-beam

Immediately after
a discharge.

Sweep (millimeters)

Voltage (kilovolts)
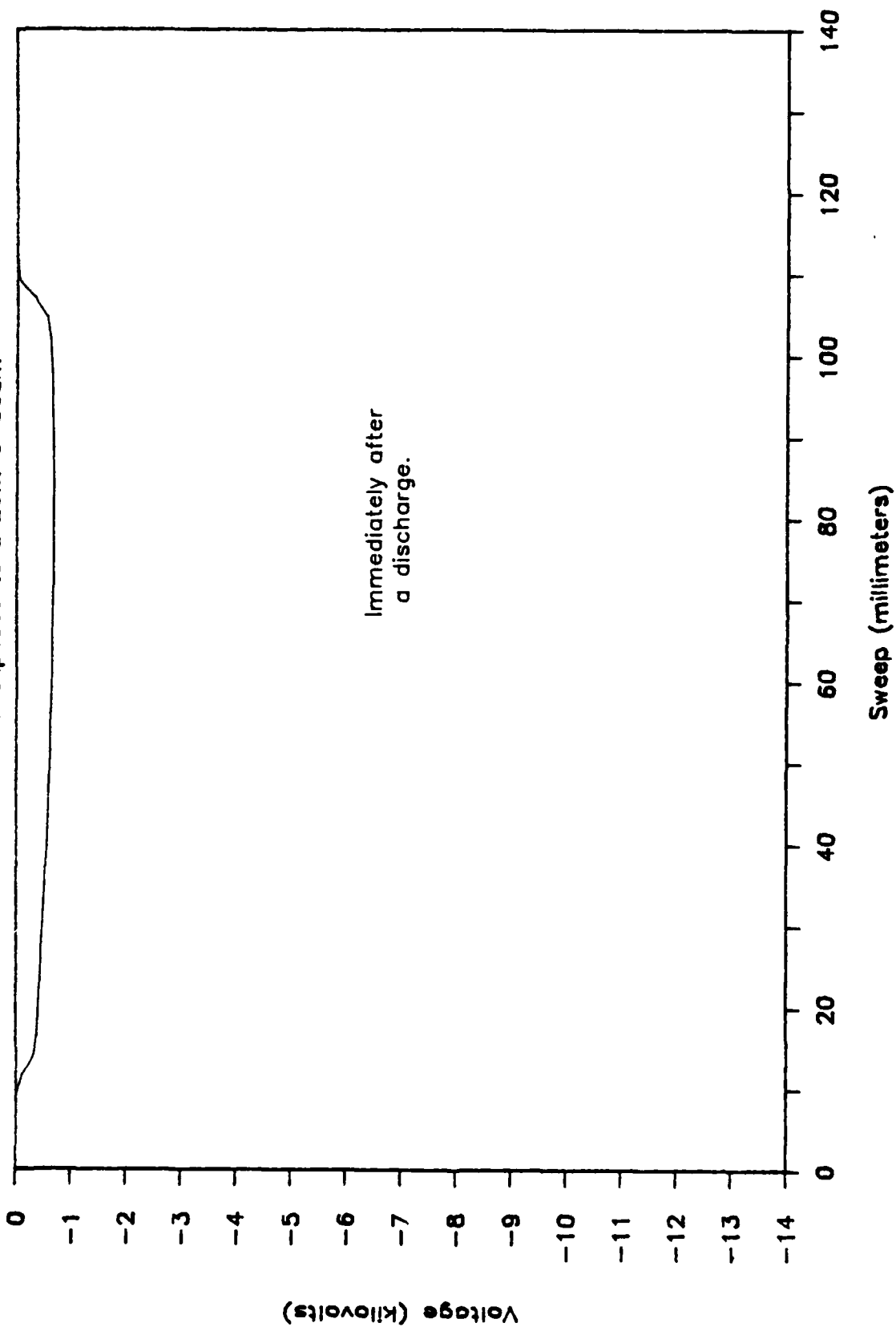
Figure 42

VOLTAGE PROFILE ON A TEFLON SAMPLE

100mm dia. exposed to a 20kv e–beam

Approx. 1 min. from previous discharge.

Sweep (millimeters)

Voltage (kilovolts)

Figure 43

APPENDIX

Thickness Scaling for Arc Discharges on Electron-
Beam-Charged Dielectrics

by

K.G. Balmain, A. Battagin, and G.R. Dubois

THICKNESS SCALING FOR ARC DISCHARGES ON ELECTRON-BEAM-CHARGED DIELECTRICS*

K.G. Balmain, A. Battagin, and G.R. Dubois
Department of Electrical Engineering
University of Toronto
Toronto, Canada M5S 1A4

Abstract

A study of arc discharges on various thicknesses of
electron-beam-charged Mylar, FEP Teflon and Kapton shows
that the peak substrate current and the energy dissi-
pated in a load resistor both exhibit maxima at a parti-
cular thickness of the order of 50 μm, for one set of
experiment parameters. The experiments also show that,
as thickness increases, this particular thickness is the
transition from near-constant to decreasing released
charge, and, for Mylar, from decreasing to near-constant
arc duration. This transition is interpreted as being
caused primarily for thin specimens by punchthrough
formation and possibly influenced by the transition from
conduction-dominated to emission-dominated charging.
Additional low-energy ion exposure is shown to weaken
and sometimes eliminate the arc discharges without ra-
dically altering the thickness scaling. At low fluxes,
the incident ions are focussed into a central spot.

Introduction

The accumulation of charge and the threat of arc
breakdown on exposed spacecraft dielectric materials
have been a matter of concern to spacecraft designers
for about fourteen years, and the first journal review
on the subject was published by Rosen in 1976 [1]. In
subsequent years, extensive laboratory simulation has
been carried out in order to study both the charge accu-
mulation and arc breakdown processes, processes which
have been reviewed recently by Frederickson [2]. Most
of the laboratory experimentation has been done on
sheets of polymeric materials which are used for space-
craft thermal control, such as Kapton and Mylar thermal
blankets and Teflon second-surface mirrors. The thick-
nesses used ranged from 12.5 to 125 μm, but to date
there has been no attempt to establish the inter-rela-
tionships between phenomena observed on specimens of
different thicknesses.

This paper addresses part of this problem, namely
the variation with specimen thickness of the electrical
properties of arc discharges, under exposure to a mono-
energetic electron beam of fixed current density, com-
bined with a low energy ion beam. If one wished to
model accurately the magnetospheric environment, one
would have to use appropriate broad-spectrum, low-
current-density sources of both electrons and ions, and
the results of such an experiment would no doubt be
different from those to be presented here. The present
objective is more limited, being to contribute to the
process of tying together the many monoenergetic-elec-
tron experiments that have been done, in the belief that
understanding those experiments is a necessary prerequi-
site to the study of more complicated situations.

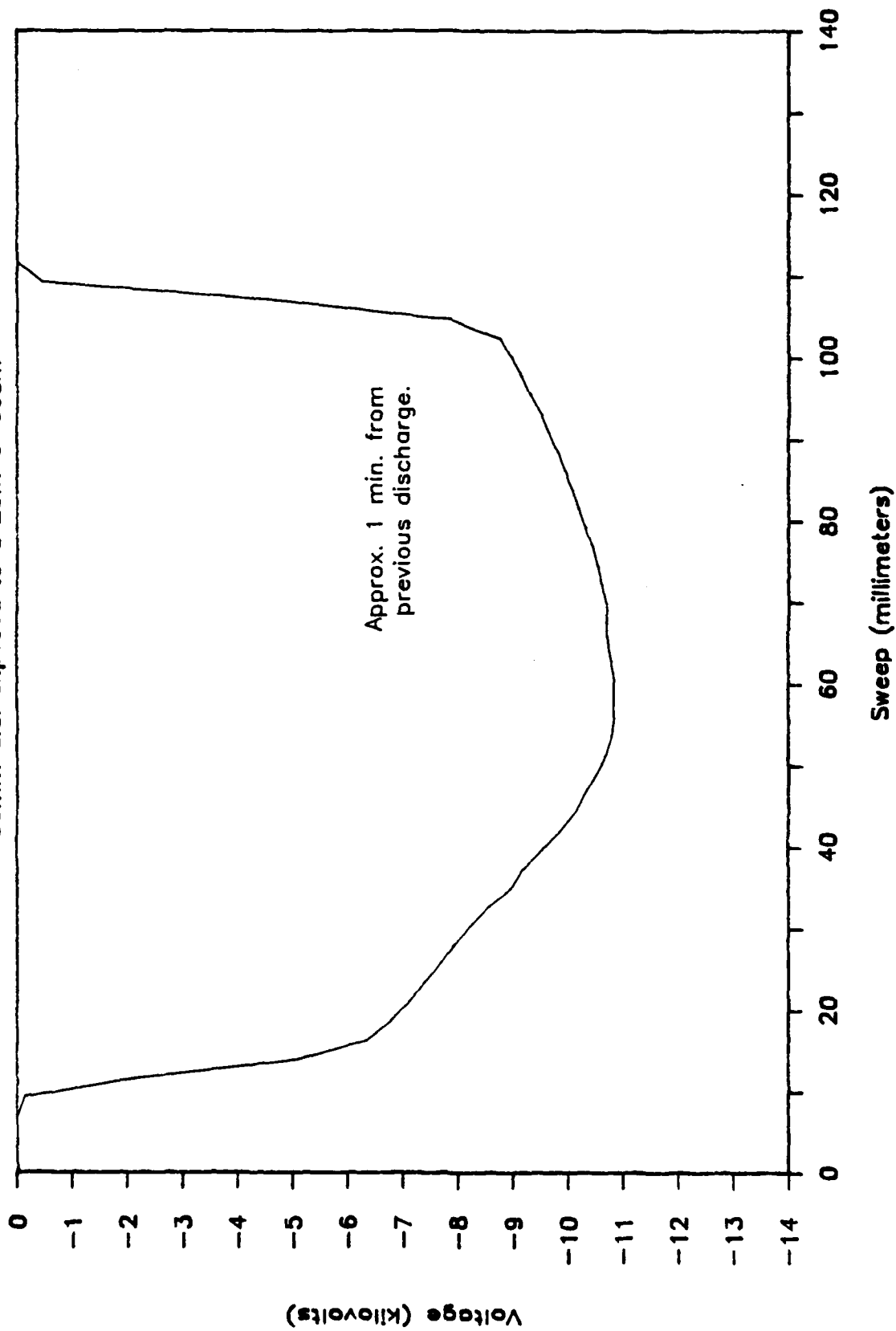The experiments to be described involve a polymer
sheet lying on a flat metal substrate and covered by a
close-fitting metal mask with a circular aperture. The
electrical quantities measured directly are the sub-
strate and mask currents as functions of time, the
method employed being to measure the voltages across
two low-value resistors connected respectively to the
substrate and the mask.

Theoretical Considerations

A dielectric sheet over a ground plane and in a
vacuum accumulates surface charge when exposed to an
incident electron beam. As time progresses, if not
interrupted by electrical breakdown, the surface charge
and potential both approach an equilibrium state which
corresponds to current balance involving the incident
electrons, the backscattered electrons, the secondary
emission from the dielectric, and the conduction through
the dielectric. It has been shown [3] that, for a mono-
energetic incident beam in which the current density J_i
actually reaches the dielectric, the equilibrium state
may be dominated either by conduction or by emission,
the transition between these two states being given for
Teflon and for a 20 kV beam accelerating voltage by

$$\frac{J_i d}{g} \simeq 2 \times 10^4 \text{ volts} \qquad (1)$$

in which d is the dielectric thickness and g is its
conductivity. The transition is not sharp but occurs
gradually over as much as an order of magnitude in
$J_i d/g$, and the transition point is not significantly
different for other good dielectrics such as Kapton.
For a constant beam accelerating voltage, the conduc-
tion-limited state is characterized by the surface
potential V being proportional to $J_i d/g$ through the re-
lation

$$V = (1-SE-BS) \, J_i d/g \qquad (2)$$

in which SE and BS are the secondary emission and back-
scatter coefficients. The emission-limited state is
characterized by the surface potential V being constant,
that is

$$eV = (BE-KE_2) \qquad (3)$$

where BE is the beam energy and KE_2 is the second-unity-
crossover emission energy at which SE+BS = 1.

Regarding the assumed uniformly charged dielectric
as a parallel-plate capacitor, one may take the charge
to be Q=CV where the capacitance C = ε A/d, A being the
area, and one may take the stored energy to be E_o=CV^2/2.
These may be written as follows, displaying their depen-
dence on V and d:

$$Q = \varepsilon A V/d \qquad (4)$$

$$E_o = \tfrac{1}{2} \varepsilon A V^2/d \qquad (5)$$

It may be assumed that a discharge involves total charge
cleanoff, which is known to be approximately true for
the strongest discharges; then Q is the total charge
flow to ground via the replacement current I from the
metal substrate supporting the dielectric. The stored
energy E_o is generally much greater than the energy E
dissipated in a low-value load resistor connecting the
substrate to ground. Making the tentative assumption
$E \propto E_o$, we would have

$$E \propto V^2/d \qquad (6)$$

The released charge is given by Q = ∫I dt. If we
assume I(t) is a symmetric triangle function with peak
current I_p and duration between half-current points
given by T, then

1

$$Q = I_p T \tag{7}$$

With the same triangular current pulse passing through a load resistor of R ohms, it is straightforward to show that

$$E = (2R/3) I_p^2 T \tag{8}$$

The following relations are deduced from (7) and (8):

$$E/Q = (2R/3) I_p \tag{9}$$

$$Q^2/E = (3/2R) T \tag{10}$$

Equations (4), (6), (9) and (10) plus the fact that, for constant incident current density J_i, conduction-limiting implies $V \propto d$ and emission-limiting implies $V =$ constant, together make it possible to estimate the thickness dependence of the properties of the arc discharge as shown in the following Table. In the table, the behavior of the released charge Q is independent of any assumptions related to E, I_p or T. However the predicted behavior of E, I_p and T with variations in thickness d depends on the assumption $E \propto E_o$. Also shown in the table are the emission-limited results for the alternative assumptions $I_p \propto 1/d$ and $I_p \propto 1/d^2$ which are based on measurements to be presented.

Table I

Conduction-dominated charging	Emission-dominated charging		
(thin dielectric)	(thick dielectric)		
$E \propto E_o$	$E \propto E_o$	$I_p \propto 1/d$	$I_p \propto 1/d^2$
$Q =$ constant	$Q \propto 1/d$	$Q \propto 1/d$	$Q \propto 1/d$
$E \propto d$	$E \propto 1/d$	$E \propto 1/d^2$	$E \propto 1/d^3$
$I_p \propto d$	$I_p =$ const.	$I_p \propto 1/d$	$I_p \propto 1/d^2$
$T \propto 1/d$	$T \propto 1/d$	$T =$ const.	$T \propto d$

This table shows that, as thickness increases, the released charge Q will change from a constant to a decreasing quantity independent of any assumptions on E or I_p. This table also suggests that the energy E dissipated in a load resistor will be a maximum at a transition thickness given by

$$d \cong 2 \times 10^4 \, g/J_i \tag{11}$$

The peak current I_p and the pulse duration T may also exhibit thickness dependence.

Experiment Parameters

A beam accelerating voltage of 20 kV was selected because of the existence of data on many experiments at this voltage. A beam current density J_b of 25 nA/cm² was chosen to allow the accumulation of an adequate quantity of discharge data in a reasonable time, although this current density is one to two orders of magnitude too high to simulate conditions around spacecraft in synchronous orbit. In the laboratory, the actual incident current density is lower than the beam current density due to beam spreading, a reasonable approximation for this case being $J_i = 0.4 \, J_b$ [4]. The low-field conductivity of FEP Teflon at room temperature and low field strength could be of the order of 10^{-20} (ohm-cm)$^{-1}$ rising to a value perhaps as high as 10^{-15} (ohm-cm)$^{-1}$ at elevated temperature (~400 K) and as the internal electric field approaches breakdown strength [4,5]. Under the extreme highest-conductivity conditions the transition thickness would be

$$d \cong 2 \times 10^4 \, g/J_i$$

$$\cong 20 \, \mu m$$

(with similar results expected for Mylar [5]) which is just within the range of available material thicknesses, these being 12.5, 25, 50, 75 and 125 μm. The conductivity for Kapton could be of the same order of magnitude or higher [6], but at room temperature. Trying to predict the transition thickness is obviously very difficult due to extreme uncertainty about the conductivity at the point of breakdown and also due to some uncertainty about the degree of beam spreading.

The experimental configuration was the same as used in the past [7]: it consisted of the dielectric sheet specimen sandwiched between a flat metal substrate and a metal aperture mask with a bevelled-edge circular aperture of area 15.9 cm². The substrate and mask were connected to the metal vacuum chamber walls ("ground") through individual 2.5 ohm resistors, the resistor voltages being used to deduce the substrate and mask currents during a discharge. The electron beam was magnetically deflected through approximately 90 degrees to permit direct viewing and photography of the specimen. Ion exposure was also available using a small Lithium oven and 100-volt-accelerator ion extractor which produced a broad flood beam of ions at a current density equal to 10% of the electron current density, comparable to relative ion current densities used in past work [8] and existing in the magnetosphere [9,10, 11]. Before the experiments, multiple Faraday cups were used to measure the incident current density distribution which was established as uniform over the mask aperture to within ± 15%. During each experiment, a single Faraday cup mounted just to the side of the mask aperture was used to monitor the incident current density which was maintained constant to within ± 10%. The dielectric specimens were used in the state "as received from the manufacturer" but it was also confirmed by a few experiments that there was no noticeable effect due to cleaning the specimens with trichloroethylene in a vapor degreaser. The vacuum pressure was always lower than 9×10^{-6} torr.

The primary measurement during an arc discharge was current I as a function of time, the peak value being designated I_p. The current was integrated to give the released charge Q, and the square of the current multiplied by the resistance (R = 2.5 ohms) was integrated to give the energy E. The current pulse duration T was measured as the time between the $I = \frac{1}{2} I_p$ points.

Experiment Results

The results for thickness scaling are presented in Figs. 1 to 4. Each graph displays up to four data curves and includes short-form designations for the curves, the short-forms having the following meanings:

Sub:e	means	Substrate: electrons only.
Mask:e	"	Mask: electrons only.
Sub:e+i	"	Substrate: electrons plus ions.
Mask:e+i	"	Mask: electrons plus ions.

The word "maximum" over the Q, E, and I_p graphs is an indicator that only the strongest discharge pulse observed for each case contributes to the data presented. Graphs for data averaged over all discharges were also plotted but are not shown. They were generally similar in shape but were significantly reduced in magnitude by the occurrence of punchthroughs after a few discharges. Among the "maximum" discharges analyzed the only cases that exhibited punchthroughs were the following:

12.5 μm Teflon with electrons only
(8 punchthroughs),

25 μm Teflon with electrons only
(4 punchthroughs),

12.5 μm Teflon with electrons and ions
(2 punchthroughs),

and 12.5 μm Mylar with electrons only
(1 punchthrough)

The pulse duration graphs displayed are of averaged data because the pulse duration is determined by arc propagation velocity and therefore is not strongly influenced by the occurrence of punchthroughs. Pulse duration graphs were plotted (but are not shown) for those discharges having the largest peak currents: these graphs were found to be generally similar to the average pulse duration graphs.

The Mylar and FEP Teflon specimen thicknesses were 12.5, 25, 50, 75 and 125 μm, and the Kapton specimen thicknesses included all of these except 12.5 μm. On the graphs, the absence of data for an available thickness indicates that no discharges were observed after an exposure period of at least 30 minutes. For example, no discharges were observed on any of the Kapton specimens under exposure to electrons plus ions, nor on the 25 μm Kapton with electron-only exposure. Also, the 12.5 μm Mylar did not discharge under exposure to electrons plus ions.

Figures 5 and 6 show typical arc discharges on the same specimen of 25 μm Mylar, under electron-only irradiation. A punchthrough is clearly identifiable as a bright spot, and essentially the whole area is covered by the arc. Figure 7 shows a luminescence pattern with 10% ion flux, and Fig. 8 shows an arc occurring under an ion flux of about 3%.

Discussion of Results: Electrons Only

The charge graphs appear to agree well with the rudimentary theory presented, and there is also a measure of apparent qualitative agreement for thin specimens under the assumption that the energy E dissipated in a substrate load resistor is proportional to the stored energy E_0. For thick specimens the slopes of the log-log graphs of measured data are shown in Table II, with the two values in parentheses being those for the initial assumptions $I_p \propto 1/d$ and $I_p \propto 1/d^2$.

Table II

Measured (predicted) substrate graph slope magnitudes for the thickest specimens irradiated with electrons only

	Charge	Energy	Peak Current
Mylar	1.1 (1,1)	3.2 (2,3)	2.0 (1,2)
Teflon	1.1 (1,1)	2.7 (2,3)	1.4 (1,2)
Kapton	1.2 (1,1)	2.8 (2,3)	1.3 (1,2)

For thin specimens the comparison is more random and is not shown. For the substrate discharge pulse duration graphs (electrons only), there is not a consistent similarity between the experiments and the predictions.

The predictions summarized in Table I are based on the premise that the specimen charges up almost to the equilibrium state before a discharge occurs. If the first discharge on a previously untested specimen exhibits a punchthrough, then experience shows that the discharge is weaker than might be expected, presumably because the discharge was triggered early by an initial breakdown at a point of weakness (such as a gaseous inclusion) which results in specimen perforation at that

point. Thus one associates punchthrough occurrence with premature and therefore relatively weak arc discharges. The punchthrough occurrences already noted could have contributed to the weaker discharges for the thinnest specimens of both Mylar and Teflon, and therefore it is not at all certain that the measured transitions in the 25 to 50 μm range were actually caused by the theoretical transition between conduction and emission domination in the charging process, a transition which could be pushed as high as 20 μm thickness only by the assumption of improbably high conductivity caused by temperatures of the order of 400K. Rather, the experimental evidence of punchthrough formation suggests that localized material weakness which affects thin specimens preferentially is the most likely cause of the observed variation of discharge properties for the thinner specimens. For the thicker specimens, emission-dominated charging appears to be the main factor controlling the variation with thickness of the discharge properties, because the released charge was found to vary with thickness as predicted, independent of whether the initial assumption was $E \propto E_0$ or an observed I_p dependence. The measured variation with thickness of energy dissipated in the load resistor appears to require the initial assumption that the peak current is proportional to something between $1/d$ and $1/d^2$. The initial assumption $E \propto E_0$ appears to be generally inappropriate for thick specimens, although it does predict correctly the slope of the pulse duration graph for Teflon.

The measured variation of pulse duration with thickness indicates that the thickness of the specimen influences arc velocity. Under electron-only exposure the velocities (mask radius divided by duration) range from 0.5×10^5 to 5.6×10^5 m/s for Mylar, from 1.8×10^5 to 7.5×10^5 m/s for Teflon, and from 2.8×10^5 to 5.0×10^5 m/s for Kapton. Arc velocity increase with increasing deposited charge in very thick specimens has been reported by Erickson and Oakley [12] and by Cooke et al. [13] for very high-energy, short-duration electron exposure but the great differences in experimental circumstances make comparison with the present work difficult.

Discussion of Results: Electrons Plus Ions

The electron-only arc photographs of Figs. 5 and 6 (both on the same Mylar specimen) show arcs that cover the entire exposed dielectric in spite of the existence of localized triggering at a punchthrough. Figure 7 is a photograph of luminescence only, in the absence of any arc, but for combined electron plus 10% ion exposure. On the photograph there are two bright regions which require explanation. The upper bright region is the specular reflection of the very dim red light from the small Lithium oven ion gun. The lower bright region disappears slowly after the ion gun is turned off and expands when the ion current density is increased. This bright region is therefore interpreted as a region of steady-state ion neutralization of embedded electron charge, which permits the electrons to approach the dielectric unimpeded and produce the bright region by impact luminescence. The bright region is approximately centrally located because the embedded electrons produce high transverse edge fields which draw the low energy ions radially inward from the specimen edge before drawing them to the surface in the middle region of the specimen. If this interpretation were correct, then, in order for steady-state neutralization to occur in the bright region when the incident ion flux density is 10% of the electron flux density, the exposed specimen area would have to be 10 times the bright-region area. In fact the area ratio is about 13, close enough to 10 to lend support to the explanation offered above.

Figure 8 shows an arc on a specimen exposed to a

3

somewhat lower incident ion current density which was not accurately measured but estimated at 3% of the electron current density. In the photograph there is an evident tendency for the arc to avoid a central region whose area is somewhat smaller than the bright region already discussed, a phenomenon consistent with the lower ion current density creating a smaller charge-neutral region which cannot support a propagating arc discharge.

Conclusions

Under electron-only exposure at one value of incident current density (25 nA/cm^2), the properties of beam-induced arc discharges on polymer sheets scale with sheet thickness in a manner which is regular and similar from one material to another indicating that a transition occurs around 50 µm thickness. For thick sheets, the released charge scales in accordance with a prediction assuming that the charge accumulation process is emission-dominated and that the released charge is proportional to the accumulated charge. A corresponding, simple prediction of scaling laws for peak current and energy dissipated in a load resistor was not achieved due to insufficient knowledge of the discharge mechanism, although a measure of consistency between peak current and energy scaling was established for thick specimens.

For thin specimens exposed to electrons only, the released-charge scaling levels off approximately as predicted by assuming that the charge accumulation process is dominated by the conductivity of the polymer, including nonlinear conductivity, but such conductivity would have to be improbably high to produce a transition between conduction and emission domination in the 20-50 µm range. A much more likely explanation based on observation is that the levelling out of released charge for thin specimens was caused by punchthrough formation and subsequent premature discharging. As for thin-specimen peak current and energy scaling, a measure of qualitative agreement with experiment was achieved by assuming that the energy dissipated is proportional to the stored energy but, again, lack of understanding of the discharge mechanism prevents the establishment of a well-founded, simple prediction.

Under electron-plus-ion exposure, a relatively bright, steady, luminescent spot was observed in the central region of the specimen. This spot was avoided by discharge arcs and therefore was interpreted as an area of ion impact and electron-ion charge neutralization. The reduction in arc strength due to the ion exposure was too great to be explained simply by postulating that the effective specimen area was reduced by the size of the ion spot. Rather, it is likely that enough ions fall outside the spot area to reduce significantly the net charge accumulated there. With ions, the arc discharges are weakened and sometimes eliminated, but the thickness-scaling graphs are not greatly changed in shape. Insofar as spacecraft are concerned, it appears that low energy ions from the ambient plasma could be drawn in to neutralize partially any exposed electron-charged dielectrics.

References

[1] A. Rosen, "Spacecraft charging by magnetospheric plasmas," IEEE Trans. Nucl. Sci., vol.NS-23, no.6, pp. 1762-1768, Dec. 1976.

[2] A.R. Frederickson, "Electric discharge pulses in irradiated solid dielectrics in space," IEEE Trans. Elect. Insulation, vol.EI-18, no.3, pp. 337-349, June 1983.

[3] R.D. Reeves and K.G. Balmain, "Two-dimensional electron beam charging model for polymer films,

[4] R.D. Reeves, Two-Dimensional Electron Beam Charging Model for Polymer Films, M.A.Sc. Thesis, Dept. of Elect. Engrg., Univ. of Toronto, 1981.

[5] V. Adamec and J.H. Calderwood, "Electrical conduction in dielectrics at high fields," Journal of Physics D, vol.8, pp. 551-560, 1975.

[6] J.B. Reagan, R.E. Meyerott, E.E. Gaines, R.W. Nightingale, P.C. Filbert, and W.L. Imhof, "Space charging currents and their effects on spacecraft systems," IEEE Trans. Elect. Insul., vol.EI-18, no.3, pp. 354-365, June 1983.

[7] K.G. Balmain and W. Hirt, "Dielectric surface discharges: dependence on incident electron flux," IEEE Trans. Nucl. Sci., vol.NS-27, no.6, pp. 1770-1775, Dec. 1980.

[8] M. Gossland and K.G. Balmain, "Incident ion effects on polymer surface discharges," IEEE Trans. Nucl. Sci., vol.NS-30, no.6, pp. 4302-4306, Dec. 1983.

[9] S.E. DeForest, "Spacecraft charging at synchronous orbit," J. Geophys. Res., vol.77, pp. 651-659, Feb. 1972. See also E.C. Whipple, "Potentials of surfaces in space," Rep. Prog. Phys., vol.44, pp. 1197-1250, 1981.

[10] J.B. Reagan, R.W. Nightingale, E.E. Gaines, R.E. Meyerott, and W.L. Imhof, "Role of energetic particles in charging/discharging of spacecraft dielectrics," Spacecraft Charging Technology 1980, NASA CP 2182/AFGL-TR-81-0270, pp. 74-85.

[11] J. Wilkenfeld, C. Mallon, and J. Horne, "Conduction and charge storage in electron-irradiated spacecraft insulators," RADC-TR-81-198, July 1981.

[12] L.M. Erickson and D.C. Oakley, "Time-resolved voltage breakdown in various insulators due to 2-MeV electrons," Lawrence Livermore Laboratory Report UCRL-51372, 5 April 1973.

[13] C.M. Cooke, E. Williams, and K.A. Wright, "Electrical discharge propagation in space-charged PMMA," Conference Record of the 1982 IEEE International Symposium on Electrical Insulation, pp. 95-101.
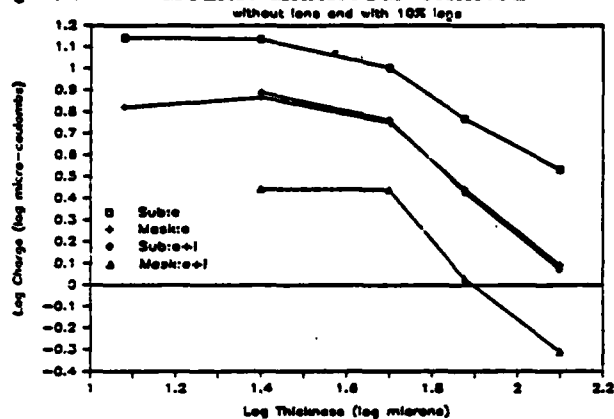
The continuation of reference [3]:

IEEE Trans. Nucl. Sci., vol.NS-28, no.6, pp. 4547-4552, Dec. 1981.

Fig.1(a) **MYLAR MAXIMUM CHARGE**
without lens and with 10% lens

Fig.2(b) **TEFLON MAXIMUM ENERGY**
without lens and with 10% lens
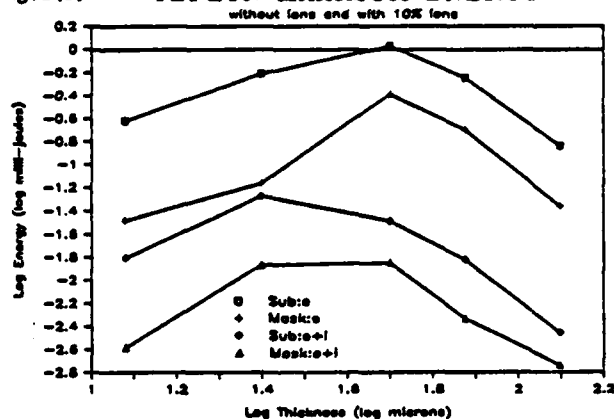
Fig.1(b) **TEFLON MAXIMUM CHARGE**
without lens and with 10% lens
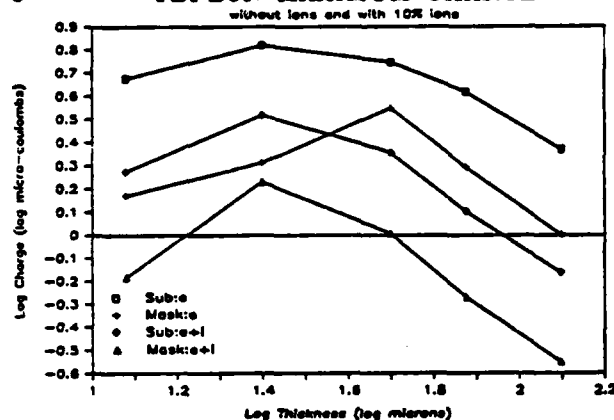
Fig.2(c) **KAPTON MAXIMUM ENERGY**
without lens
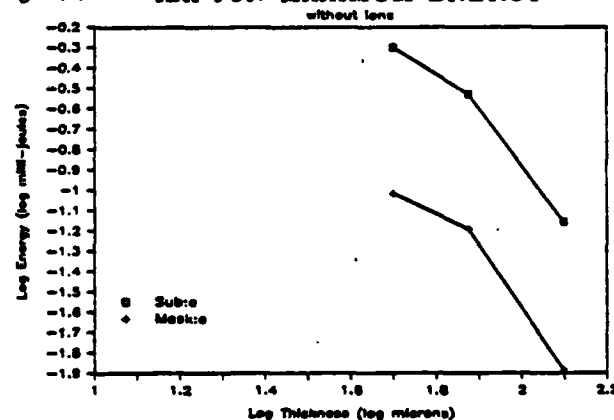
Fig.1(c) **KAPTON MAXIMUM CHARGE**
without lens
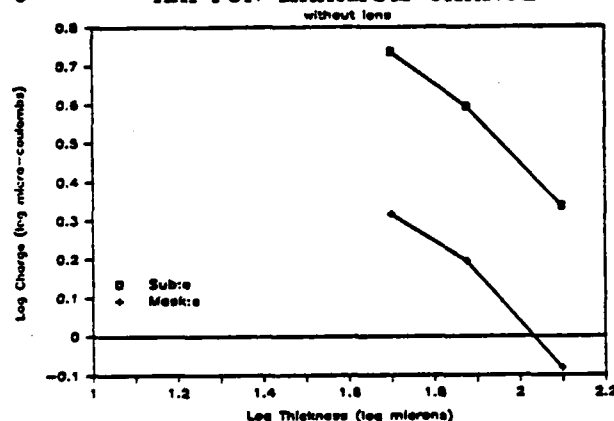
Fig.3(a) **MYLAR MAXIMUM CURRENT PEAKS**
without lens & with 10% lens
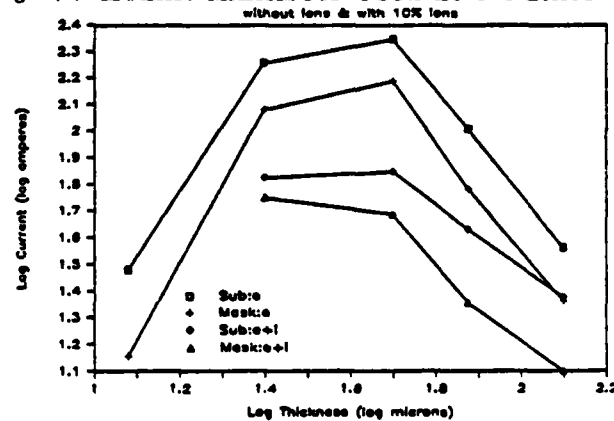
Fig.2(a) **MYLAR MAXIMUM ENERGY**
without lens and with 10% lens
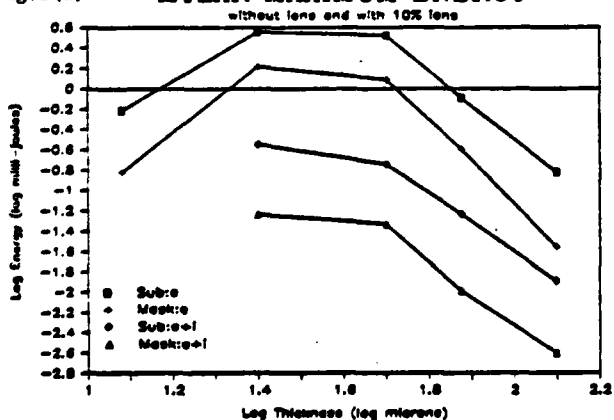
Fig.3(b) **TEFLON MAXIMUM CURRENT PEAKS**
without lens & with 10% lens

5
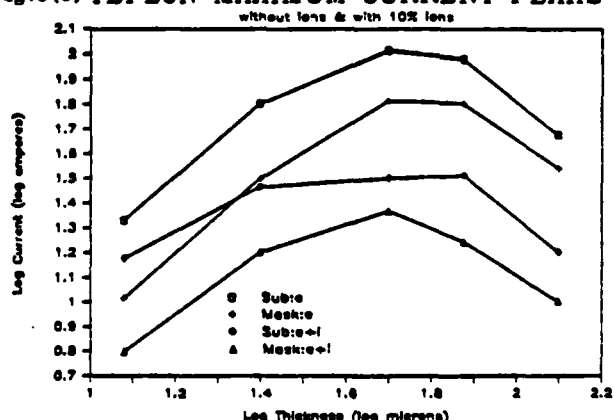
Fig.3(c) KAPTON MAXIMUM CURRENT PEAKS
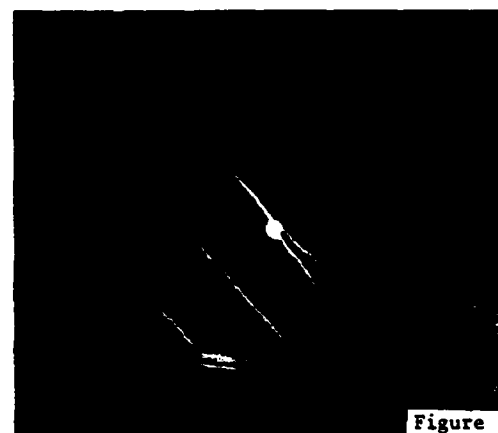
without lens
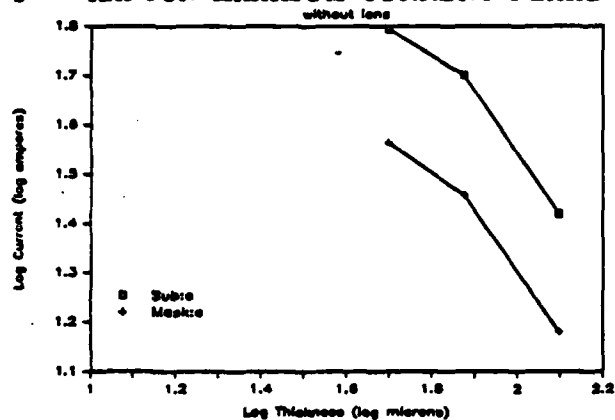
Fig.4(a) MYLAR PULSE DURATION

without lens and with 10% lens
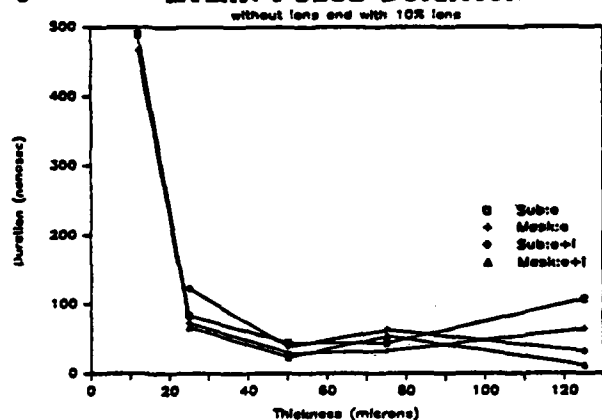
Fig.4(b) TEFLON PULSE DURATION

without lens and with 10% lens
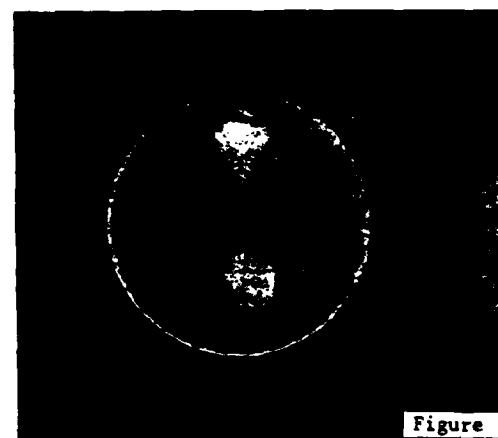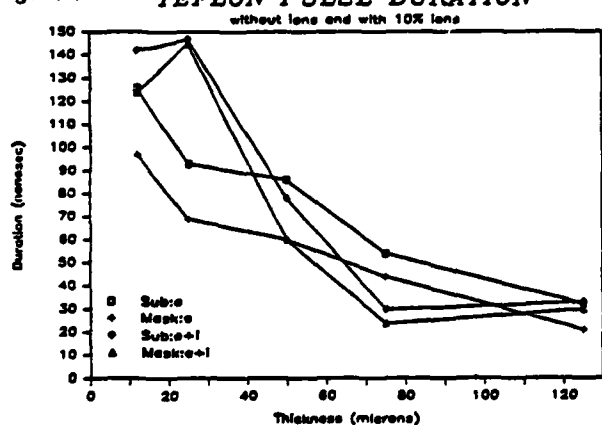
Fig.4(c) KAPTON PULSE DURATION

without lens and with 10% lens

Figure 5

Figure 6

Figure 7

Figure 8

6

END
FILMED

5-86

DTIC